THE UNIVERSITY OF CHICAGO

DOPAMINERGIC MODULATION OF HIPPOCAMPAL CA1: UNCOVERING THE ACTIVITY DYNAMICS OF VTA AND LC INPUTS DURING BEHAVIOR AND LEARNING

A DISSERTATION SUBMITTED TO
THE FACULTY OF THE DIVISION OF THE BIOLOGICAL SCIENCES
AND THE PRITZKER SCHOOL OF MEDICINE
IN CANDIDACY FOR THE DEGREE OF
DOCTOR OF PHILOSOPHY

COMMITTEE ON NEUROBIOLOGY

BY
CHAD MICHAEL HEER

CHICAGO, ILLINOIS
DECEMBER 2023

This dissertation is dedicated to my parents, for listening intently as I recited everything I learned from 'The Discovery Channel' as a kid and for instilling in me the value of an education.

TABLE OF CONTENTS

LIST OF FIGURES

ACKNOWLEDGMENTS

Here I want to thank all of the people who have supported me throughout the past six years including my advisor, Dr. Mark Sheffield. I first met Mark during my interviews at The University of Chicago and immediately noticed his passion for research, ability to ask and pursue meaningful scientific questions, and great communication skills. Hoping to gain some of these skills myself, I joined the lab as Mark's second graduate student. His genuine excitement, availability and mindfulness were invaluable as I learned how to ask interesting questions, run experiments, analyze data, write grants and manuscripts, and communicate my science. Throughout the troubleshooting eras, new discoveries, and addressing of reviewers comments, his support was unwavering. His genuine care for me as both a scientist and person made completing a PhD during a pandemic feel much more achievable. I am extremely grateful for all of the ways he invested in me and in this dissertation.

Along with Mark, I want to thank all of other members of the lab who made this dissertation possible. Seetha Krishnan, who served as a second mentor throughout my PhD, always willing to drop what she was doing to help me code, run an experiment, or just chat about science and life. Her collaborations with the reward-noreward project made it possible, exciting and enjoyable, and transformed it into a much more compelling set of experiments. I want to thank Can Dong, Chery Cherian, Madeline Klinger and Joe Dipietro, for teaching me how to do mouse surgeries, VR-experiments, and 2-photon imaging, and making my first years in the lab fun, exciting, and successful. Thanks to Antoine Nadar for always answering analysis questions, Heather Macomber for improving on our axon imaging, Anqi Jiang for her unwavering positivity, and Douglas Goodsmith for always being willing to help and keeping the lab running. I also want to thank the army of undergrads that have supported the lab and my project, especially Denisse Morales-Rodriguez, Phoebe Cao, Zinnia Saha, and Anthony James Jr.

I am also greatful for the support of my thesis committee members: Dr. Narayan 'Bobby' Kasthuri, Dr. Daniel McGehee, and Dr. Xiaoxi Zhuang for their intellectual, moral, and logisitic support. They were extremely helpful over the past year, helping me finsih up my expeirment and analysis, and guiding my transition to the next steps. I also thank the rest of the neuroscience community at The University of Chicago for making science thrilling and achievable, while also making space for us graduate students as people.

None of this dissertation would have been possible without the support of my friends and family. Thanks to my family for always supporting my interests in science since elementary school and for providing me with the means and freedom to pursue my dreams. I want to thank Dalton, Jordan, Katie, Craig, Mel, Madeleine, Brittany and the rest of my Chicago friends with whom I shared many drinks, played countless board games, talked infinitely about sports, vented endlessly about grad school, and had so much fun with.

Finally, I want to thank my partner, Cassidy McPherson, for her endless encouragement and support. You made the last few years of grad school so much more meaningful, made everyday brighter, and helped reignite my passions for science and teaching when I needed it most. There is no one else I would rather go through the next stages of life with.

ABSTRACT

Dopaminergic activity in the hippocampus modulates synaptic plasticity, alters place cell activity, and affects hippocampal dependent learning and memory processes. Traditionally these effects were attributed to the release of dopamine from sparse projections originating in the ventral tegmental area (VTA) and extending to the hippocampus. However, the role of VTA inputs in dopaminergic modulation of the hippocampus has recently been brought into question, as denser inputs from the locus coeruleus (LC) have been shown to release dopamine in the dorsal hippocampus, and impact hippocampal dependent learning and memory. To dissect the impacts of both VTA and LC dopaminergic circuits on hippocampal activity and memory, we functionally imaged the activity of VTA and LC axons in dorsal CA1 (dCA1). During spatial navigation, VTA inputs exhibited a ramping to reward signal that depended on the animals' reward expectation. Inhibiting VTA dopaminergic neurons largely replicated the effects of reward expectation extinction: reducing overrepresentation of rewarded locations, inducing place field remapping, and decreasing place field trial-to-trial reliability. We conclude that reward expectation restructures CA1 place cells and determines map reliability through the modulation of dopaminergic VTA-CA1 reward-proximity signals. In contrast, LC inputs were devoid of the reward-proximity signal observed in VTA axons and instead exhibited velocity correlated activity and increases in activity prior to motion onset. Interestingly, a marked divergence emerged in novel VR environments. LC axon activity sharply and persistently increased for over a minute, while the previously observed VTA axon reward-proximity signal disappeared. We conclude that LC inputs to dCA1 encode the animals' brain state, as changes in behavior and environmental novelty are associated with heightened arousal. This observation further strengthens the roles of LC neurons in influencing brain states and in novelty encoding in the hippocampus. Together, these findings demonstrate VTA and LC inputs encode unique information, likely contributing to differential modulation of hippocampal activity during behavior and learning.

CHAPTER 1

INTRODUCTION

Memory is an essential function of the brain. In order to survive, animals must be able to not only acquire and store information from previous experiences, but also rapidly access relevant memories and update them as necessary. Without this ability, animals would be unable to learn and identify potential hazards, remember and locate food sources, navigate complex social interactions, and adapt to ever changing environments. In fact, memory is an integral component of nearly all other cognitive functions, shaping how the world is perceived and interacted with. In humans, memories are a central aspect of identity. They shape our relationships, our personality, and how we communicate and interact with the world around us. Understanding how memories are formed, updated, and recalled is critical to our understanding how brains function and has been a major goal of neuroscientists for decades.

Memory can be divided into two categories: implicit(non-declarative) and explicit (declarative) memories. Implicit memories refer to memories that do not require conscious awareness and can only be demonstrated through actions. These memories include procedural memories, or the memories that allow individuals to get better at motor tasks. While individuals are not aware of these memories, they explain how people improve at riding a bike or playing the piano with practice. These memories depend heavily on function of the basal ganglia (Foerde and Shohamy 2011) and cerebellum (H 2008) as dysfunction of either of these structures leads to deficits in procedural memories. The other type of implicit memory is conditioning, involving the pairing of an unconditioned stimulus with a conditioned stimulus to evoke a conditioned response. The classic example of conditioning is Pavlov's dog where dogs were trained to salivate at the ringing of a bell by pairing the bell with a reward. Depending on the response elicited, these memories can involve function of the amygdala and cerebellum (Squire 2004).

In contrast, declarative memories refer to memories that can be consciously recalled. These memories are most often thought of when referring to memory and can be further divided into semantic and episodic memories. Semantic memories are memories of facts and concepts that can be recalled without knowing when the information was obtained, while episodic memories are memories of experienced events that include information what occurred, when and where it occurred, as well as the emotions associated to the event. Both types of explicit memories depend on the function of the hippocampus. However, the precise circuit mechanisms underlying the storage, updating, and recall of explicit memories are not fully understood and are the focus of this thesis.

1.1 The identification of the hippocampus as a key component of episodic memory

The idea that the hippocampus plays a vital role in the formation of new declarative memories largely came about following the studies of patient H.M. (Henry Molaison). After suffering from epilepsy, patient H.M. underwent bilateral removal of parts of his medial temporal lobes including both hippocampi (Scoville and Milner 1957). While this solved his epilepsy, it caused some unforeseen complications. He was unable to form new declarative memories or recall events that occurred shortly before the surgery. However, his declarative memories that existed well before his surgery were undisturbed. These observations inspired the idea that the hippocampus is necessary for the formation of new declarative memories and recall of recently formed memories. Over time these memories are consolidated, and their recall then becomes independent of the hippocampus. Additionally, his procedural memories were unaffected eventually leading to our understanding of multiple memory systems that exist in the brain (Cohen and Squire 1980). Although H.M.'s lesions extended beyond the hippocampus (Corkin et al. 1997) and parts of his hippocampus remained intact (Annese et al. 2014), many behavioral studies of humans and animals with hippocampal lesions have

further demonstrated the role of the hippocampus in declarative memory.

At the same time as investigations into the functional role of the hippocampus, the first recordings of hippocampal neuron activity in rodents were being conducted. These initial recordings revealed the presence of neurons who are selectively active at specific places within a given environment, earning these cells the title of place cells (J. O'Keefe and Dostrovsky 1971). Together, the firing activity of hippocampal place cells was theorized to serve as a cognitive map, or an internal representation of an external environment, and allow an animal to identify its location in an environment (John O'Keefe and Nadel 1978). Indeed, it is possible to reconstruct the trajectory of an animal using its hippocampal activity patterns (M. Wilson and B. McNaughton 1994; Krishnan et al. 2022) supporting the role of the hippocampus in spatial navigation. There is now a growing body of evidence that this activity is used beyond spatial navigation and serves as a representation of environmental information for episodic memories. For example, sequences of place cell activity that occur during navigation are repeated during rest, and disruption of these replay events impairs spatial memory (Carr, Jadhav, and Loren M Frank 2011; Foster and Matthew A. Wilson 2006; Sadowski, Jones, and Jack R. Mellor 2016; Ven et al. 2016; M. Wilson and B. McNaughton 1994). Additionally, recent studies have shown the congitive map includes other non-spatial information, as place cells have been shown to be modulated by time (Eichenbaum 2017), color (Leutgeb 2005), odor (Save, Nerad, and Bruno Poucet 2000; S. Zhang and Denise Manahan-Vaughan 2015), novelty(Larkin 2014), and reward (Hollup et al. 2001; Kobayashi et al. 2003; Dupret et al. 2010; McKenzie et al. 2013; Mizumori and Tryon 2015; Zaremba et al. 2017; Gauthier and Tank 2018). The encoding of these various contextual features of experience by cognitive maps strongly indicates they are a representation of episodic memory, encoding general experiences in space in time. Indeed, non spatial cognitive maps have been observed in hippocampal activity with neurons constructing maps of abstract value space (Knudsen and Wallis 2021) and time (Eichenbaum 2017). Together, these findings support the role of

hippocampal place cells in both spatial navigation and episodic memory.

1.2 The anatomy of the hippocampus

The first description of the hippocampus was published in 1587 in the 1st issue of the *Anatomicarum Observationum Liber* (Book of Anatomical Observations) by Italian anatomist, Giulio Cesare Aranzio (Arantius) (Engelhardt 2016). This curved structure deep in the temporal lobe, resembled a seahorse to Arantius, earning it the name hippocampus, or seahorse in Latin. While its anatomical boundaries were updated and redefined, the name persisted, and the hippocampus is used today to describe this curved structure found deep in the medial temporal lobe. Anatomical studies have since demonstrated that this archicortical structure is conserved across may taxonomic classes including mammals, birds, and reptiles (Allen and Fortin 2013). In mammals, the hippocampus is easily identifiable due to the presence of a single, densely packed pyramidal neuron layer (*stratum pyramidalis*), a basal dendrite layer (*stratum oriens*), and an apical dendrite layer (*stratum radiatum*), rather than six sparser layers in many parts of the cortex. The hippocampus can then be divided into two regions; the dentate gyrus (DG), and cornus ammonis (CA), which itself can be divided into CA1, CA2 and CA3. In rodents, these two hippocampal regions from interlocking U's with the dorsal U composing the three subregions of the cornus ammonis. Unlike the neocortex, information in the hippocampus largely flows in one direction through a trisynaptic circuit. The entorhinal cortex, which receives multimodal information from many cortical areas, is the main input to the hippocampus through the perforant path which largely synapses onto DG neurons. DG neurons project onto CA3/CA2 neurons through mossy fibers, which in turn project onto CA1 neurons through Schaffer collaterals. CA1 neurons then project out of the hippocampus into the subiculum and parahippocampal areas. Each of these four subregions has distinct anatomical and physiological properties which have been theorized and shown to support the hippocampus's role in episodic memory formation.

How does the hippocampus the structure and physiology of the different hippocampal subregions support its role in episodic memory formation? To understand this, it is helpful to explain the role of the hippocampus in terms of the Hippocampal Index Theory (Teyler and DiScenna 1986). In this theory, the hippocampus does not serve as the site of memory storage but rather plays a role like that of a reference card at a library. Just as a reference card does not provide the detailed information in a book but provides the means to quickly locate and obtain the correct book, the hippocampus is theorized to serve as a means of storing information about where a memory is located and how to retrieve said memory. Therefore, during recall of a memory, the hippocampus would provide a means to reactivate the correct pattern of cortical activity. Overtime, these memories are consolidated, and the hippocampus is no longer needed recall, just as a reference card would no longer be needed after a book has been found multiple times.

The hippocampus's connections with neocortical areas supports this idea. It receives highly processed information from all sensory modalities through its main excitatory inputs from the entorhinal cortex. These connections with neocortical areas provide the hippocampus with information about the cortical activity patterns that occurred during learning that could then be stored in the hippocampus . Additionally, the hippocampus sends its major outputs to the subiculum and then out to many cortical areas. Therefore, during recall the hippocampus is perfectly situated to reactivate the cortical activity patterns necessary for recall. These reciprocal connections with cortical areas provide the hippocampus with information about the cortical activity patterns that occur during learning and a way to reactivate those patterns during recall.

The hippocampal index theory depends on the idea that the specific firing patterns of neurons that occur during learning can reliably be reactivated during recall. This idea was first theorized by Donald Hebb in 1949. Simplified, the Hebbian theory is the idea that "cells that fire together, wire together", and predicts the presence of cellular mechanisms that allow

for the strengthening of the connections between two neurons. More specifically, it states that when the firing of one neuron reliably precedes the firing of another neuron, changes will occur in the connections, or synapses, between these two neurons allowing the activity of the first neuron to evoke activity more efficiently in the downstream neuron. Indeed, it has since been discovered that there is a wide range of cellular mechanisms devoted to the strengthening and weakening of synapses. These mechanisms extend beyond the plasticity proposed by Hebb, and are considered to serve as the cellular basis of learning and memory and considerable evidence supports this idea (Martin, Grimwood, and R. G. Morris 2000; Citri and Malenka 2008; Magee and Grienberger 2020).

However, not all events are remembered. Animals must be able to ignore irrelevant stimuli but also reliably form memories from single experiences with rewarding, or life-threatening stimuli. It has been theorized that neuromodulators can serve as filter, controlling which events are remembered (Dayan 2012; Palacios-Filardo and Jack R Mellor 2019). Rather than acting directly on ion channels to excite or inhibit neurons, neuromodulators act on metabotropic receptors which utilize signaling cascades to modulate neurons in a number of ways. They can cause changes in cell excitability, synaptic efficacy, and even promote the removal or formation of synapses, thus providing neuromodulators with a means to gate when memories are formed. The hippocampus receives neuromodulatory inputs from several brain areas but the strongest are seratonergic inputs from median raphe nucleus, cholinergic inputs from medial septal nucleus/diagonal band of Broca, dopaminergic inputs from the ventral tegmental area (VTA), and noradrenergic inputs from the locus coeruleus (LC) (Palacios-Filardo and Jack R Mellor 2019). Each of these neurotransmitters has been shown to impact hippocampal synaptic plasticity and hippocampal dependent learning in memory. However, dopamine activity in the hippocampus has been shown to play many roles in hippocampal dependent learning including spatial learning (Silva et al. 2012; McNamara et al. 2014; Lisman and Grace 2005; Edelmann and Lessmann 2018), novelty encoding (Chowdhury et

al. 2022; Wagatsuma et al. 2018; Kempadoo et al. 2016), aversive learning (Tsetsenis et al. 2019), and reward learning (N. Hansen and D. Manahan-Vaughan 2014; Assar et al. 2016; Azevedo et al. 2019). Additionally, the main source of dopamine in the dorsal hippocampus has been brought into question (Kempadoo et al. 2016; Takeuchi et al. 2016; Duszkiewicz et al. 2019). Therefore, my thesis focuses on the role of dopaminergic inputs on hippocampal function.

1.3 Dopaminergic neuromodulation of the hippocampus

There are dopamine receptor subtypes that can be divided into D1 like receptors (D1 and D5 receptors) due to their positive effect on adenylate cyclase activity (AC) and D2 like (D2, D3 and D4 receptors) receptors that downregulate AC activity. Therefore, these receptors play opposing roles in the regulation of AC activity, impacting cAMP levels in the cytosol and therefore effecting Ca2+ which is involved in many types of synaptic plasticity (Jean-Martin Beaulieu and Raul R. Gainetdinov 2011). Throughout the dorsal hippocampus, D1R are expressed most strongly in granule cells of the DG (Gangarossa et al. 2012; Wei et al. 2018) but are also found in the *stratum oriens* and *stratum radiatum* of CA3-CA1 where they are found on both pyramidal neurons and interneurons (Yao, Spealman, and J. Zhang 2008). D2Rs are mainly expressed in mossy cells in the dorsal DG (Wei et al. 2018) but have also been reported in the *s.l.m.* of CA3-CA1 (C Charuchinda et al. 1987). In the ventral hippocampus, D1R and D2Rs are more strongly expressed in CA1 and the subiculum (Puighermanal et al. 2017; Wei et al. 2018). The variable expression across the longtitudinal axis and hippocampal subregions hints towards different roles of dopamine across these regions.

Most of the research investigating dopamine's actions in the hippocampus has investigated its impact through D1Rs. However, there is evidence indicating that D2Rs modulate LTD (Z. Chen et al. 1995; Rocchetti et al. 2015), play a role in food and drug seeking (Assar

et al. 2016; Azevedo et al. 2019), and in the acquisition of conditioned place preferences (Assar et al. 2016) highlight a distinct role of these receptors. The focus on D1Rs is likely because have been shown to play a significant role in the regulation of synaptic plasticity and hippocampus dependent memory (N. Hansen and D. Manahan-Vaughan 2014; Huang and Kandel n.d.)(Hansen 2012, Hansen 2014, Kandel 1994). In slice preps, activity of D1Rs has been shown to modulate early and late LTP and LTD in schaffer collaterals (Huang and Kandel n.d.; Lisman and Grace 2005; N. Hansen and D. Manahan-Vaughan 2014; Z. Chen et al. 1995), mossy fibers (Hagena and Denise Manahan-Vaughan 2013), and perforant path (Kusuki et al. 1997; Wieschollеck and Denise Manahan-Vaughan 2014). DA has been shown to play a role in spike timing-dependent plasticity in Schaffer collaterals (J.-C. Zhang, Lau, and Bi 2009; Edelmann and Lessmann 2011; Yang and Dani 2014), a physiologically relevant form of synaptic plasticity thought to serve as the neural correlates of memory formation. The wide range and potentially contrasting roles of dopamine seen highlight importance of experiments describing the activity of DA inputs and therefore DA concentrations during spatial navigation and learning tasks, as different concentrations of DA could lead to contrasting effects on learning and memory due to the different binding affinities of DA receptors (Cumming 2011).

In-vivo activity of D1Rs has been shown to influence many hippocampal dependent forms of learning and memory. D1Rs play an important role in spatial memory formation, as their activity during and after encoding significantly impacts memory retention and retrieval in many different spatial learning tasks (O'Carroll et al. 2006; Silva et al. 2012; Xing et al. 2010; Granado et al. 2008). Additionally, inhibition of D1Rs leads to impairments in the acquisition and reinstatement of morphine (Assar et al. 2016), cocaine (Burgdorf et al. 2017) and nicotine-induced (Tang and Dani 2009) conditioned place preference. In contextual fear conditioning experiments, D1Rs play a role in the acquisition and extinction but not recall of contextual fear (Tsetsenis et al. 2019). Importantly, D1Rs have been shown to

play an important role in encoding novelty in the hippocampus. Dopamine is released in the hippocampus during exposure to spatial novelty, facilitates LTP and influence memory formation (S. Li et al. 2003; Liu et al. 2009; Moncada and Viola 2007). During exposure to spatial environments, the stable formation of place cells has been shown to be dependent on cellular mechanism underlying LTP (Mark E.J. Sheffield, Adoff, and Daniel A. Dombeck 2017) and D1Rs (Wagatsuma et al. 2018) further supporting the role of dopamine in spatial memory formation. Although there is the potential for different effects of dopamine between the ventral and dorsal hippocampus, I will focus on dopaminergic inputs to the dorsal hippocampus for a couple of reasons. First, much more is known about the role of the dorsal hippocampus in episodic learning and memory largely due to the difficulty of recording from the ventral hippocampus. Therefore, we will be able to connect the function of dopaminergic inputs to the known dynamics of the dorsal hippocampus. Secondly, there is controversy over the source of the dopamine in the dorsal hippocampus, highlighting a need for further investigations of dopaminergic inputs to these regions.

1.4 Ventral tegmental area inputs to the dorsal hippoacmpus

Traditionally, dopaminergic inputs from the ventral tegmental area (VTA) were thought to serve as the main source of dopamine in the dorsal hippocampus. This midbrain region is an important part of the brains reward circuitry and it thought to provide a reward prediction error to many parts of the brain (Schultz 1998). Dopaminergic neurons in the VTA will respond strongly to unexpected rewards, but once an association has been learned between a cue a reward, they will be active at the cue but not when the reward is delivered. However, if the reward is omitted there will be a reduction in VTA neurons activity at the time when the reward is delivered. These findings supported the idea that these neurons signal a reward prediction error, or the difference between the expected value and the actual value of a given timepoint. Reward prediction errors are an important component of reinforcement

learning models (Sutton and Barto 1981; Dabney et al. 2020), which attempt to explain how individuals ought to act to maximize reward. Therefore, VTA DA neurons are thought to signal when to update the value of a given cue or action, and their projections to the hippocampus may provide them with a way to gate when the value representations of an environment or cue should be updated. Recent experiments demonstrate a wide degree of heterogeneity in the activity of VTA DA neurons (Engelhard et al. 2019) while others highlight a disconnect between VTA activity and RPE (Kim et al. 2020; Mohebi et al. 2019; Howe et al. 2013). These findings highlight the importance of careful characterization of projection specific VTA neuron activity during different behaviors.

Furthermore, some controversy exists regarding the strength of VTA DA projections to the dorsal hippocampus. VTA DA neurons project strongly to the ventral hippocampus, however their projections to the dorsal hippocampus are very sparse (Takeuchi et al. 2016; Wagatsuma et al. 2018; Adeniyi, Shrestha, and Ogundele 2020). While some studies have reported a near absence in VTA DA projections to the dorsal hippocampus (Takeuchi et al. 2016; Wagatsuma et al. 2018), others have reported neurons innervating *s.o.* (Adeyelu and Ogundele 2023; Rosen, Cheung, and Siegelbaum 2015; McNamara et al. 2014) and *s.r.* (McNamara et al. 2014; Rosen, Cheung, and Siegelbaum 2015) of CA1 and CA3. It is not clear how these axons connect to and release dopamine in the dorsal hippocampus. They could connect to dendrites, act on presynaptic terminals, or act through bulk volume transmission of dopamine (Rice and Patel 2015; Borroto-Escuela et al. 2015; Agnati et al. 1995). Additionally, it is now understood that the VTA is composed of a heterogenous population of GABAergic, glutamatergic and dopaminergic neurons (Adeniyi, Shrestha, and Ogundele 2020; Han et al. 2020; Morales and Margolis 2017). Recent evidence seems to suggest that most inputs to the dorsal hippocampus from the VTA are glutamatergic rather than dopaminergic (Adeniyi, Shrestha, and Ogundele 2020; Adeyelu and Ogundele 2023; Han et al. 2020) which may explain the contrast between recent findings of VTA DA inputs and

original tracing studies showing strong VTA innervation of the dorsal hippocampus (Gasbarri et al. 1994). These glutamatergic inputs innervate all layers of CA1 and the hilus of DG (Han et al. 2020), impact pyramidal neuron excitability (Adeniyi, Shrestha, and Ogundele 2020; Adeyelu and Ogundele 2023), and influence contextual fear conditioning and opioid induced place preference (Han et al. 2020). While a picture of VTA projections to the dorsal hippocampus is being developed, further experiments need to be conducted to characterize the subregion specific anatomy of these inputs.

Although VTA DA projections to the dorsal hippocampus are sparse, they have been demonstrated to impact hippocampal function and hippocampal dependent learning and memory (McNamara et al. 2014; Rosen, Cheung, and Siegelbaum 2015; Mamad et al. 2017). In vivo optogenetic stimulation of VTA DA inputs to dCA1 during learning increases the persistence of reward-location associations, increases the stability of CA1 place cells across days, and increases the rate of sharp wave ripples (SWRs) (McNamara et al. 2014). A recent study demonstrated that optogenetic suppression of VTA DA neurons evokes place avoidance, and biases place cell activity away from the location of suppression, while optogenetic stimulation of these inputs can influence place cell activity and shift place fields towards the stimulated location (Mamad et al. 2017). Together these findings indicate that VTA inputs to dCA1 can influence learning of reward locations and may influence the overrepresentation of reward locations by place cells (Gauthier and Tank 2018).

In-vitro Low levels of optogenetic stimulation of VTA DA inputs to dCA1 depressed Schaffer collateral activity through D4 receptor dependent inhibition by parvalbumin-expressing interneurons. However, high levels of optogenetic stimulation, increase Schaffer collateral activity through a D1 receptor dependent mechanisms (Rosen, Cheung, and Siegelbaum 2015). These findings suggest that VTA DA neurons can bidirectionally modulate the flow of information in the hippocampus by serving as a gate between CA3 and CA1. Additionally, optogenetic stimulation of VTA DA inputs modulates the connectivity between pyramidal

neurons and interneurons (Adeyelu and Ogundele 2023; Adeniyi, Shrestha, and Ogundele 2020). It is possible that VTA DA inputs to dCA1 may act through interneurons allowing them to have an outsized effect on hippocampal function . While there is considerable diversity among interneurons (Booker and Vida 2018), they are largely characterized by dense local connections that provide strong local inhibition. By modulating a small number of interneurons, VTA DA inputs could therefore extend an impact onto a wide range of hippocampal neurons.

1.5 Locus coeruleus inputs to the hippocampus

The effects of VTA DA release in the dorsal hippocampus have been additionally confounded by the findings that locus coeruleus (LC) inputs also release DA in the dorsal hippocampus (Kempadoo et al. 2016; Takeuchi et al. 2016). LC neurons are typically thought of as being noradrenergic. However, DA is in the synthesis pathway of NE, and in norepinergic neurons, DA is first loaded into vesicles where it is then converted into norepinephrine by dopamine β-hydroxylase. There is now considerable evidence that this dopamine can be released prior to being converted and impacts hippocampal dependent learning and memory (Wagatsuma et al. 2018; Kempadoo et al. 2016; Takeuchi et al. 2016). It has also been shown that most of the clearance of dopamine in the dorsal hippocampus occurs through norepinephrine transporters (NET) (Borgkvist et al. 2012). This suggests that NET positive axons from the LC are present in sites where dopamine is released and may be the source of dopamine themselves.

The LC sends widespread projections throughout the brain and has a wide range of behavioral effects. Studies have demonstrated a strong relationship between LC activity and arousal levels (Aston-Jones and Bloom 1981; McCarley and Hobson 1975), and wakefulness (Isaac and Berridge 2003), with LC activity being strongly correlated with many arousal measures including pupil diameter (Reimer et al. 2016). LC neurons are also thought to play

a role in attention, as LC activity can effect receptive fields of visual cortex neurons (Shulman, Remington, and McLean 1979), modulate odour discrimination in the olfactory bulb (Bouret and Sara 2002), frequency tuning in the auditory cortex (Martins and Froemke 2015), and improve performance in visual tasks (Waterhouse and Navarra 2019). Furthermore, LC neurons have been shown to play an important role in modulating plasticity and learning and memory (Eschenko 2018; Yamasaki and Takeuchi 2017). In support of the wide range of effects of LC activity, recent findings have demonstrated that the LC is not a homogenous region as once believed (Noei et al. 2022). Instead, it is now believed that the LC is modular, with neurons in different regions of the LC projecting to separate and distinct brain regions (Chandler, Gao, and Waterhouse 2014; Kebschull et al. 2016; Uematsu et al. 2017). These modular regions in the LC likely receive different inputs, allowing them to have different activity and therefore lead to the different effects of LC inputs to different brain regions (Noei et al. 2022). These findings highlight a need for projection specific characterization of LC neuron activity during behavior.

LC neurons appear to innervate the dorsal hippocampus more densely than VTA DA neurons, with LC axons found in all layers of CA1, CA3, and DG (Kempadoo et al. 2016; Takeuchi et al. 2016; Wagatsuma et al. 2018) with the densest projections being found in the DG and stratum lucidum of CA3 (Loy et al. 1980). These inputs were thought to act through release of norepinephrine which binds to alpha-adrenergic receptors to regulate neuronal excitability (Segal, Markram, and Richter-Levin 1991) and beta-adrenergic receptors to regulate synaptic plasticity. B-adrenergic receptors have been reported to modulate perforant path (Edison and Harley 2012), mossy fiber (Hagena and Denise Manahan-Vaughan 2012), and schaffer collaterals synapses (Goh and Denise Manahan-Vaughan 2013). Norepinephrine activity in the hippocampus is involved in the formation of spatial and contextual fear memories (J. Ji, X. Zhang, and B. Li 2003; J.-Z. Ji, X.-H. Zhang, and B.-M. Li 2003), short and long term memory consolidation (Gibbs and Summers 2002), memory retrieval

(Thomas 2015), and extinction learning (André, Wolf, and Denise Manahan-Vaughan 2015). Because LC neurons are activated by arousal and novelty and norepinephrine activity modulates hippocampal LTP and hippocampal dependent learning and memory, it has been proposed that these inputs can provide a signal for when novel or salient events should be encoded (Hagena, Niels Hansen, and Denise Manahan-Vaughan 2016). In support of this idea, it has been demonstrated that optogenetic activation of LC inputs to the dorsal hippocampus promotes spatial learning (Kempadoo et al. 2016), drive novelty induced memory enhancement (Takeuchi et al. 2016), potentiates schaffer collateral synapses (Takeuchi et al. 2016), and drives overrepresentation of newly rewarded locations (Kaufman, Geiller, and Losonczy 2020). Additionally, inhibition of these inputs impairs learning of novel contexts (Wagatsuma et al. 2018), impairs memory linking (Chowdhury et al. 2022), and reduces the stability of place fields across days (Wagatsuma et al. 2018). All these findings were found to be dependent on D1Rs while beta-adrenergic receptors played no role supporting the idea that LC inputs can influence dorsal hippocampus function through the release of dopamine.

It is clear dopamine has profound effects on hippocampal activity and therefore hippocampal dependent learning and memory. However, both potential sources of dopamine can impact hippocampal function, shape place cell activity, and effect learning and memory. To disentangle the role of these two inputs in spatial learning and memory, it is important to characterize the activity of these inputs during behavior. Because of the heterogeneity of both VTA DA and LC neurons, this characterization must be specific to the projections to the hippocampus. So far, no study has investigated the projection specific activity of VTA DA inputs and only one has investigate activity of LC inputs (Kaufman, Geiller, and Losonczy 2020). Kaufman et al. demonstrated that as an animal is navigating for reward LC axons in dCA1 have activity correlated with velocity supporting previous findings of LC activity during movement (Reimer et al. 2016). Additionally, these neurons fire at novel reward locations and this activity can influence place cell locations, suggesting they play a

role in the establishment of overrepresentation of reward locations. However, on its own, LC input stimulation did not influence place fields indicating there may be other mechanisms driving this process (Kaufman, Geiller, and Losonczy 2020). While the findings of Kaufman et al start our understanding of how LC inputs are active during spatial navigation, they only looked at activity during spatial navigation in a familiar environment for rewards and did not address how VTA inputs may be active during the same tasks. Investigating how these inputs are active during spatial learning of novel contexts would provide insight into how these inputs influence novelty encoding in the hippocampus.

In chapter 1, I describe the first recordings of VTA DA inputs to the hippocampus and observed ramping to reward activity that is dependent on the animals' reward expectation. I establish, in work with Seetha Krishnan, the effects of reward expectation on hippocampal place cell activity and demonstrate these effects are largely mediated through the activity of VTA DA neurons. Our results indicate that reward expectation restructures CA1place cells and determines map reliability through the modulation of VTA-DA input reward-proximity signals. In the second chapter, I compare the activity of VTA DA inputs to the activity of LC inputs to dCA1. This work reveals distinct encoding across the two inputs, with VTA DA neurons exhibiting ramping to reward activity and LC inputs showing activity correlated with velocity and an increase in activity prior to motion onset. Additionally, LC inputs drastically increase in activity for $>$ 1 minute following exposure to a novel environment while the ramping activity VTA DA disappears in the novel environment. This work demonstrates VTA and LC inputs encode unique information, likely contributing to distinct roles in modulation of hippocampal activity and episodic memory.

CHAPTER 2

REWARD EXPECTATION EXTINCTION RESTRUCTURES AND DEGRADES CA1 SPATIAL MAPS THROUGH LOSS OF A DOPAMINERGIC REWARD PROXIMITY SIGNAL

This chapter is a full reprint of **"Reward expectation extinction restructures and degrades CA1 spatial maps through loss of a dopaminergic reward proximity signal"** In: *Nature Communications* 13.1, p. 6662. issn: 2041-1723. doi: 10.1038/s41467-022-34465-5.(Krishnan et al. 2022), in which I was a co-first author. The work is included with permission from all authors.

2.1 Abstract

Hippocampal place cells support reward-related spatial memories by forming a cognitive map that over-represents reward locations. The strength of these memories is modulated by the extent of reward expectation during encoding. However, the circuit mechanisms underlying this modulation are unclear. Here we find that when reward expectation is extinguished in mice, they remain engaged with their environment, yet place cell over-representation of rewards vanishes, place field remapping throughout the environment increases, and place field trial-to-trial reliability decreases. Interestingly, Ventral Tegmental Area (VTA) dopaminergic axons in CA1 exhibit a ramping reward-proximity signal that depends on reward expectation and inhibiting VTA dopaminergic neurons largely replicates the effects of extinguishing reward expectation. We conclude that changing reward expectation restructures CA1 cognitive maps and determines map reliability by modulating the dopaminergic VTA-CA1 reward-proximity signal. Thus, internal states of high reward expectation enhance encoding of spatial memories by reinforcing hippocampal cognitive maps associated with reward.

2.2 Introduction

Individual pyramidal cells in the hippocampus fire action potentials in specific regions of an environment, known as their place field1. Specific populations of place cells represent cognitive maps of specific environments (Colgin, E. I. Moser, and M.-B. Moser 2008; Bostock, Muller, and Kubie 1991). As animals become familiar with an environment, hippocampal place fields become more stable and many of them are reinstated whenever the animal navigates the environment (Ziv et al. 2013; Dong, Madar, and M. E. J. Sheffield 2021; Hainmueller and Bartos 2018). When environmental cues change, hippocampal place cells "remap" through changes in firing rate and place field locations, thought to be an integral part of navigational and memory processes (Colgin, E. I. Moser, and M.-B. Moser 2008; Bostock, Muller, and Kubie 1991; Dong, Madar, and M. E. J. Sheffield 2021; RU Muller and JL Kubie 1987). Place cells and the maps they comprise allow animals to acquire, store, code, and recall environments (Goode et al. 2020; Robinson et al. 2020). In addition, place cells are modulated by external context variables that include odors and colors (Michael I. Anderson and Kathryn J. Jeffery 2003) but also include internal context variables such as attention (Kentros et al. 2004; André A. Fenton et al. 2010), decisions of future trajectories (Wood et al. 2000; Zhao, Hsu, and Spruston 2022; Kinsky et al. 2020) and fear (Marta A. P. Moita et al. 2004; Peter J. Schuette et al. 2020). Reward expectation (or reward prediction) is another internal context variable that could modulate cognitive maps as it has a powerful influence on hippocampal-dependent memories (Rouhani and Niv 2021; Jang et al. 2019; Stanek et al. 2019). However, the influence of reward expectation on cognitive maps remains unclear and some evidence suggests cognitive maps may be independent from reward expectation (Éléonore Duvelle et al. 2019; Tabuchi, Mulder, and Wiener 2003; Wikenheiser and Redish 2011).

Rewards themselves are represented through a distinct population of reward cells (Gauthier and Tank 2018) and an over-representation of place cells tuned to rewarded locations in

CA1 (Hollup et al. 2001; I. Lee et al. 2006; Kaufman, Geiller, and Losonczy 2020; B. Poucet and Hok 2017; Mamad et al. 2017). The over-representation of reward locations by place cells requires learning (Kaufman, Geiller, and Losonczy 2020) and is dependent on the probability a reward will be delivered at those locations (B. Poucet and Hok 2017). This suggests that it is reward expectation that determines over-representation of reward locations rather than the attainment of the reward itself, although this remains to be determined. Furthermore, cues distant from reward locations can predict the attainment of future reward, i.e., lead to them (Howe et al. 2013). Therefore, over-representation of reward locations by place cells does not explain how reward expectation might influence the encoding of locations that are distant from, but lead to, rewards. What is also unclear is how changes in reward expectation within an environment might influence the place cell code in the hippocampus, or the time course over which such changes may occur.

The learned associations between isolated cues and future rewards involves dopaminergic circuits that respond to reward predicting cues and act as a learning signal (Sutton and Barto 1981). Dopaminergic circuits that encode reward expectation project to the hippocampus from the ventral tegmental area (VTA) (Gasbarri et al. 1994) and influence hippocampal function, synaptic plasticity, and synaptic transmission (Mamad et al. 2017; Martig and Mizumori 2011; McNamara et al. 2014). Recent work has begun to elucidate the role of reward expectation and dopamine circuits during spatial navigation and has uncovered a spatial proximity to reward signal emanating from the VTA that ramps up in activity as animals approach an expected reward location (Howe et al. 2013; Engelhard et al. 2019; Sosa and Giocomo 2021; Guru et al. 2020; Kim et al. 2020). Like the classic studies of reward learning, spatial locations during navigation that predict future reward trigger increases in dopamine release. As the animal approaches the reward, dopamine levels ramp up as locations closer to reward are better predictors of the reward, i.e., they increase reward expectation. This suggests that reward expectation may influence the encoding of space during

navigation through the effects of dopamine modulation, possibly through ramping dopamine signals (Sosa and Giocomo 2021), but whether these signals exist in the hippocampus has yet to be demonstrated experimentally, as is their influence on cognitive maps.

Spatial memories encoded in the hippocampus are represented by populations of place cells that create a cognitive map, and reward expectation influences these memories through dopaminergic circuits (Rouhani and Niv 2021; Jang et al. 2019; Stanek et al. 2019; Wikenheiser and Redish 2011; Martig and Mizumori 2011; McNamara et al. 2014). We therefore hypothesized that changing reward expectation would modulate place cell properties and transform the structure of the cognitive map (remapping) driven by dopaminergic signals from the VTA. However, testing this hypothesis is challenging as manipulating rewards to change reward expectation alters navigation behaviors that affects place cells(B. L. McNaughton, Barnes, and J. O'Keefe 1983). We therefore developed a paradigm that changes reward expectation in head-restrained mice repeatedly traversing an unchanging virtual linear track. Importantly, mice in this setup showed matched navigation behaviors and engagement with their environment across many trials during changes in reward expectation, allowing us to isolate the influence of reward expectation on place cells. This head-restrained setup allowed for continuous 2-photon calcium imaging of large populations of place cells in CA1 as well as direct calcium imaging of dopaminergic axons from VTA in CA1 during changes in reward expectation. We also inhibited dopaminergic neurons in the VTA to further test our hypothesis.

2.3 Results

2.3.1 Lowering reward expectation changes spatial encoding of an unchanging spatial environment in CA1

Mice were trained to run on a treadmill along a 2 m virtual linear track for water rewards (rewarded condition: R) delivered at the track end (Fig.2.1 a, b), after which they were teleported back to the start of the track. Well-trained mice learned the location of the reward and pre-emptively licked before the reward location (pre-licking), providing a lap-wise behavioral signal of reward expectation (Supp Fig. 2.6). On experimental day (Fig. 2.1b), mice ran in R for 10 min before water reward was unexpectedly removed (unrewarded condition: UR). Interestingly, mice continued pre-licking for a few laps in UR, as though still expecting a reward (see "Licking behavior" section in "Methods"; Fig. 2.1c.iii and Supp Fig 2.6). After mice traversed UR for 10 min, reward was reintroduced (re-rewarded condition: RR).

Additionally, using 2-photon calcium imaging of dorsal CA1 pyramidal neurons expressing the genetically encoded calcium indicator GCaMP6f (T.-W. Chen et al. 2013) (Fig. 2.1a), we measured population activity while mice were switched across conditions: R-UR-RR (Fig. 2.1b, c). Behavior and activity in an example mouse are shown in Fig. 2.1c. We found that removing reward caused a dramatic change in population activity (Fig. 2.1c.i, population activity is represented as a raster plot where cells with correlated activity are arranged next to each other, see Methods). This was not a consequence of time or running behavior (Supp Figs. 2.7 and 2.8) and like changes in pre-licking, did not occur immediately after reward removal (Fig. 2.1c). To quantify this, we trained a naive Bayesian classifier with all the extracted cells on the initial laps in R and used the trained classifier to predict track position on the final laps of R and all laps in UR and RR (Methods). We found that the decoder was able to accurately predict position on the final laps in R and initial laps in

UR before abruptly underperforming (Fig. 2.1d).

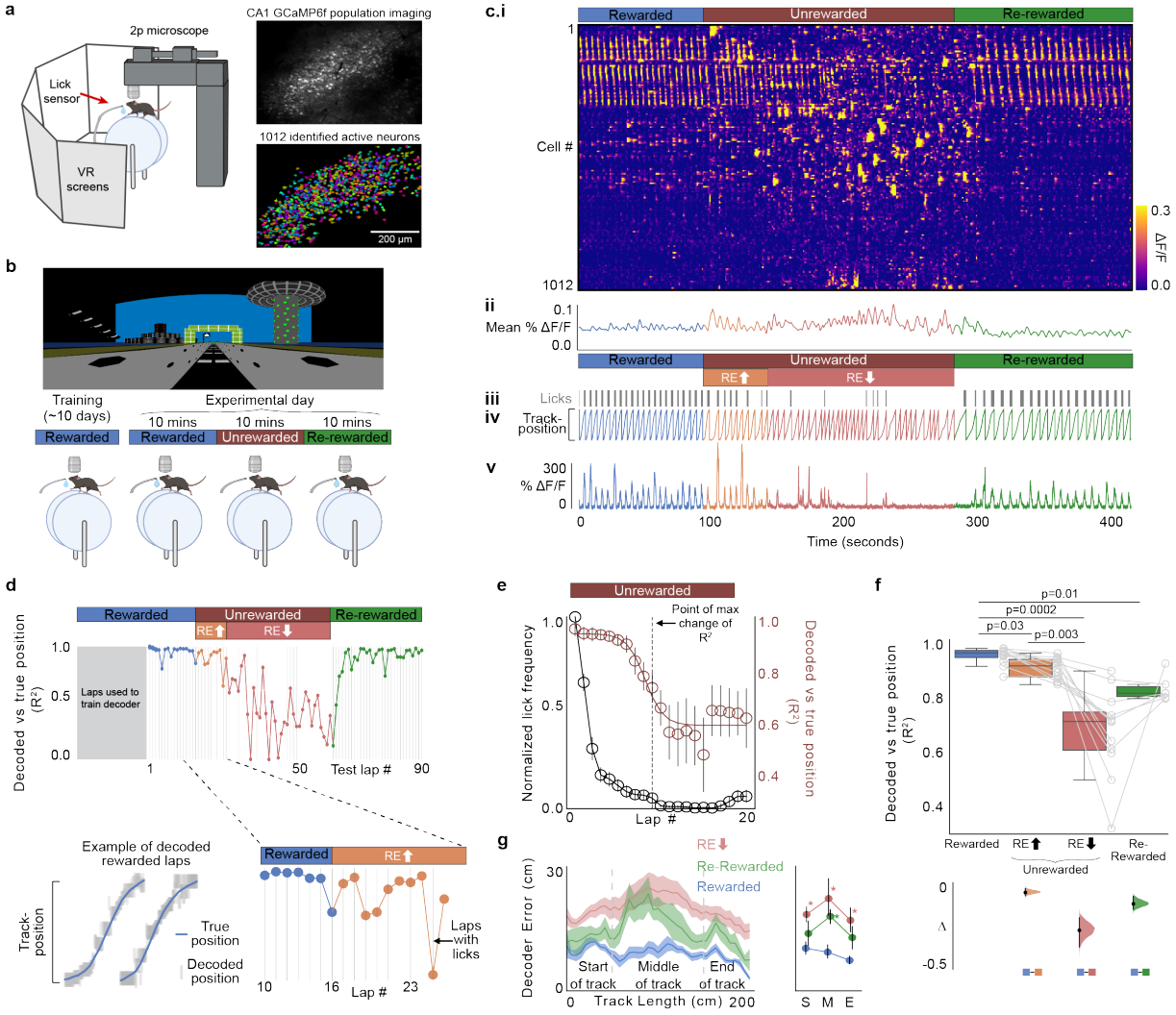

Figure 2.1: **Diminished reward expectation restructures spatial encoding in the hippocampus a,**Experimental setup (left), created with BioRender.com. A typical field of view in CA1 (right, top). Extracted regions of interest, randomly colored (right, bottom). **b,** Experimental protocol. Image of virtual track (top). Changing reward contingencies (bottom, Rewarded (R), Unrewarded (UR), Re-Rewarded (RR)), created with BioRender.com. **c,** i: Rasterplot representing fluorescence changes ($\Delta F/F$) of cells in A across time. Cells (y-axis) are arranged with the most correlated cells next to each other. ii: Mean $\Delta F/F$ of the cells in (i). iii: Mouse licking behavior. iv: Mouse track position. v: $\Delta F/F$ from an example cell. Laps before animal stops consistently licking in UR were considered laps with high reward expectation (REhigh, orange laps) and after licking stops are laps with low reward expectation (RElow, red laps, see Methods). **d,** A Bayesian decoder was trained on CA1 activity from initial laps in R and tested on remaining laps.

Figure 2.1, continued: (Top) Coefficient of determination (R^2) between true and predicted position of tested laps, (bottom right) zoomed in. (Bottom left) An example fit. Gray lines indicate laps with licks. **a**–**d** are from the same animal. **e** Mean decoder R^2 fitted with a reverse Boltzmann Sigmoid ($r = 0.94$; magenta), mean lick frequency normalized to maximum licks (black) for each lap in unrewarded condition. Error bars indicate s.e.m. The point of maximum change in R^2 as calculated from the fit is indicated by the dashed line. **f** (Top) Boxplots (see methods for definition) show distribution of mean decoder R^2 in the different conditions. Circles represent individual animals. P values were obtained using a two-sided Paired t test. (Bottom) Bootstrapped mean differences (Δ) with 95% Confidence Intervals (CI) (error bar). X-axis indicates the comparisons made. **g** (Left) Mean decoder error by track position. Shading indicates s.e.m. (Right) Mean decoder error binned by track position as indicated by gray bars in the left panel. Error bars indicate 95%CI. S: Start of the track, M: Middle of the track, E: End of the track. Asterisk (*) indicates significant p values ($P < 0.01$, two-sided paired t test) obtained by comparing R with other conditions at each position. $n = 12$ mice used for **f, g**.

Because mice pre-licked for a few laps in UR, we asked if decoder underperformance was associated with reduced reward expectation. In all mice (n = 12), we quantified the average pre-licking and decoder fit on each lap after reward removal by running a rolling average (Fig. 2.1e, see Methods). On average, pre-licking continued for a few laps before rapidly dropping, and interestingly, decoder performance sharply dropped around the same lap when pre-licking reached zero. This decreased decoder accuracy with decreased pre-licking indicates that hippocampal spatial encoding remains unchanged following reward removal, until reward expectation diminishes, at which point the spatial code abruptly transforms.

To further quantify this, we identified the lap on which pre-licking stopped in each mouse (Methods). For clarity, we labeled the laps with pre-licking as having high reward expectation (REhigh) and the laps after pre-licking stopped as having low reward expectation (RElow). Indeed, decoder accuracy in REhigh laps was similar to R and was significantly lower in RElow laps (Fig. 2.1, mean decoder R^2 [95% confidence intervals (CIs)]: R = 0.95 [0.93 0.97], REhigh = 0.90 [0.87 0.93], RElow = 0.65 [0.54 0.75]). This held true independent of our definition of when licking stopped (Supp Fig. 2.9). The decoder accuracy somewhat recovered following reward re-introduction in RR laps, although it remained lower than in R (RR = 0.82 [0.77 0.87]). Reduced decoder performance during RElow was not explained

by differences in time or running velocity (Supp Figs. 2.7 and 2.10).

To quantify these changes further, we analyzed decoder error across the track by measuring the absolute distance between the true position from the position predicted by the decoder at each point on the track. Interestingly, in RElow, decoder error had increased at all locations across the track (Fig. 2.1g), and not just around the reward site, as may have been predicted (Hollup et al. 2001; I. Lee et al. 2006; Kaufman, Geiller, and Losonczy 2020; B. Poucet and Hok 2017; Mamad et al. 2017). As observed before, in RR, decoder error decreased across the track but remained lower than in R (Fig. 2.1g). These data provide evidence against spatial encoding being independent from reward expectation21 and demonstrate that changing reward expectation drastically alters spatial encoding at all locations within an unchanging spatial environment.

2.3.2 Changes in spatial encoding associated with diminished reward expectation are not due to disengagement with the environment

Next, we tested an alternate explanation; that disengagement with the environment in RElow laps was responsible for the changes in spatial encoding (Kentros et al. 2004; André A. Fenton et al. 2010; Pettit, Yuan, and Harvey 2022). We noticed that mice in R slowed down as they approached the reward site, exhibiting engagement with the VR environment (Gauthier and Tank 2018) (Supp Figs. 2.11 and 2.12). To confirm this, we exposed mice to a dark environment without any virtual cues and indeed found an absence of this approach behavior (n = 6, Supp Fig. 2.11a). We therefore interpret approach behavior on each lap as a behavioral readout of engagement with the environment. In UR we observed changes in velocity throughout the track, but approach behavior remained intact on most laps in UR (n = 12, 170/244 laps, 70%). This was true even after mice stopped licking (RElow: Engaged; Supplementary Figs. 6 and 7). In contrast, laps displaying disengagement with VR were less frequent (RElow: Disengaged, 74/244, 30%, Supp Figs. 2.11 and 2.12). Importantly, we

found a similar reduction in decoder performance in UR when using only RElow engaged laps (Supp Fig. 2.11b, Mean decoder R^2 [95% CI]: R = 0.95 [0.93 0.97], REhigh = 0.90 [0.87 0.93], RElow: Engaged = 0.65 [0.49 0.81]), although disengaged laps did further reduce decoder performance (RElow: Disengaged = 0.31 [0.06 0.5]). The disengaged laps were uniformly distributed throughout RElow (see example laps in Supp Fig. 2.12). The proportion of disengaged laps also did not progressively increase with time, as was observed in Pettit et al. (Pettit, Yuan, and Harvey 2022). The probability of disengaged laps in the first half of RElow was similar to the second half (P = 0.14). Furthermore, the distribution of disengaged laps throughout the session did not differ from a uniform distribution (P = 0.7). The influence of disengagement on CA1 spatial representations is in agreement with a recent paper (Pettit, Yuan, and Harvey 2022), but is not the main focus of this paper.

Using an alternate method to measure engagement with the VR environment, we quantified pupil area during running in R and UR conditions as pupil diameter has been shown to be a measure of attentional/arousal state (n = 5, Supp Fig. 2.11c-f) (Beatty 1982; Bradley et al. 2008). We observed a distinct pattern of pupil area changes during laps in R which included an increase in pupil area near the end of the track. To quantify if within lap pupil area dynamics were altered in UR compared to R, we calculated the Pearson's correlation coefficient of each lap's pupil area dynamics to the mean pupil area dynamics from all laps in R. We first ensured that any changes in pupil area correlation in UR were not due to changes in animal behavior in UR (Supp Fig. 2.13). Engaged laps in UR in each animal were then defined as laps where the correlation coefficient was greater than or equal to the mean correlation coefficient of laps in R (the remaining laps were defined as disengaged laps). 71% of these engaged laps were also classified as engaged laps using the approach behavior described above (57/80 laps; chance levels = 37%). We again found that animals were engaged on most laps in UR (n = 5, 80/106, 75%) after licking stopped (RElow: Engaged, Supp Fig. 2.11e) and found a similar reduction in decoder performance when using

only these laps (Supplementary Fig. 2.11f, mean decoder R^2 [95% CI]: R = 0.91 [0.81 1.00], REhigh = 0.83 [0.71 0.94], RElow: Engaged = 0.57 [0.34 0.79], RElow: Disengaged = 0.43 [0.13 0.74]). Therefore, using two distinct measures of engagement with the VR environment, approach behavior and pupil area, we conclude that changes in spatial encoding in UR are not due to disengagement with the VR environment but instead are due to lowered reward expectation. However, because disengagement further influences spatial encoding, we focused further analysis on engaged laps (laps with approach behavior) during RElow to isolate the effects of RElow without confounds introduced by disengagement with the VR environment (Pettit, Yuan, and Harvey 2022).

2.3.3 Lowering reward expectation induces place cell remapping

The changes in spatial encoding in UR suggests changes in activity patterns of place cells (remapping). Place cell (PC) remapping is linked to encoding changes within environments or distinct environments as well as separated exposures to the same environment across days (Colgin, E. I. Moser, and M.-B. Moser 2008; Ziv et al. 2013; Dong, Madar, and M. E. J. Sheffield 2021; RU Muller and JL Kubie 1987; Mark E.J. Sheffield, Adoff, and Daniel A. Dombeck 2017). We explored if changes in reward expectation may induce remapping in an unchanging spatial environment within a single session. We first defined PCs in R and constructed a population firing vector using these cells for each lap in R-UR-RR and correlated these vectors across the session using only those laps in UR that showed engagement with the VR (only RElow: Engaged laps, Fig. 2.2a). Correlations showed pronounced transitions in population activity around the lap when licking stops (REhigh to RElow) and again following reward re-introduction (RElow to RR). To adequately quantify these transitions, we clustered the lap-by-lap PV correlations and calculated the probability of laps being part of the cluster to which R laps belong (see Methods). The lap-wise cluster probability traces revealed dips in probability when transitioning from REhigh to RElow and not between R

and REhigh (Fig. 2.2a bottom; mouse 3 correlation drops a lap before our definition of low reward expectation) confirming changes in place cell activity occurring as animals stop licking and not immediately following reward removal. Moreover, the probability increased to a certain extent in RR laps. This is most apparent in mouse 1 which comes all the way back to R levels. However, mice 2 and 3 did not show a similar reinstatement nor was there an immediate transition in cluster probability following reward reintroduction.

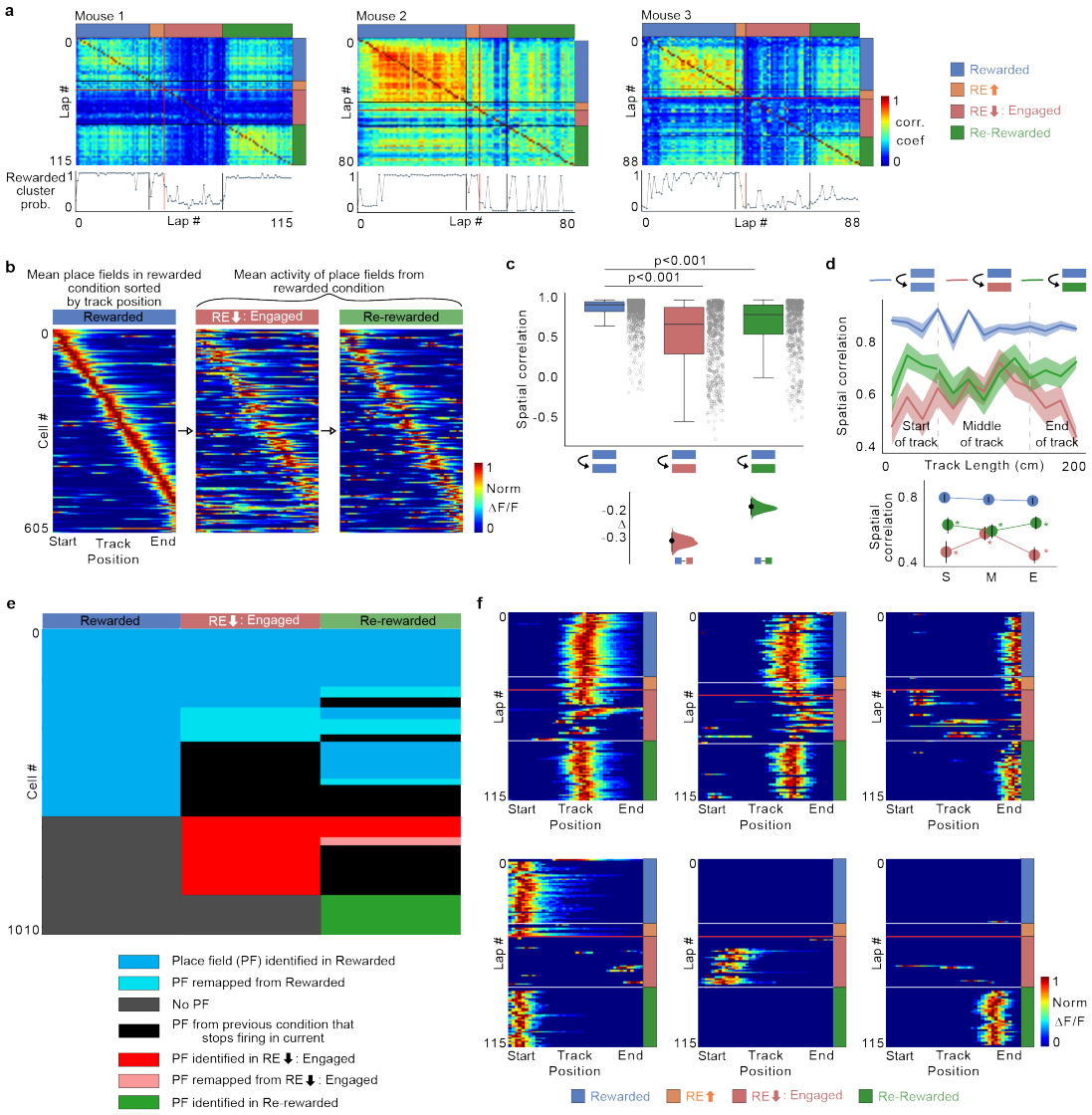

Figure 2.2: **Diminished reward expectation leads to place cell remapping across all track locations and loss of reward overrepresentation**

Figure 2.2, continued: a,(Top) Population vector correlations between place cell activity in each lap in all conditions in 3 animals. In laps with low reward expectation, only Engaged laps were used (RElow: Engaged). (Bottom) Probability of laps belonging to the Rewarded cluster following 1000 iterations of k-means clustering (see Methods). Red line indicates the lap where pre-licking stops, and black lines divide each condition. **b,** Place fields defined in R plotted across all conditions. Activity of each place cell was normalized to peak in R and sorted by its center of mass along the track. **c,** Boxplots show distribution of place field spatial correlation for cells (circles) within R condition (blue) and between R and other conditions. P values were obtained using two-sided paired t test. (Bottom) Bootstrapped mean differences (Δ) with 95% CI (error bar). X-axis indicates the comparisons made. **d,** (Top) Same data, averaged by track position. Shading indicates s.e.m. (Bottom) Average correlation binned by track position indicated by gray lines in the top panel. S: Start of the track, M: Middle of the track, E: End of the track. Asterisk (*) indicates significant P values (two-sided paired t test, $p < 0.01$) obtained by comparing R (blue) with other tasks at each position. Both **d**, **e** use n = 605 place cells defined in R. **e,** Fate of place cells identified in different conditions. Place fields identified in R (blue) can be stable throughout RElow (blue) and RR (blue). They can also remap in RElow and RR (light blue) or lose their place field completely (black). New place fields can form in RElow (red) and be stable (red) or remap (light red), in RR. New place fields can also form in RR (green). **f,** Example place cell activity in the different conditions. White lines divide each condition and the red line indicates lap defined as when pre-licking stops.

We next analyzed the RElow period in UR in these 3 mice as they had sufficient numbers of engaged laps in all conditions (R-UR-RR) to define place fields using only the engaged laps and removing disengaged laps (see Supp Fig. 2.14 for analysis on all mice using both engaged and disengaged laps). We found RElow caused partial remapping as shown by a drop in the spatial correlation of place fields between R and UR conditions (using only RElow: Engaged laps; Fig. 2.2b–d). Interestingly, partial remapping caused by RElow occurred at all locations throughout the environment, and not just at locations near the reward site (Fig. 2.2d). As observed with the population firing vector correlations, the extent of remapping was reduced in RR—i.e., the R map seemed to somewhat return in RR (Fig. 2.2b–d).

To further analyze place field dynamics, we determined the fate of individual place fields throughout R-UR (RElow: Engaged laps only)-RR. We found 27.9% of place fields found in R (605 PFs in R, n = 3) remained stable throughout R-RElow-RR (169/605; Fig. 2.2e blue throughout). In RElow, R place fields either remained stable (222/605, 36.7%; Fig.

2.2e blue, middle column), disappeared (249/605, 41.2%; Fig. 2.2e black, middle column), or remapped (134/605, 22.1%; Fig. 2.2e cyan, middle column). In addition, new place fields formed in RElow (296/663 of all place fields found in RElow, 44.6%; Fig. 2.2e red, middle column). More R-place fields retained their fields in RR (311/605, 51.4%; Fig. 2.2e blue, right column), but other R-place fields remapped in RR (89/605, 14.7%; Fig. 2.2e cyan, right column). Furthermore, of the place fields that disappeared in RElow some reappeared in RR (126/249; 50.6%; Fig. 2.2e blue adjacent to black, right column). Only a small proportion of those that were newly formed in RElow remained stable in RR (64/296 new PFs in RElow; 21.6%; Fig. 2.2e red, right column) and a larger percentage disappeared in RR (204/296; 68.9%; Fig. 2.2e black adjacent to red, right column). Finally, of the 674 place fields found in RR, 140 were newly formed (20.8%; Fig. 2.2e green, right column). These place field dynamics were also observed when place fields from all mice were analyzed that included engaged and disengaged laps (Supp Fig. 2.14) and were not observed in control mice that stayed in R for a matched number of laps (Supp Fig. 2.15). Example of the lap-by-lap dynamics of individual place cells throughout R-UR-RR are shown in Fig. 2.2. In summary, transitioning to RElow restructures the CA1 place code at all locations within an unchanging spatial environment through the disappearance, emergence, and remapping of place fields. Although a component of the structure returns when transitioning back to RR, the original structure remains changed, and further restructuring takes place. This suggests that the CA1 spatial code of an environment is dependent on reward expectation and the history of reward expectation. This supports the idea that CA1 performs context discrimination in an unchanging spatial environment.

2.3.4 Place fields show diminished reliability and increased out-of-field firing following lowered reward expectation

The quality of hippocampal spatial encoding is related to memory performance (Kentros et al. 2004; Rotenberg et al. 1996). Qualitatively, increased reliability of firing across multiple traversals through the same location, low out-of-field firing, and decreased place field width are general indicators of better spatial encoding accuracy. Measuring these properties, we asked whether place fields in RElow were of the same or reduced quality compared to place fields in R. Plotting place fields defined in each condition, we found a total number of place fields that tiled the track to be similar in R, RElow (using only Engaged laps), and RR (n = 3, Fig. 2.3a, findings from all animals using both engaged and disengaged laps are shown in Supp Fig. 2.16). We quantified place cell properties and found that the place fields in RElow had degraded on every measure of spatial encoding we used (see Methods): place field trial-to-trial reliability (Wikenheiser and Redish 2011) (Rewarded = 0.47 [0.38 0.57], RElow: Engaged = 0.32 [0.15 0.48]), out/in place field firing ratio (Rewarded = 0.10 [0.07 0.13]; RElow: Engaged = 0.16 [0.12 0.20]) and place field width (Rewarded = 53.34 [43.87 62.81]; RElow: Engaged = 60.56 [48.07 73.06]), across all locations (Fig. 2.3b). There was also a small decrease observed in firing intensity (Rewarded = 0.36 [0.31 0.40]; RElow: Engaged = 0.31 [0.23 0.40]). These place field properties returned to or approached R levels in RR, except firing intensity which remained low in RR (Fig. 2.3b, Reliability 0.41 [0.31 0.51]; Out/In Field Firing 0.12 [0.08 0.15]; Place field width (cm) 54.08 [46.86 61.31]; Firing Intensity 0.29 [0.24 0.34]). The degradation of place fields in RElow and return in RR was also observed when we included engaged and disengaged laps together (Supp Fig. 2.16) and was not due to time (Supp Fig. 2.17). This demonstrates that diminished reward expectation leads to a spatial code in CA1 with low quality place fields at all locations, suggesting a weakened spatial memory representation of the environment (Kentros et al. 2004; Rotenberg et al. 1996).

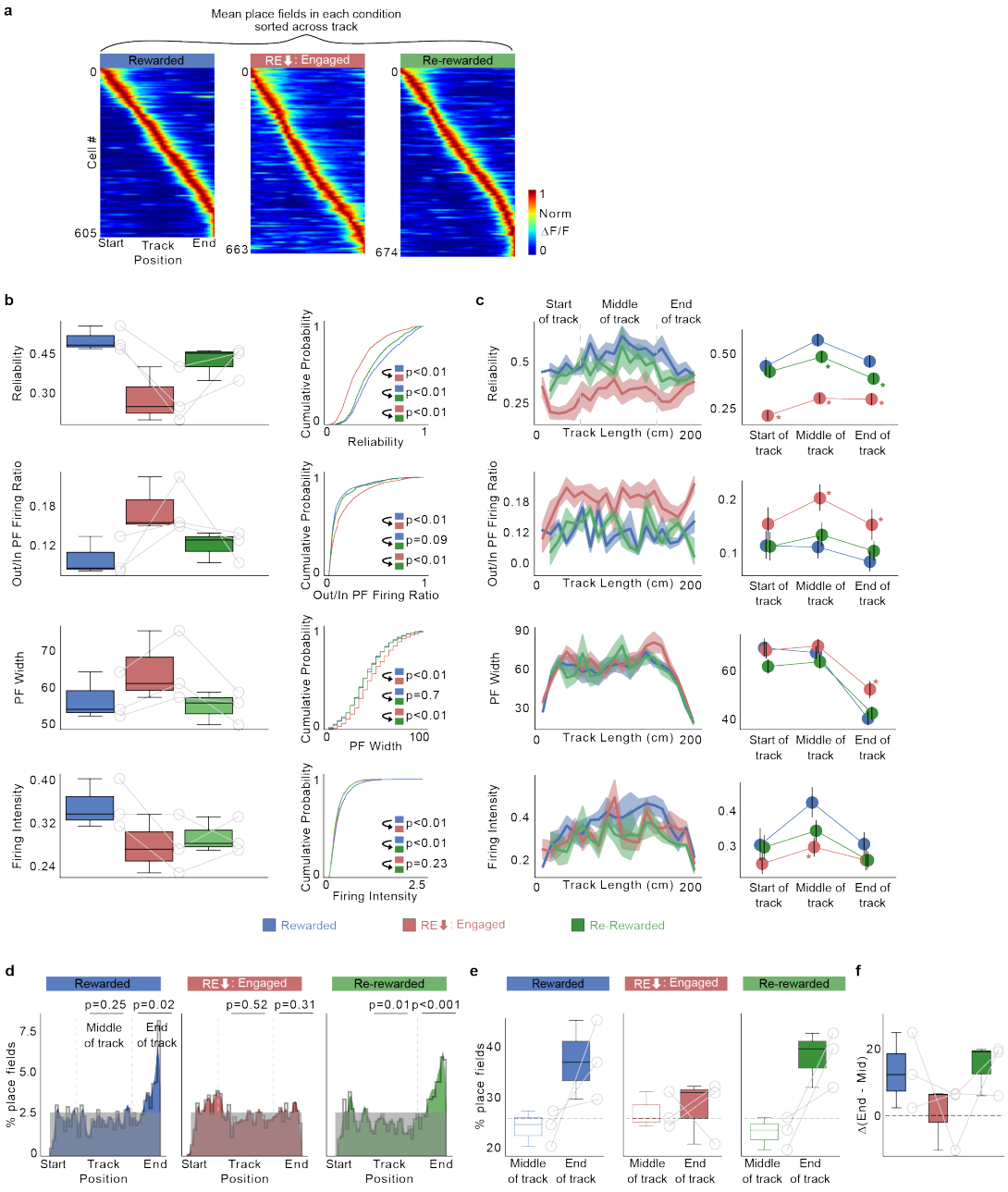

Figure 2.3: **Diminished reward expectation leads to inferior spatial encoding by unreliable place cells across the entire environment. a,**Place fields defined and sorted in each condition pooled from all mice (n = 3 mice). Each cell's activity normalized to its peak and cells are sorted by their center of mass along the track. **b,** Place cell parameters calculated independently from each condition are displayed as a boxplot of average per animal (left), cumulative histogram (right). P-values were calculated using a two-sided t test.

Figure2.3, continued: c, (left) Mean place cell parameters across track location. Shading indicates s.e.m. (right) Average correlation binned by track position indicated by gray lines in the left panel. S: Start of the track, M: Middle of the track, E: End of the track. Asterisk (*) indicates significant P-values (two tailed KS-test, $p < 0.01$) obtained by comparing R (blue) with other tasks at each position. **d,** Distribution of place field center of mass (COM) locations in each condition pooled from all mice (n = 3 mice). Plots show observed density (gray line), uniform distribution (gray shade) and Gaussian distribution of place field density (color). P-values (two-sided t test) were obtained by calculating the place field distribution with the uniform distribution. **e,** Percentage of place fields in the middle of the track versus end of the track in each animal (circles). **f,** Difference between end of track and middle of track place field percentages in each animal (circles, n = 3 mice). Dashed line in **e**, **f** indicates the percentage expected from a uniform distribution across the track. All place field calculations in RElow condition were done on Engaged laps (RElow: Engaged). Number of cells in b–d; R: 605, RElow Engaged: 663, RR: 674.

Finally, we compared the degradation of place cells following reward expectation extinction to a novel never-reinforced environment (Supp Fig. 2.18). We found that the spatial decoding and place cell parameters were poor in the initial laps of the novel environment, however, with time, as the animal learned the environment and developed reward expectation (Supp Fig. 2.18b), these properties became better and comparable to properties in R and RR (Supp Fig. 2.18c-e). Both reliability and out/in field firing ratio in RElow matched the levels of the initial trials in the novel environment and remained so throughout the session until reward expectation was reinstated in RR (Supp Fig. 2.18c-e). This further demonstrates that reward expectation enhances the spatial code in CA1.

2.3.5 Lowering reward expectation eradicates the over-representation of reward location and disrupts reward cell firing

One of the striking features of CA1 place cells is the accumulation of place fields near learned rewarded locations (Hollup et al. 2001; I. Lee et al. 2006; Kaufman, Geiller, and Losonczy 2020; B. Poucet and Hok 2017; Mamad et al. 2017). We similarly found an over-representation of place fields near the reward site in R (Fig. 2.3d–f left, I; Supp Fig. 2.16c-e). Interestingly, this over-representation disappeared once reward expectation diminished

(Fig. 2.3d, e middle, f; Supp Fig. 2.16c-e). Of the place cells in R that disappeared in RElow, 41.8% (104/249, n = 3) were at the end of the track (150–200 cm). Furthermore, the new place cells that appeared in RElow, were equally distributed on the track length (0–50 cm: 77/296 (26%), 50–100 cm: 83/296 (28%), 100–150 cm: 62/296 (21%), 150–200 cm: 74/296 (25%)). When reward was reinstated in RR, the over-representation of the reward site reappeared (Fig. 2.3d, e right, f; Supp Fig. 2.16c-e). However, not all the place fields that disappeared around the reward zone in RElow reappeared in RR (61/104, 58.6% reappeared), instead, the increased density around the reward site was also derived from the new place cells that formed fields in RR (0–50 cm: 31/140 (22%), 50–100 cm: 24/140 (17%), 100–150 cm: 18/140 (13%), 150–200 cm: 67/140 (48%)). Thus, place fields near reward sites act like typical place fields, i.e., they are largely context-specific. Such changes were not observed in control mice (Supp Fig. 2.17). This demonstrates that transitioning from REhigh to RElow abolishes place field over-representation of the previously rewarded site. Reinstatement of reward expectation (as in RR) restores over-representation of the reward site with an overlapping yet distinct ensemble of place cells.

It was recently shown that a small fraction of cells distinct from place cells exist in the CA1 that encode reward regardless of position or environment (Gauthier and Tank 2018). We looked for these "reward cells" and defined them based on their reward activity in 2 distinct VR environments (Supp Fig. 2.19). We found that these reward cells did not account for the over-representation of the reward site by place cells in R (Supp Fig. 2.19b). We also found that the correlation of reward cell activity between R and RElow was significantly less than within R or between R and RR (Supp Fig. 2.19c, d). Importantly, reduced correlation in reward cell activity was only observed in RElow and not in REhigh laps in UR (see example cells in Supp Fig. 2.19d). These findings show that transitioning from REhigh to RElow disrupts the additional coding of specific reward sites by place and reward cells.

2.3.6 Bilateral VTA inhibition largely replicates lowering reward expectation

Ventral Tegmental Area (VTA) dopaminergic inputs to the hippocampus have been implicated in shaping and stabilizing spatial representations (McNamara et al. 2014; Sosa and Giocomo 2021) and VTA/dopamine encode changes in reward expectation (Schultz, Dayan, and Montague 1997). We therefore hypothesized that inhibiting VTA dopaminergic neurons would mimic the effects of lowering reward expectation. To do this, we bilaterally injected Cre-dependent AAV expressing the inhibitory DREADD receptor hM4D(Gi) (Armbruster et al. 2007) and mCherry in VTA of DAT-Cre mice and imaged from dorsal CA1 cells expressing GCaMP6f (Fig. 2.4a, b). On experimental day, mice ran in R for 10 min before being removed and injected intraperitoneally either with saline (control) or one of two different ligands for the hM4D(Gi) receptor—Descholoroclozapine (DCZ) (Nagai et al. 2020) or Clozapine-N-oxide (CNO) (Armbruster et al. 2007). Due to the slower kinetics and known off-target actions of CNO, DCZ was also used to inactivate VTA DA neurons. After the injections (45 mins after CNO injections and 10 mins after DCZ injections due to the faster metabolism of DCZ), mice were placed back in R for 10–20 min. Each mouse after training went through 4 days with imaging: Day1: R-UR-RR switch; Day2: Saline session, Day3: CNO, Day4: DCZ session (Fig. 2.4c). The same FOV was imaged throughout all days of imaging and place cells were extracted from each imaging session (see Methods). This protocol allowed us to compare the effect of lowering reward expectation and VTA inhibition on hippocampal neural activity in the same mice.

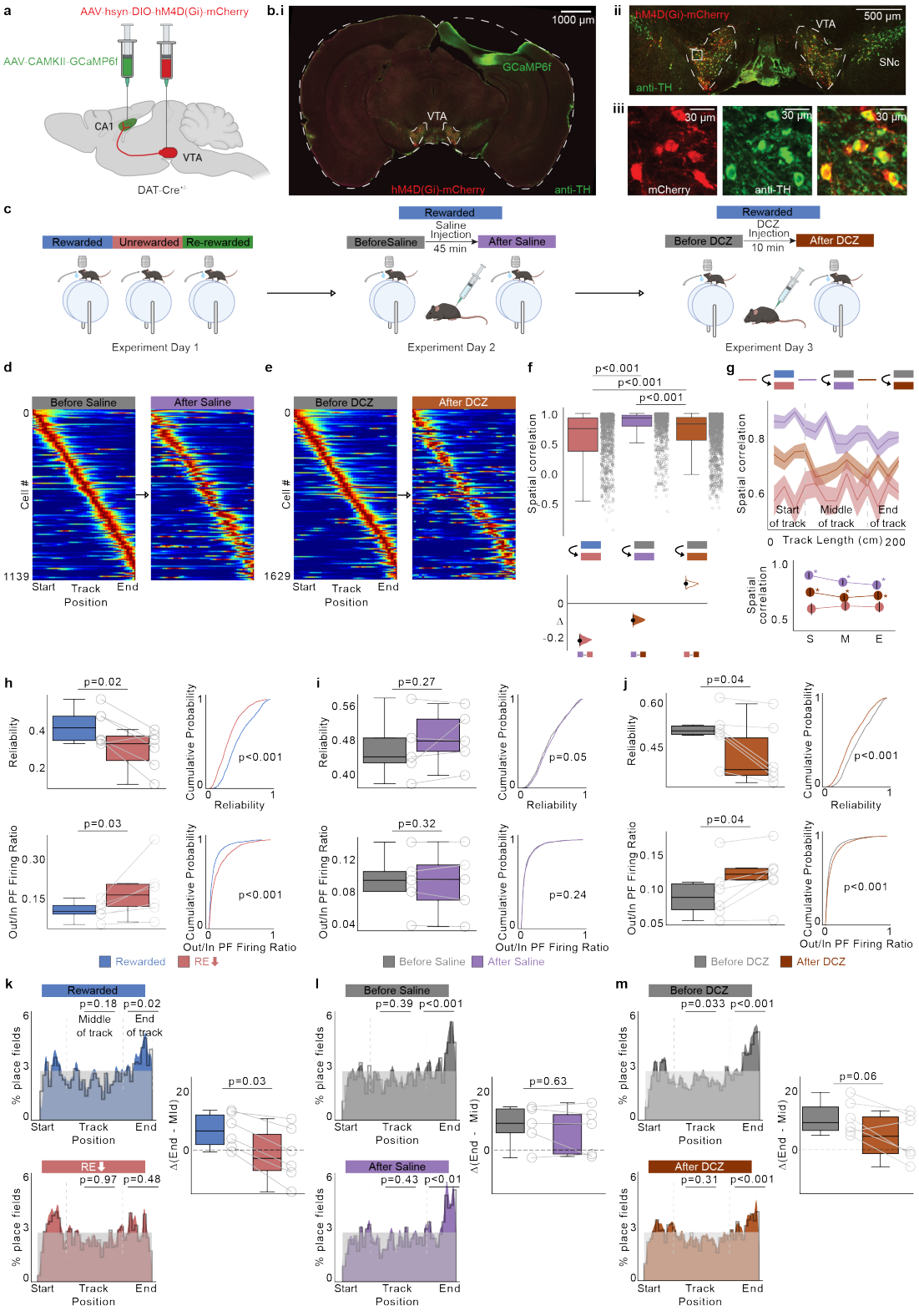

Figure 2.4: **Bilateral inhibition of VTA dopaminergic neurons largely replicates**

Figure 2.4, continued: ... the effects of low reward expectation on place cells. a, Schematic representation of procedure, created with BioRender.com. **b,** i, ii: Representative coronal brain section from 1 of 6 mouse brains expressing hm4D(Gi)-mCherry (red) in VTA, GCaMP6f in dorsal CA1(green), and immunostained for Tyrosine Hydroxolase (TH- green). iii: hm4D(Gi)-mCherry expression (left), TH expression (middle) and overlapping expression (right) in example VTA neurons. **c,** Experimental protocol. **d, e,** Place fields defined in the Before Saline/Before deschloroclozapine (DCZ) condition and plotted across After Saline/After DCZ administration. Activity of each place cell was normalized to peak in the Before conditions and sorted by their center of mass. **f,** (Top) Boxplots show distribution of place field spatial correlation (circles) in R/RElow (left, n = 6 mice), Before Saline/After Saline (middle, n = 5 mice) and Before DCZ/After DCZ (right, n = 6 mice). Place cells were defined in the former condition. P-values were obtained using two tailed KS-test. (Bottom) Bootstrapped mean differences (Δ) with 95% CI (error bar). **g,** (top) Same data, averaged by track position. Shading indicates s.e.m. (bottom) Average correlation binned by track position indicated by gray lines in the top panel. S: Start of the track, M: Middle of the track, E: End of the track. Asterisk (*) indicates significant P values (two tailed KS-test, $p < 0.01$) obtained by comparing UR (red) with other tasks at each position. **h-j,** Place cell parameters in each condition are displayed as boxplot of average per animal (left) and cumulative histogram (right, p-values, two-sided paired t test). **k-m,** (left) Distribution of place field center of mass (COM) locations in each condition pooled from all mice. Plots show observed density (gray line), uniform distribution (gray shade) and Gaussian distribution of place field density (color). P-values (two-sided t test) were obtained by calculating the place field distribution with the uniform distribution. (right) Difference between end of track and middle of track place field percentages in each animal (circles). Dashed line indicates the difference expected from a uniform distribution across the track (P-values, two-sided paired t test). Number of cells in **f-g** and **k-m**; R/RElow: 928, Before Saline/After Saline: 1139, Before DCZ/After DCZ: 1629.

We found that inactivation by both DCZ and CNO yielded similar results (Fig. 2.4 and Supp Fig. 2.22), demonstrating a shared mechanism of action and the timing differences following CNO and DCZ injections and exposure to R, 45 mins versus 10 mins, respectively, does not affect the results. DCZ and CNO administration caused a decrease in lap running speed in R (Supp Fig. 2.22, Mean speed (m/s) [95% CI]: Before Saline 42.74 [41.12 44.36], After Saline 42.75 [41.34 44.17], Before DCZ 41.99 [40.26 43.73], After DCZ 25.96 [24.30 27.62], Before CNO 43.18 [41.26 45.10], After CNO 25.71 [24.03 27.39]) but approach behavior (demonstrating engagement) and anticipatory licking remained (Supp Fig. 2.21). We then measured spatial correlation of place fields before and after DCZ/CNO administration and found a reduction at all locations across the track, similar to the effects in RElow

(Fig. 2.4d–g and Supp Fig. 2.22a-c). This decrease was not observed in the saline control (Fig. 2.4d–g). To test whether these changes might be due to decreased lap speed after DCZ/CNO administration, we split our saline control data into fast velocity and slow velocity laps (Supp Fig. 2.23a). We found a small reduction in spatial correlation on the slow velocity laps compared to the fast laps (Supp Fig. 2.23b, c), but this was much smaller than the effects induced by DCZ and CNO (Fig. 2.4d–g and Supp Fig. 2.22a-c).

Interestingly, we found a decrease in lap velocity in control mice following injections (CNO injected in mice with no DREADD expression; Supp Fig. 2.20C, $p < 0.001$). However, this decreased lap speed did not lead to the same changes in place cells we observed in our experimental groups (Supp Fig. 2.20d, e), further indicating that decreased running speed is not the cause of place cell changes we report in our experimental groups injected with CNO/DCZ with DREADD expression in VTA DA neurons (Fig. 2.4d–g; Supp Fig. 2.22a-c).

We next measured the lap-by-lap reliability of place fields and the out of field firing ratio, two properties most affected by RElow. We found a similar decrease in place field reliability and increase in out-of-field firing in DCZ and CNO as in RElow (Fig. 2.4h, j, Supp Fig. 2.22d, Mean [95%CI]: Reliability: Rewarded = 0.41 [0.31 0.52], RElow = 0.29 [0.17 0.40], Before DCZ = 0.48 [0.38 0.58], After DCZ = 0.41 [0.31 0.51], Before CNO = 0.42 [0.31 0.52], After CNO = 0.35 [0.24 0.47]. Out/In Field Firing: Rewarded = 0.10 [0.06 0.13], RElow = 0.17 [0.06 0.29], Before DCZ = 0.10 [0.05 0.14], After DCZ = 0.12 [0.08 0.16], Before CNO = 0.10 [0.05 0.15], After CNO = 0.12 [0.07 0.17]). This was not the case in the saline controls (Fig. 2.4i, Mean [95%CI]: Reliability: Before Saline = 0.45 [0.34 0.55], After Saline = 0.46 [0.39 0.54], Out/In Field Firing: Before Saline = 0.09 [0.04 0.14], After Saline = 0.09 [0.04 0.14]), even in the slow velocity saline control laps (Supp Fig. 2.23d, Mean [95%CI]: Reliability: Before Saline fast velocity = 0.51 [0.46 0.57], After Saline slow velocity = 0.45 [0.32 0.58], Out/In Field Firing: Before Saline fast velocity = 0.09 [0.04 0.13],

After Saline slow velocity = 0.09 [0.04 0.14]). Lastly, we found DCZ and CNO tended to induce a reduction in place field over-representation of the reward site compared to saline controls, but this did not reach significance (Fig. 2.4m; p = 0.06) and the effect size was less than RElow (Fig. 2.4k–m and Supp Fig. 2.22e), suggesting other neuromodulators might be involved in over-representation. Additionally, both the reduction in over-representation and the changes in reliability and out-of-field-firing ratio were not observed in control animals expressing tdTomato in VTA DA neurons instead of DREADDs and injected with CNO and DCZ (Supp Fig. 2.20). Together, these data indicate that the effects on CA1 spatial encoding with changing reward expectation are largely driven by VTA dopaminergic inputs.

2.3.7 VTA inputs to CA1 encode reward expectation through a proximity to reward signal

To further investigate how the VTA regulates CA1 encoding, we recorded from VTA dopaminergic (DA) axons directly in CA1 using 2-photon imaging of axon-GCaMP7b specifically expressed in VTA DA axons of DAT-Cre mice (Fig. 2.5a). We found that individual DA axons ramped up in activity as mice moved closer to the reward site on each traversal of the environment in R (Fig. 2.5b–d; n = 7 axons from 6 mice). The activity of these ramping DA axons peaked right before the reward site and then rapidly returned to baseline levels after reward was received (Fig. 2.5c, d). DA-axon-ramps decayed in slope and amplitude when mice were switched to UR and disappeared in RElow (Fig. 2.5b–d). DA-axon-ramps started to return early in RR and were almost back to R levels late in RR (Fig. 2.5e, h). To further quantify DA-axon-ramp dynamics, we measured the slope and max peak of the ramps on each lap throughout R-UR-RR from 5 axons that were imaged throughout all conditions (Fig. 2.5i–l and Supp Fig. 2.24). We found DA-axon-ramps were consistent in R but decayed abruptly after a few laps in UR (Fig. 2.5j and Supp Fig 2.24). Similarly, average pre-licking continued for a few laps before rapidly dropping, indicating DA axon-ramps are impacted by

reward expectation. DA-axon-ramps were on average smaller in UR compared to R during REHigh laps but disappeared in RElow laps (Fig. 2.5k; n = 7, Mean [95%CI]: Slope*max: R = 1.00 [1.00, 1.00], REHigh = 0.57 [0.40, 0.74], RElow = 0.24 [0.03, 0.45]). DA-axon-ramps were not different in R versus RR (Fig. 2.5k; n = 5 , Mean [95%CI]: $Slope * max$: R = 1.00 [1.00, 1.00], RR = 1.23 [-0.28, 2.74]). These data demonstrate that VTA DA axons in CA1 encode the animal's proximity to reward and disappear when rewards are no longer expected.

To investigate the emergence of DA-axon-ramps with learning, we switched a subset of mice to a novel (N) VR environment while continuously imaging VTA DA axons (n = 5 axons from 5 mice; Supp Fig. 2.25). We found DA axon activity had much lower peaks in N and were much more locked to reward delivery rather than ramping with proximity to reward (Supp Fig. 2.25b, c). However, activity peaks increased with experience in N and DA-axon-ramps started to develop towards the end of the session (Supp Fig. 2.25d), revealing DA-axon-ramps are a learned signal requiring repeated environment-reward associations.

We found two axons with distinct types of signals that did not ramp to reward (Supp Fig. 2.26). One of these encoded the animal's velocity and was not sensitive to the R-UR transition (Supp Fig. 2.26a-c). The other responded to being in VR environments by decreasing activity relative to being in a dark environment (Supp Fig. 2.26d). These findings show that VTA DA axons in CA1 predominantly encode the animal's proximity to reward, but there exists heterogeneity across the population of DA axons with some axons encoding other features of experience (Engelhard et al. 2019).

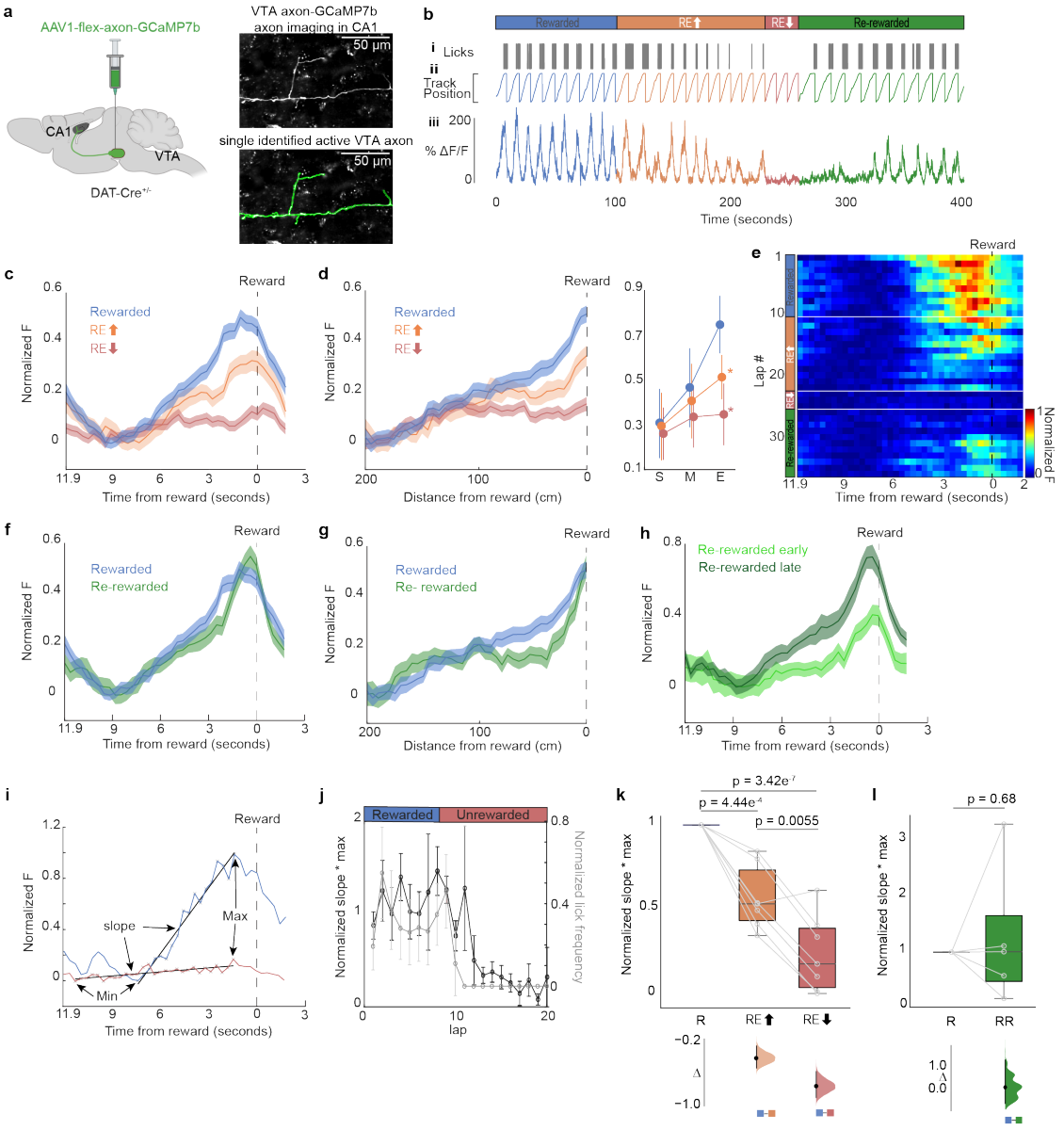

Figure 2.5: **Activity of dopaminergic VTA axons in CA1 ramp up to reward a,** Schematic representation of injection procedure created with BioRender.com (left). Example CA1 field of view of VTA axons (right, top). Extracted region of interest (right, bottom). **b,** Example mouse. i: Mouse licking behavior. ii: Mouse track position. iii: $\Delta F/F$ from an example ROI. **c,** Fluorescent activity of axons (7 axons in 6 mice) in R (blue), REhigh (orange-RE arrow), and RElow (red-RE arrow) experimental conditions averaged by time to reward. Shaded areas represent s.e.m. **d,** Same data, averaged by position (left). Mean with 95% CI (error bar) of starting 50 cm (S), middle 100 cm (M), and end 50 cm (E)(right). Asterisk ($*$) indicates significant p-values (two-sided paired t test, $p < 0.01$) obtained by comparing R (blue) with other tasks at each position. **e,** Normalized fluorescence of an example axon in the different conditions binned by time to reward. White lines divide each condition, and the dashed line represents time of reward delivery.

Figure 2.5, continued: f, Fluorescent activity of VTA axons (5 axons in 5 mice) in R(blue) and RR (green) averaged by time to reward. Shaded areas represent s.e.m. **g,** Same data averaged by position. **h,** RR time binned fluorescent activity divided into early (light green) and late laps (dark green) and averaged by time to reward. **i,** Example showing how the max and slope of time binned fluorescence data was determined in an R (blue) and RElow (red) lap. **j,** Mean slope∗max for laps in the R and Unrewarded (black, n = 7) and mean lick frequency normalized to maximum licks (gray), error bars represent s.e.m. **k, l,** Boxplot shows distribution of mean slope∗max of axons (circles) within R, REhigh, and RElow (k; n = 7 axons) and within R and RR (l; n = 5 axons). P values were obtained using a two-sided paired t test. (Bottom) Bootstrapped mean differences (Δ) with 95% CI (error bar) are shown at the bottom. X-axis indicates the comparisons made.

2.4 Discussion

During wakeful exploration animals continuously experience external events, some of which are robustly encoded into memory for future recall. A key aspect of whether external events become encoded into memory depends on the internal state of the animal during encoding (Kentros et al. 2004; Tarder-Stoll et al. 2020). Here we found that changes in reward expectation within unchanging spatial environments alters the structure and trial-to-trial dynamics of place codes in CA1 likely through the modulation of a ramping to reward signal in dopaminergic inputs from VTA to CA1. This is supported by several observations: 1, reward removal led to diminished reward expectation which caused an abrupt restructuring of the place code that included place cell remapping, the loss of some place fields, and the formation of new place fields at all locations within the environment, plus a loss of place field over-representation of the reward zone. 2, place code restructuring only occurred after the reward expectation diminished and not following reward removal 3, place cells encoding the environment during low reward expectation were degraded in quality exhibiting low trial-to-trial reliability and high out-of-field firing at all locations 4, bilateral inhibition of dopaminergic neurons in the VTA during high reward expectation largely mimicked the effects of lowering reward expectation 5, dopaminergic axons from the VTA to CA1 encoded a ramping to reward signal during high reward expectation that disappeared after lowering re-

ward expectation. These results provide evidence that the structure and robustness of spatial memory encoding in the hippocampus is determined by dopaminergic inputs from the VTA that is dependent on the animal's internal state of reward expectation during navigation.

Reward contingencies in navigation tasks have been shown to modulate place cells (Wikenheiser and Redish 2011; Gauthier and Tank 2018; I. Lee et al. 2006; Martig and Mizumori 2011; Tryon et al. 2017). Most studies in this area either alter reward magnitudes or move reward locations, and many times include a decision-making component in their behavioral task. These factors all modulate place cells in some way, depending on the specifics of the experiment. What has been difficult to achieve in this research area is a complete removal of rewards for long enough to alter, and measure, reward expectation yet maintain matched navigation behavior. This is a necessary step to assess the influence of changing reward expectations on place cells without confounds caused by changes in navigation behavior (B. L. McNaughton, Barnes, and J. O'Keefe 1983). Our behavioral set-up allowed us to match navigation behaviors, even when reward was not expected. Specifically, head direction, location occupancy, location sequences leading to reward, running speed, and pupil area were the same in rewarded and unrewarded conditions for many trials. A number of factors led to this matched behavior: (1) Mice were head-fixed; (2) The behavior was simple and stereotyped (mice run on a linear treadmill along a linear track); (3) Mice were first trained to run to a very high level with reward to establish high reward expectation before reward was removed; (4) Many traversals of the environment could be achieved in short succession (5 traversals/min). In conjunction with our ability to measure reward expectation on a trial-by-trial basis, this matched behavior allowed us to specifically connect the influence of reward expectation on place cells in real-time.

Interestingly, our data show that the presence (or consumption) and subsequent absence of reward itself has little influence on spatial encoding in CA1 as shown by very little difference in the spatial code between R and UR when RE is high on the first few laps. Sharp

wave ripples and place cell replay events occur more frequently during reward consumption which might reflect a reward-related feedback signal that could influence the place code for the environment, but this does not seem to be the case (Singer and Loren M. Frank 2009; Knudsen and Wallis 2021). Instead, it is only after animals learn to associate or disassociate reward from the environment and change their reward expectation that we observe changes in the place cell code. The structure of the map, place cell over-representation of the reward location, and trial-by-trial reliability/out-of-field firing were all modulated only when reward expectation changed, not when reward was removed/added. This demonstrates that the act of reward attainment does not in itself modulate place cells in the hippocampus, which may have been the case through a reward-related feedback signal. Instead, the animal's internal state of reward expectation is a stronger driver of place cell encoding than the external reward. Reward cells in this region have recently been described that encode reward independently of space (Gauthier and Tank 2018). We did identify these cells, and found that they too were modulated by reward expectation rather than reward per se. Therefore, our data suggests internal states of reward expectation rather than reward attainment modulate hippocampal spatial encoding of locations within environments.

Such changes in the place code in an unchanging spatial environment could reflect the animal's attempts to infer whether they are in a different "state" of the world (Knudsen and Wallis 2021), something that has been observed in the prefrontal cortex (Durstewitz et al. 2010; Karlsson, Tervo, and Karpova 2012). The sensory cues remained constant but internal expectation of reward did not, and this was sufficient to induce partial remapping along with other changes in the place code. From the perception of the mice, the state of the world changed as the locations within the environment became devalued by lowering reward expectation and no longer predicted the presence of a reward. The value of the sensory experience thus alters the CA1 place code, suggesting that the hippocampus does not simply represent spatial information, but flexibly encodes the value of space and is able

to discriminate contexts within an unchanging spatial environment (Knudsen and Wallis 2021). This could be due to mice disengaging from their environment once it is no longer valued. A recent paper showed that when mice disengage with their environment CA1 place codes degrade41. However, we measured two distinct features—approach behavior and pupil area—as a readout of engagement and found mice in our experiments remain engaged on many trials even when reward expectation is low. For instance, mice decelerated as they approached the end of the track on many trials even when reward expectation had diminished. This approach behavior was likely due to mice anticipating hitting the VR wall at the end of the track which triggers a 2s delay before teleportation to the start of the track. This was not due to stereotyped behavior as switching mice to a dark environment with no spatial cues eradicated approach behavior. Therefore, mice in our set up were engaged with their spatial environment following lowered reward expectation on many trials. The changes in the place code we observe are therefore unlikely due to disengagement with the environment and are instead most likely due to reduced reward expectation. Although our mice show signs of engagement, we cannot rule out that they are less engaged than during high reward expectation and our engagement measures are not sensitive enough to capture more subtle changes. Reduced engagement could therefore contribute to the place cell changes we report here. In agreement with Pettit et al.(Pettit, Yuan, and Harvey 2022), we did find obvious disengaged trials during low reward expectation and these trials show further place code changes beyond those caused by reduced reward expectation. We therefore add to the Pettit et al. (Pettit, Yuan, and Harvey 2022) findings by demonstrating extensive changes in CA1 place coding caused by lowered reward expectation during engagement (or minimally lowered engagement) with the environment. This implicates additional internal states in modulating place coding beyond environment engagement-disengagement.

The process of switching reward expectation from high-low-high led to a greater distinction between representations in the two high reward expectation conditions than when

reward expectation was held high throughout the session (as was the case in control animals that maintained high reward expectation throughout a time-matched session). This suggests the CA1 chunks external events into distinct episodes based on changes in internal state, even when external events remain the same. In other words, when internal expectations are constant, unchanging external events are encoded as a single contextual episode. When internal expectations change and then return to original levels, unchanging external events are encoded as distinct contextual episodes. This encoding of episodic information within the CA1 network is consistent with its proposed role in capturing temporal and contextual episodes (Smith and Mizumori 2006).

DA activity in CA1 is known to play an important role in hippocampal-dependent reward learning (Lisman and Grace 2005) and DA VTA inputs to CA1 have been shown to modulate reward learning (McNamara et al. 2014). Optogenetic activation of VTA axons during learning of new goal locations enhances the subsequent reinstatement of spatial representations and stabilizes memory performance(McNamara et al. 2014). The stability of CA1 spatial representations is reduced by inactivation of VTA neurons (Martig and Mizumori 2011) or CA1 DA receptor antagonism (Barter et al. 2015). Here, we also find that spatial representations are more stable when VTA DA neurons are active (during high reward expectation) and destabilize when VTA DA activity is reduced (during lowered reward expectation and during VTA DA inhibition). What is missing from previous studies is a direct connection between the animal's internal state of reward expectation and how changing reward expectation changes spatial representations and VTA DA activity. Our findings fill this gap and we additionally reveal that bilateral inhibition of VTA DA neurons: 1, decreases the trial-to-trial reliability and increases the out-of-field firing of place fields. 2, reduces reward site over-representation by place fields. 3, largely replicates the effects of lowering reward expectation. We also reveal the natural VTA DA dynamics in CA1 and their response to changes in reward expectation (further discussion below), which, as far as we know, has never been

measured. Our findings therefore replicate previous work on VTA DA influences on spatial representations and memory but add to this area by showing the natural dynamics of VTA DA inputs to CA1 and their influence on spatial representations in real-time during changes in reward expectation. We also show the "fate" of individual place cells through changes in reward expectation, revealing heterogeneity of responses at the single cell level (some place fields disappear when reward expectation is lowered, some remap, some cells form new place fields, and some maintain their place fields). One caveat is that VTA inhibition did cause lap velocity to reduce - a known role of VTA dopaminergic neurons(Barter et al. 2015)—which itself could cause changes to place coding(B. L. McNaughton, Barnes, and J. O'Keefe 1983). We addressed this by comparing slow and fast velocity laps in saline controls to see if place cell differences could be observed, and we did find small differences. Therefore, reduced velocity likely contributes to the observations we made during VTA inhibition but given the small effect size of velocity it is unlikely to explain all the changes. Our findings instead support a framework whereby diminished reward expectation causes diminished DA release from VTA in CA1, leading to an abrupt restructuring of place coding that includes a loss of over-representation of rewards sites, plus a degradation in the quality of place coding.

In support of this idea, we show that VTA DA neurons in the hippocampus exhibit ramping to reward activity that diminishes following the removal of rewards. Similar activity has been observed in VTA DA neurons and their projections to several brain areas using various techniques (Howe et al. 2013; Kim et al. 2020; Guru et al. 2020; Mohebi et al. 2019). It is not entirely clear whether this ramping activity signals reward prediction error (RPE) (Kim et al. 2020) or value (Howe et al. 2013; Mohebi et al. 2019). However, our findings that VTA axon activity peaks prior to expected reward locations in familiar environments but peaks at the location of unexpected rewards in novel environments supports the established idea that VTA DA neurons signal RPE. Importantly, this ramping activity diminished over the course of several trials following reward removal, was completely absent in RElow, and rapidly re-

established in RR mimicking the timing of changes to reward expectation and hippocampal place cell codes we observed. Thus, we hypothesize that this ramping activity provides reward expectation information to the hippocampus through DA release that is required to maintain specific excitatory drive to place cells or postsynaptic responses within place fields. However, we did not specifically manipulate this input in our DREADD experiment, which targeted all DA VTA neurons and not just DA inputs to CA1. Future experiments should be designed to specifically manipulate the VTA-CA1 DA input to further test our hypothesis.

Interestingly, we found that although our CNO/DCZ inhibition experiments largely replicated the results of lowering reward expectation, it did not cause a corresponding inhibition of pre-licking. This suggests a distinct brain region might encode reward expectation and send parallel signals to both VTA, to drive DA ramps, and to a lower-order center that drives pre-licking. In our CNO/DCZ experiment we inhibited the VTA component of this circuit which appears to leave intact the parallel circuit to licking centers. Indeed, there is evidence for such a reward expectancy center in PFC(Watanabe 1996).

Although VTA DA inputs to CA1 are sparse, manipulation of this pathway has large effects on spatial memory (McNamara et al. 2014; Gomperts, Kloosterman, and Matthew A Wilson 2015; Duszkiewicz et al. 2019) and many subtypes of DA receptors are expressed throughout CA1 on pyramidal cells, Interneurons, and astrocytes (Edelmann and Lessmann 2018; Jennings et al. 2017). The influence of this sparse input could be amplified by the types of connections VTA DA inputs make. A recent paper showed that VTA DA inputs to Nucleus Accumbens make "spinule" connections that increase the surface area between DA inputs and their postsynaptic targets, potentially amplifying their influence (Wildenberg et al. 2021). Volume transmission is another potential mechanism that could amplify DA's influence on the hippocampus (Edelmann and Lessmann 2018). Local interneurons and/or astrocytes expressing DA receptors could further amplify DA's influence in CA1 through their many connections with pyramidal cells. While we did not measure DA release in the

hippocampus and cannot directly attribute the effects of bilateral VTA DA neuron inhibition to DA activity, studies have demonstrated that these neurons can impact hippocampal place cell stability through DA receptor dependent mechanisms(McNamara et al. 2014). DA regulates synaptic transmission and dendritic excitability(Tritsch and Sabatini 2012) and high dendritic excitability of CA1 basal dendrites has been linked to place field emergence, precision, and long term stability (Mark E.J. Sheffield, Adoff, and Daniel A. Dombeck 2017; M. E. J. Sheffield and Daniel A. Dombeck 2015). Interestingly, VTA DA inputs are located in the Stratum Oriens of CA1 where basal dendrites of pyramidal cells reside and express D5 receptors (Adeniyi, Shrestha, and Ogundele 2020). We hypothesize that DA increases dendritic excitability to increase dendritic branch spike prevalence across basal dendrites when reward expectation is high. High dendritic branch spike prevalence stabilizes place fields and increases their precision and reliability(Mark E.J. Sheffield, Adoff, and Daniel A. Dombeck 2017; M. E. J. Sheffield and Daniel A. Dombeck 2015). Following diminished reward expectation, loss of DA reduces branch spike prevalence, destabilizing place fields (restructuring the place code at the population level) and reducing their trial-to-trial precision and reliability. This hypothesis remains to be tested.

Although the presence of DA-ramps in CA1 means the level of DA release is not equal across the track, attractor-like dynamics could ensure DA influences place cells at all locations. For instance, place cells with place fields closer to the end of the track receive greater levels of DA release, but are part of a larger place cell sequence (possible attractor network) with cells that have place fields at the beginning of the track that receive lower levels of DA. Based on the known connectivity of CA1 neurons, this may arise from local inhibition within CA1 or driven by input from CA3, which does have recurrent connectivity to support attractor dynamics and also receives dopaminergic input (Gasbarri et al. 1994; Lisman and Grace 2005; Rolls 2007). Furthermore, place cells sequences are replayed during immobility and reward enhances the fidelity and increases the frequency of replays which could

further stabilize place cell sequences associated with high reward expectation that include place fields throughout the entire track and not just ones close to the reward site (Ambrose, Pfeiffer, and Foster 2016; Bhattarai, J. W. Lee, and Jung 2020; Gillespie et al. 2021). A hypothesis generated from this framework would be that DA ramps increase replay fidelity and/or frequency. Indeed, optogenetic stimulation of DA neurons in VTA enhances replay events in CA1, suggesting the DA ramps we observed may be the natural brain signal that leads to a similar enhancement of CA1 replay events.

An alternative source of dopamine in CA1 could be coming from locus coeruleus (LC) fibers which impact hippocampal learning and memory in a DA dependent manner (Kempadoo et al. 2016). LC has been shown to encode reward expectation (Bouret and Sara 2004) and a recent study found optogenetic stimulation of LC-CA1 inputs at a goal induced a shift in place fields towards the goal, whereas inhibition decreased overrepresentations of new goal locations suggesting these inputs help establish overrepresentation of reward locations (Kaufman, Geiller, and Losonczy 2020). However, these inputs only showed activity locked to new goal locations but not familiar locations and have not been shown to influence pre-existing overrepresentation of goal locations or place fields throughout an environment. Therefore, it is unlikely that these inputs are the main driver for restructuring of the place code observed during diminished reward expectation. It is possible LC inputs do have some influence, though, as inhibition of VTA by DCZ or CNO did not induce the same effect size as lowering reward expectation, implicating other neuromodulatory systems beyond VTA. Serotonergic inputs to the hippocampus from the Raphe Nuclei also encode reward related information, so could further modulate CA1 place codes during changes in reward expectation74. Given the importance of strongly encoding reward-related memories it is not surprising that reward-related information is distributed across multiple neuromodulatory systems that project to the hippocampus. However, our findings suggest VTA DA is the main system in modulating dorsal CA1 during changes in reward expectation during spatial

navigation.

An outstanding question is what drives the DA ramps in VTA. Ramps seem to require animals to know where they are and how far they are from a reward. This implicates the hippocampus and the place codes represented there in providing spatial information to the VTA (Guru et al. 2020). It has been proposed that a loop may exist between the hippocampus and VTA whereby the hippocampus sends information through the subiculum, accumbens, and ventral pallidum to the VTA (Lisman and Grace 2005). This pathway could inform DA neurons in VTA of the animal's position relative to reward. These neurons could then ramp up their firing as the animal approaches expected reward locations, modulating the value of locations based on their distance from reward locations. The DA released in the hippocampus thus serves to stabilize the structure of place codes and maintain reliable place fields along trajectories that lead to expected rewards (Guru et al. 2020).

2.5 Methods

2.5.1 Subjects

All experimental and surgical procedures were in accordance with the University of Chicago Animal Care and Use Committee guidelines. For this study, we used 10–12-week-old male $C57BL/6J$ wildtype (WT) mice and $Slc6a3^{(}Cre+/-)$ ($DAT-Cre^{(}+/-)$) mice (23–33 g). Male mice were used over female mice due to the size and weight of the headplates (9.1 mm $\times$ 31.7 mm, 2 g) which were difficult to firmly attach on smaller female skulls. Mice were individually housed in a reverse 12h light/dark cycle at 72°F and 47% humidity, and behavioral experiments were conducted during the animal's dark cycle.

2.5.2 Mouse surgery and viral injections

Mice were anesthetized (1–2% isoflurane) and injected with 0.5 ml of saline (intraperitoneal injection) and 0.5 ml of Meloxicam (1–2 mg/kg, subcutaneous injection) before being weighed and mounted onto a stereotaxic surgical station (David Kopf Instruments). A small craniotomy (1–1.5 mm diameter) was made over the hippocampus (1.7 mm lateral, -2.3 mm caudal of Bregma). For population imaging, a genetically-encoded calcium indicator, AAV1-CamKII-GCaMP6f (pENN.AAV.CamKII.GCaMP6f.WPRE.SV40 was a gift from James M. Wilson – Addgene viral prep #1 00834-AAV1; https://www.addgene.org/100834/; RRID:Addgene_100834) was injected (50 nL at a depth of 1.25 mm below the surface of the dura) using a beveled glass micropipette leading to GCaMP6f expression in a large population of CA1 pyramidal cells. For DREADD experiments, craniotomies were made over the hippocampus and bilaterally over the ventral tegmental area (VTA) (± 0.5 mm lateral, 3.1 mm caudal of Bregma) of $DAT - Cre^{(} + /-)$ mice. A genetically encoded DREADD receptor (pAAV-hSyn-DIO-hM4D(Gi)-mCherry was a gift from Bryan Roth (Addgene viral prep # 44362-AAV1; http://n2t.net/addgene:44362; RRID: Addgene_44362) or tdTomato (pAAV-FLEX-tdTomato was a gift from Edward Boyden (Addgene viral prep # 28306-AAV1; http://n2t.net/addgene:28306; RRID: Addgene_28306) was injected (200 nL at a depth of 4.4 mm below the surface of the dura). For axon imaging, a small craniotomy was made over the ventral tegmental area (VTA) (0.5 mm lateral, -3.1 mm caudal of Bregma) of $DAT - Cre^{(} + /-)$ mice. A genetically-encoded calcium indicator, pAAV-Ef1a-Flex-Axon-GCaMP7b (pAAV-Ef1a-Flex-Axon-GCaMP7b was a gift from Rylan Larsen - Addgene plasmid # 135419; http://n2t.net/addgene:135419; RRID: Addgene_135419) was packaged into AAV1 and injected (200 nL at a depth of 4.4 mm below the surface of the dura) leading to axon-GCaMP7b expression in dopaminergic VTA neurons. Afterwards, the site was covered up using dental cement (Metabond, Parkell Corporation) and a metal head-plate (9.1 mm × 31.7 mm, Atlas Tool and Die Works) was also attached to the skull with the cement. Mice

were separated into individual cages and water restriction began the following day (0.8–1.0 ml per day). For axon imaging, mice were put on water restriction 3 weeks after viral injection to provide time for increased expression of axon-GCaMP7b. On the 7th day of water restriction, mice underwent another surgery to implant a hippocampal window as previously described (Daniel A. Dombeck et al. 2010). Following implantation, the head-plate was reattached with the addition of a head-ring cemented on top of the head-plate which was used to house the microscope objective and block out ambient light. Post-surgery mice were given 2–3 ml of water/day for 3 days to enhance recovery before returning to the reduced water schedule (0.8–1.0 ml/day). Expression of GCaMP6f reached a somewhat steady state 20 days after the virus was injected.

2.5.3 Behavior and virtual reality

Our virtual reality (VR) and treadmill setup was designed similar to previously described setups (Mark E.J. Sheffield, Adoff, and Daniel A. Dombeck 2017; Heys, Rangarajan, and Daniel A. Dombeck 2014). The virtual environments that the mice navigated through were created using VIRMEn(Aronov and Tank 2014). 2 m linear tracks rich in visual cues were created that evoked numerous place fields in mice as they moved along the track at all locations (Fig. 2.1a)(Bourboulou et al. 2019). Mice were head restrained with their limbs comfortably resting on a freely rotating styrofoam wheel ('treadmill'). Movement of the wheel caused movement in VR by using a rotatory encoder to detect treadmill rotations and feed this information into our VR computer, as in refs. (Mark E.J. Sheffield, Adoff, and Daniel A. Dombeck 2017; Aronov and Tank 2014). Mice received a water reward (4 µL) through a waterspout upon completing each traversal of the track (a lap), which was associated with a clicking sound from the solenoid. Licking was monitored by a capacitive sensor attached to the waterspout. Upon receiving the water reward, a short VR pause of 1.5 s was implemented to allow for water consumption and to help distinguish laps from one another rather than

them being continuous. Mice were then virtually teleported back to the beginning of the track and could begin a new traversal. Mouse behavior (running velocity, track position, reward delivery, and licking) was collected using a PicoScope Oscilloscope (PICO4824, Pico Technology, v6.13.2). Pupil tracking was done through the imaging software (Scanbox v4.1, Neurolabware) at 15 frames per sec, using Allied Vision Mako U-130b camera with a 25 mm lens and a 750 nm longpass IR filter. IR illumination from the objective was used to illuminate the pupil for tracking. Behavioral training to navigate the virtual environment began 4–7 days after window implantation (30 min per day) and continued until mice reached >4 laps per minute, which took 10–14 days (although some mice never reached this level). This high level of training was necessary to ensure mice continued to traverse the track similarly after reward was removed from the environment. Initial experiments showed that mice that failed to reach this criterion typically did not traverse the track as consistently without reward. Such mice were not used for imaging. The rate of success in training mice to reach this criterion was 60%. In mice that reached criteria, imaging commenced the following day. Additionally, since we are testing changes in reward expectation, only animals that displayed pre-licking in the familiar environment before reward delivery were used for imaging.

2.5.4 Two-photon imaging

Imaging was done using a laser scanning two-photon microscope (Neurolabware). Using a 8 kHz resonant scanner, images were collected at a frame rate of 30 Hz with bidirectional scanning through a 16x/0.8 NA/3 mm WD water immersion objective (MRP07220, Nikon). GCaMP6f and GCaMP7b were excited at 920 nm with a femtosecond-pulsed two photon laser (Insight DS + Dual, Spectra-Physics) and emitted fluorescence was collected using a GaAsP PMT (H11706, Hamamatsu). The average power of the laser measured at the objective ranged between 50–70 mW. A single imaging field of view (FOV) between 400–700

µm equally in the x/y direction was positioned to collect data from as many CA1 pyramidal cells or dopaminergic axons as possible. Time-series images were collected through Scanbox (v4.1, Neurolabware) and the PicoScope Oscilloscope (PICO4824, Pico Technology, v6.13.2) was used to synchronize frame acquisition timing with behavior

2.5.5 Imaging sessions

The familiar environment was the same environment that the animals trained in. The experiment protocol for single day imaging sessions is shown in Fig. 1a. Each trial lasted 8–12 min and was always presented in the same order. 6 mice were exposed to Rewarded (R), Unrewarded (UR) and Re-Rewarded environments (RR), in that order. An additional 6 mice were exposed to only R and UR. Mice on average ran 34 ± 2 (mean ± 95% CI) laps in the Rewarded condition, at which point, reward was turned off and imaging in the Unrewarded environment continued (28 ± 4 laps). In the Unrewarded condition, both reward and auditory cue associated with the reward (solenoid click) were disabled. In n = 6 animals, reward was then turned on again (Re-rewarded) and mice ran 27 ± 3 laps. To identify reward cells, the 6 mice that went through R-UR-RR were also introduced to a Novel-rewarded environment (NR; 31 ± 5 laps). The Novel-rewarded environment (N) had distinct visual cues, colors and visual textures, but the same dimensions (2 m linear track) and reward location (end of the track) as the familiar environment. Furthermore, to rule out the possibility that observed changes in population activity were due to time, mice were exposed to only the familiar Rewarded environment for 20 min (control, n = 6).

2.5.6 DREADD experimental protocol

To activate hM4D(Gi) receptor and silence VTA dopaminergic neurons, two ligands were used - Deschloroclozapine dihydrochloride (DCZ, MedChemExpress)(Nagai et al. 2020) and Clozapine N-Oxide (CNO, Enzo Life Sciences, Inc)(Armbruster et al. 2007). Due to the slow

kinetics and known off-target effects of CNO, DCZ was used as an additional method for inactivation(Nagai et al. 2020).

CNO was dissolved in DMSO at a 5 mg/mL concentration and stored at -80°C. On experiment day, CNO solutions were thawed at room temperature and diluted to 0.6 mg/mL with saline (details on saline). DCZ was dissolved in DMSO at 5 mg/mL concentration and stored at -80°C. On experiment day, DCZ solutions were thawed at room temperature and diluted to 0.02 mg/mL with saline.

Once DREADD or tdTomato (control) injected DAT-Cre mice met training criteria, they were habituated to the injection process. They were exposed to the familiar rewarded environment for 10 min. Afterwards, they were removed from the VR set up, placed in the holding room, and injected with 150 µL of a 12% DMSO/Saline solution. After 30–45 min, they were placed back in the VR setup and exposed to the familiar rewarded environment for an additional 10 min. This was repeated for 3–5 days to acclimate mice to the injection procedure.

The experimental protocol for the first day of DREADD experiments was identical to the reward manipulation experiments described above. At the end of the imaging session, a 1 minute time-series movie was collected at a higher magnification and then averaged to aid as a reference frame in finding the same imaging plane on subsequent days. On Experiment Day 2, mice were first exposed to R for 8–12 min. The mice were removed from the VR set up and placed in a holding room where they were immediately injected with 150 µL of a 12% DMSO/ Saline solution. 35 min after injection mice were placed back on the VR setup and the same imaging plane was found. At the 45 min post injection mark, mice were again exposed to R for 15–20 min. The procedure for Experiment Day 3 was identical to Day 2 except mice were injected with 5 mg/kg CNO in a 0.6 mg/mL solution instead of the DMSO/Saline solution or with 0.1 mg/kg DCZ of a 0.02 mg/mL solution. Due to the faster kinetics of DCZ, mice were placed back in R after 10 min post injection.

2.5.7 Histology and brain slices imaging

We checked the VTA expression of hm4D(Gi)-mCherry to confirm adequate coverage of dopaminergic VTA neurons. Mice were anesthetized with isoflurane and perfused with 10 ml phosphate-buffered saline (PBS) followed by 20 mL 4% paraformaldehyde in PBS. The brains were removed and immersed in 30% sucrose solution overnight before being sectioned at 30 µm-thickness on a cryostat. Brain slices were collected into well plates containing PBS. Slices were washed 5 times with PBS for 5 min then were blocked in 1% Bovine Serum Albumin, 10% Normal goat serum, 0.1% Triton X-100 for 2 h. Brain slices were then incubated with 1:500 rabbit-α-TH (MAB318, Sigma Aldrich) in blocking solution at 4°C. After 48 h, the slices were incubated with 1:1000 goat-α-rabbit Alexa Fluor 488 secondary antibody (A32731, ThermoFisher) for 2 h. Brain slices were then collected on glass slides and mounted with a mounting media with DAPI (SouthernBiotech DAPI-Fluoromount-G Clear Mounting Media, 010020). The whole-brain slices were imaged under $\times$10 and x40 with a Caliber I.D. RS-G4 Large Format Laser Scanning Confocal microscope from the Integrated Light Microscopy Core at the University of Chicago.

2.5.8 Image processing and ROI selection

Time-series images were preprocessed using Suite2p (v0.10.1) (Pachitariu et al. 2017). Movement artifacts were removed using rigid and non-rigid transformations and assessed to ensure absence of drifts in the z-direction. Datasets with visible z-drifts were discarded (n = 2). For multi-day datasets (DREADD Experiments), imaging planes acquired from each day were first motion corrected separately. ImageJ (v1.53, NIH) was then used to align the motion corrected images relative to each other by correcting for any rotational displacements. The images across all days were then stitched together and motion corrected again as a single movie. For population imaging, regions of interest (ROIs) were also defined using Suite2p (Fig. 2.1a) and manually inspected for accuracy. Baseline corrected $\Delta F/F$ traces across

time were then generated for each ROI and filtered for significant calcium transients, as previously described (Mark E.J. Sheffield, Adoff, and Daniel A. Dombeck 2017; M. E. J. Sheffield and Daniel A. Dombeck 2015; Daniel A. Dombeck et al. 2010). Finally, we used raster plots(Stringer and Pachitariu 2019) to visualize the $\Delta F/F$ population activity of neurons across time and across all conditions (Fig. 2.1c and Supp Figs. 2.7 and 2.8). In these raster plots, neurons were clustered and sorted such that neurons with correlated activity were next to each other on the vertical axis (https://github.com/MouseLand/rastermap). For visual clarity, only neurons with at least 2 transients above 10% $\Delta F/F$ over the time of the experiment were included in the raster plot and the 2-D plots were interpolated using a hanning filter.

For axon imaging, ROIs were first defined using Suite2p and manually inspected for accuracy. ROIs were then hand drawn over all segments of Suite2p defined active axons using ImageJ to ensure all axon segments were included for analysis. Fluorescent activity for each ROI was extracted and highly correlated ROIs (Pearson correlation coefficient $\geq$ 0.7) were combined and fluorescent activity for the combined ROI was extracted. Baseline corrected $\Delta F/F$ traces across time were then generated for each ROI using a larger sliding window of 2000 frames.

2.5.9 Licking behavior

Licking data was collected using a capacitive sensor on the waterspout. Well trained mice showed a higher proportion of licks (pre-licking) in the region immediately preceding the reward in R (Supp Fig. 2.6). This anticipatory licking behavior continued for a few laps in UR (5 ± 1 lap) and decayed exponentially (Fig. 2.1e) except for some animals (4/12) that randomly licked in later laps. To calculate anticipatory licking in UR, we defined a reward zone which started from the average track position at which the animal started pre-licking in R and ended after teleportation. We calculated the presence of any licks within this zone

to quantify anticipatory licking in UR in the absence of a reward. The lap where pre-licking stops in UR was then defined as the lap following 2 consecutive laps with an absence of these licks.

2.5.10 Position decoding

We trained a naive Bayes decoder (scikit-learn, v1.0.2, Python) to predict the spatial location of the animal on the linear track from population activity within each mouse. Population activity consisted of $\Delta F/F$ traces from all identified cells organized as NxT, where N is number of cells and T is the total number of frames from an imaging session. Each lap traversal on the 2 m track was discretized into 40 spatial bins (each 5 cm wide). Time periods where the animal was stationary were filtered out (speed $<$ 1cm/s) and the decoder was only trained on frames belonging to running periods $>$ 1 cm/s. Running behavior and population activity before and after filtering is shown in Supp Fig. 2.8 and Fig. 2.3c, respectively. To ensure decoder performance was not confounded by teleportation, we considered the end of the track as continuous with the beginning of the track so that the topology of the track was treated as a circle.

To assess how well a decoder trained in R was able to decode the animal's spatial location in other conditions (Fig. 2.1d–g), the decoder was trained on the first 60% of laps in R. The resulting model was evaluated on the remaining laps in R and on all laps in UR and RR (Fig. 2.1d). Quality of fit was assessed by calculating the coefficient of determination (R^2) between the actual location of the animal and the location predicted by the decoder. Decoder error was quantified as difference in actual and decoded position in cm (Fig. 2.1g). We also trained and tested decoders within each condition in each mouse (Supp Fig. 2.18). Here, to assess decoder performance and to account for population activity changes across time, we employed a cross-validation approach by sliding the tested laps (20% of laps) by one each time and training on the remaining laps (80% of laps). Furthermore, to account for different

numbers of laps across conditions, we down sampled each condition to match the condition with the least number of laps.

2.5.11 Decoder performance with different behavioral parameters

Licking behavior To analyze the relationship between decoder error and licking, we identified the lap when licking had stopped in UR when 2 consecutive laps had no licks, and then divided the data into laps before licking stopped (REhigh, before licking stops) and laps after licking stopped (RElow, after licking stops). We found that if we instead used different criteria to identify when licking had stopped, i.e., the first lap with no licks, or 4 consecutive laps with no licks, our results were unaffected. This was also true if instead of defining when licking stopped in UR we simply grouped laps together based on the presence or absence of licks (Supp Fig. 2.9). However, with 6 consecutive laps with no licks, our results differed (Supp Fig. 2.9). We obtained the lap wise decoder fit (R^2) and lick frequency in UR in each animal and ran a rolling average with a sliding window of 3 laps (Fig. 2.1e). The average decoder fit across laps formed an S-shaped curve. We fit this mean R^2 to a reverse Boltzmann Sigmoid curve (scipy.curve_fit, v1.7.3, Python, Fig. 2.1e, coefficient of determination of curve fit with mean decoder = 0.94). To calculate the inflection point at which the rate of decrease in R^2 reaches the maximum, we calculated the first point where the second derivative of the fit reached 0 (lap 10, Fig. 2.1e).

Time taken to complete a lap This was calculated as the total time (in seconds) taken by the animal to run from 0 to 200 cm. We assessed if there was any correlation between the decoder fit and the time the animal took to complete a lap. To do so, we created a histogram of the distribution of time taken to complete a lap in R and UR (Supp Fig. 2.10). For each animal, we divided the laps in UR into those that overlapped with the histogram in R (Matched velocity laps) and those that did not (Slower velocity laps). The average time taken to complete a lap in the matched laps was 7.34 $\pm$ 0.46 s in R and 7.41 $\pm$ 0.40 s in UR.

The slower speed laps took 19.99 ± 1.85 s. Most of the laps belonged to the Matched speed laps and consisted of 70% of the total laps run by all animals in UR. Results are shown in Supp Fig. 2.10.

Engagement with VR-approach behavior In R, mice slowed down as they approached the end of the track. We postulated that if mice were continuing to pay attention to where they were in VR when reward was removed, they would display a similar approach behavior. As a control, we first recorded running behavior of trained animals in the dark (n = 6), without any visual cues, to ensure that well trained mice were not displaying a stereotypical behavior independent from VR. To assess approach behavior, instantaneous velocity was calculated at each point along the 2 m track. This velocity trace was then smoothed by averaging it over 5 cm bins. In the dark, there were no signs of stereotyped behavior that looked like approach behavior (Supp Fig. 2.11a). The degree of this approach behavior at the end of the track was calculated as the ratio between lap velocity in the middle (100–150 cm) and end (175–200 cm) of the track as indicated above the traces in each condition. On average (mean ± 95% CI), this ratio was 1.01 ± 0.03 in the Dark, 1.3 ± 0.02 in the Rewarded condition and 1.22 ± 0.02 in the Unrewarded condition. Engaged laps in each animal after licking stops (RElow) were then defined as laps where the approach ratio was greater than or equal to mean $/pm 1.5 * standarddeviation$ of the ratio in the Rewarded Condition (rest were defined as disengaged laps). In total, number of laps in each condition were obtained as follows: REhigh:Engaged = 90, RElow:Engaged = 170, RElow:Disengaged = 74. Mean ± 95% CI approach ratio in each condition: REhigh:Engaged = 1.26 ± 0.04, RElow:Engaged = 1.3 ± 0.02, RElow:Disengaged 1.02 ± 0.03. To ensure matched behavior in Rewarded and RElow conditions and that the disengaged laps do not skew our results, only engaged laps were extracted from animals for further analysis. Only one animal continued to randomly pre-lick at laps after our definition of lick stop. Of those laps (n = 10 laps), 5 were classified as engaged and 5 as disengaged. Reanalyzing the data excluding these laps did not change

the decoder error. n = 3/6 animals that went through the R-UR-RR paradigm had enough engaged laps (>12) to define place fields and their results are displayed in Figs. 2.2 and 2.3. (see Supp Figs. 2.14 and 2.16 for all animals).

Engagement with VR-pupil measures To obtain images with dark pupils and high contrast around the borders of the pupils, pupil images were inverted, and their brightness/contrast was adjusted. Pupil area, pupil center of mass (COM), and blinking area were obtained using FaceMap (v0.2.0) (Stringer and Pachitariu 2019). Pupil data during blinking periods (frames where blinking area < mean – twice the standard deviation of the blinking area) was removed and the pupil data was interpolated to match the 2-photon imaging frame rate (30 fps). The pupil data was filtered to exclude time periods where the animal was immobile (speed < 1 cm/s).

Pupil area correlation To obtain a pupil area trace for each lap, we binned the track into 40 bins (5 cm wide) and calculated the mean pupil area of each bin. For each mouse, the average pupil area of each bin across all laps in the familiar rewarded condition was calculated and served as a template pupil area trace. The pupil area correlation was then measured as the Pearson correlation coefficient between the template pupil area trace and the lap's pupil area trace. High pupil area correlation laps were defined as laps whose pupil area correlation $>= mean - 1.5 * std$ of the pupil area correlation for rewarded laps.

Mean eye movement Eye movement for each frame in a condition was calculated as the difference between the pupil's center position and the mean center position of the pupil during the condition. The mean eye movement for each lap was then calculated.

Blinking ratio Defined as the number of frames defined as blinking periods divided by the total number of frames in each lap.

Freezing ratio Defined as the number of frames where the animal was immobile (speed < 1 cm/s) divided by the total number of frames in each lap.

2.5.12 Defining place fields

Place fields were identified as described in previous studies (Mark E.J. Sheffield, Adoff, and Daniel A. Dombeck 2017; M. E. J. Sheffield and Daniel A. Dombeck 2015; Daniel A. Dombeck et al. 2010) with a few key differences. The 2 m track was divided into 40 position bins (each 5 cm wide). The running behavior of the animal was filtered to exclude time periods where the animal was immobile (speed $<$ 1 cm/s). Filtering was done to ensure that place cells were defined only during active exploration. In UR, only RElow frames after the licking stopped (see section on "Licking behavior") were included for place cell analysis. Separately, RElow:Engaged laps only were included for place cell analysis (Figs. 2.2 and 2.3, see "Animal engagement with VR" section). Place fields across the entire track were extracted if they began firing on the track (see clipped cells at the end of the track in Fig. 2.2b). Cells that began firing at or after reward delivery and during teleportation were excluded from this analysis (although see Reward cells below). Extracted place fields satisfied the following criteria and the same criteria was used for all conditions and all mice: 1. Their width was $>$ 10 cm (except for fields that are clipped at the end of the track). 2. The average $\Delta F/F$ was greater than 10% above the baseline. 3. The average $\Delta F/F$ within the field was $>$4 times the mean $\Delta F/F$ outside the field. 4. The cell displayed calcium transients in the field on $>$30% of laps. 5. The rising phase of the mean transient was located on the track. 6. Their p-value from bootstrapping was $<$0.0575. Multiple place fields within the same cell were treated independently.

2.5.13 Place field parameters

To calculate the various place field parameters, we binned the track into 40 bins (5 cm wide) and measured the mean $\Delta F/F$ of each bin. The data of each place field was a Lx40 matrix where L is the number of laps traversed by the animal. For all measures other than out-of-field firing and spatial correlation, transients outside the defined place field region were

removed.

Center of mass(COM) The COM from all traversals L was calculated as described in (M. E. J. Sheffield and Daniel A. Dombeck 2015). Briefly, COM for each traversal was calculated as,

$$COM_L = \frac{\sum_i F_i x_i}{\sum_i F_i} \tag{2.1}$$

where F is the $\Delta F/F$ in each bin i and xi is the distance of bin i from the start of the track.

Reliability Reliability of a place cell is the consistency with which it fires at the same location across multiple lap traversals. To calculate this, we computed the Pearson correlation between each lap traversal to obtain an L $\times$ L matrix. To obtain the reliability index, the average of this correlation matrix was multiplied by the ratio of number of laps with a significant calcium transient within the field and the total number of laps. The reliability index is 1.0 if the cell fires at the same location in each lap and 0.5 if it fires at the same position but only in half the laps, and so on.

Out/in place field firing ratio This was computed as the ratio between the mean $\Delta F/F$ in bins outside the place field and the mean firing in bins within the place field.

Width Width of the place field was computed as the distance between the spatial bin at which the mean place field rose above 0 and the spatial bin when it decayed back to 0. For place fields at the end of the track that were clipped the end of the place field was considered as the end of the track.

Firing intensity Firing intensity of the place field was calculated as the peak $\Delta F/F$ of the mean place field

Population vector correlation To determine level of similarity in spatial representations from lap-to-lap in the different conditions, population vector (PV) correlations were calculated. For each of the 40 spatial bins, population vectors were defined as the mean rate of firing for each place cell in that bin. The correlation between the population vector in one lap versus another lap was then calculated and the correlations were averaged over all

positions (Fig. 2.2a).

K-means clustering K-means clustering was performed on the calculated lap-wise population vectors. The elbow method was used to determine the optimal number of clusters. For all animals, the method determined this to be 3. K-means clustering was performed 1000 times. Each time, the Rewarded cluster was determined as the cluster ID to which most rewarded laps belong to. The probability of all laps (in R, UR and RR) belonging to the Rewarded cluster was then calculated over the iterations (Fig. 2.2a).

Spatial correlation with Rewarded condition To calculate the consistency of firing of the place cells defined in R across different conditions, we calculated the Pearson correlation coefficient between mean place cell activity defined in R and the mean of the L $\times$ 40 matrix of the same cells in other conditions. The within-session correlation was calculated from control animals (n = 6 mice). The control rewarded condition (the duration control mice were in this condition matched experimental mice that experienced R-UR-RR) was divided into two halves and the correlation coefficient was calculated between the mean place cell firing in the two halves.

Place field parameters in DREADD experiments All place cells and associated parameters were calculated and quantified as described above for R-UR-RR experiments.

2.5.14 Reward over-representation

To compute the density of place cells along the track, the COM of all place fields in all animals were fitted to a gaussian distribution (mean $\pm$ standard deviation of the gaussian distribution in cm in different conditions, R: 114 $\pm$ 55, UR: 102 $\pm$ 54, RR: 112 $\pm$ 58, N: 108 $\pm$ 53, DREADD Experiments: R: 110 $\pm$ 55, UR: 103 $\pm$ 54, Before Saline: 113 $\pm$ 55, After Saline: 114 $\pm$ 54, Before CNO: 113 $\pm$ 57, After CNO: 109 $\pm$ 56, Before DCZ: 113 $\pm$ 56, After DCZ: 106 $\pm$ 55) and a uniform distribution to extract regions of place cell overrepresentation (Figs. 2.3d–f and 2.4k–m and Supp Figs. 2.16c, 2.20g, 2.22e, 2.23e). To compare changes in

place field density across conditions between the middle of the track (50–150 cm) and end of the track (150–200 cm), we divided the middle of the track into 50 cm bins and averaged place cell density across the bins.

2.5.15 Reward cells

Reward cells were defined as described in24. Briefly, a cell was defined as a reward cell if it fired at the reward zone on the track (40 cm before reward) and around reward delivery (2 seconds before and after reward delivery) in both R and NR. The reward zone on the track was chosen based on the area of high place field density before the reward in R and N (Supp Fig. 2.19a). In total, we found 43 such cells from 6 animals, both on track and around reward delivery (Supp Fig. 2.19a). These cells constituted 0.9% of all active cells recorded. To compare reward cell firing across all conditions, we computed the lap wise firing of these cells in time around reward delivery (Supp Fig. 2.19). Their COM in time around reward delivery, reliability and correlation with R was then calculated similar to place cells.

2.5.16 Axon imaging analysis

To characterize the activity of VTA axons, their activity was divided into time and positional bins. For positional bins, the 2 m track was divided into 40 position bins (each 5 cm wide) and the mean fluorescent activity in each bin for every lap was calculated. For time bins, we aligned each lap with the reward delivery and divided the lap into 40 time bins. The average time to reward was 11.9 s ($\pm$ 0.25 s, SEM) and the time after reward was 2 s. Therefore, to align each laps reward delivery and maintain roughly equal time bins, the time before reward was divided into 34 time bins and the time after reward was divided into 6 time bins. To account for potential shifts in baseline fluorescence in both position and time binned data, the binned fluorescence data was subtracted by the minimum bin fluorescence for each lap. The binned data was then normalized by dividing by the maximum bin fluorescence for each

mouse and pooled across mice. Finally, the average binned fluorescence was calculated for each task condition.

DA ramp slope and max To characterize the ramping activity observed in VTA axons, the maximum and slope of the time binned fluorescence data were calculated for each lap. The maximum was defined as the maximum bin value of the time binned fluorescence data for each lap. The maximum values for each lap were then normalized by dividing by the average maximum value in the Rewarded condition for each mouse. To calculate the slope of the curve in the Rewarded condition, the maximum value near the end of the track (within 15 bins of lap end) and the minimum value near the beginning of the track (within 25 bins of lap start) were determined for each lap. In all other experiment conditions, the range of bins used to find the maximum and minimum values were restricted to the nearest and furthest bins where the maximum and minimum were found in the Rewarded condition for each mouse. A line was then fit to the data points between the defined maximum and minimum values using the matlab fitlm function. The slope of this line was found and normalized by dividing by the average slope in the Rewarded condition for each lap. The slope*max was calculated as the product of the slope and maximum values for each lap and was normalized by dividing the average slope*max in the Rewarded condition for each mouse. The average maximum, slope and slope*max in each experimental condition were calculated for each mouse.

Velocity encoding To investigate velocity encoding in a VTA axon, we aligned the activity of the axon to motion initiation. Motion epochs were identified as periods where the animal's velocity ≥ 1 cm/s for at least 1 s. Motion epochs were aligned to motion initiation, or the first frame where velocity ≥ 1 cm/s. The $\Delta F/F$ data and velocity 2 s prior to motion initiation and 8 s after motion initiation were collected for each motion epoch. Velocity was normalized by dividing by the maximum velocity of each motion epoch. The average $\Delta F/F$ and velocity of all motion epochs was calculated for each experiment condition.

2.5.17 Statistics

For data distributions, a Shapiro–Wilk test was performed to verify if the data was normally distributed. If normality were true, where applicable, a paired or unpaired Student's t test was used. For non-normal distributions, a paired Wilcoxon signed rank test or an unpaired Mann–Whitney U-test was used. To compare between distributions, a two-tailed Kolmogorov–Smirnov (KS) test was used. For samples with five data points or less, only a non-parametric test was used. Multiple comparisons were corrected with Bonferroni post hoc. Throughout the manuscript, boxplots are plotted to display the full distribution of the data. The box in the boxplot ranges from the first quartile (25th percentile) to the third quartile (75th percentile) and the box shows the interquartile range (IQR). The line across the box represents the median (50th percentile). The whiskers extend to 1.5*IQR on either sides of the box and anything above this range is defined as an outlier. Significance tests were performed with and without outliers. P-values calculated without outliers have been displayed in the figure panels. To model the probability distribution in the datasets and get an accurate idea of the data shape, a kernel density estimate was fitted to the data distribution and is shown alongside histograms. Cumulative probability distribution functions were compared using a KS test. We employed estimation statistics to ascertain the level of difference between distributions by using the DABEST (v0.3.1, Data Analysis with Bootstrap-coupled Estimation) package82. Estimation plots display the median difference between two conditions against zero difference, with error bars displaying 95% confidence intervals of a bootstrap generated difference (5000 resamples). A kernel density fit (shaded curve) on the resampled difference is also displayed alongside. This difference was compared against zero. Correlations were performed using Pearson's correlation coefficient. Data preprocessing and analysis was done on MATLAB (Mathworks, Version R2018a) and Python 3.7.4 (https://www.python.org/).

2.5.18 Figure graphics

All figure graphics including Figs. 2.1a, b, 2.4b, c, and 2.5a and Supp Figs. 2.18a and 2.20a were created using BioRender.com.

2.5.19 Reporting summary

Further information on research design is available in the Nature Portfolio Reporting Summary linked to this article.

2.6 Data availability

Raw imaging data are extremely large and not feasible for upload to an online repository but are available upon request at sheffield@uchicago.edu. Processed source data for all figures and associated statistical analysis are provided with the paper. Source data are provided with this paper.

2.7 Code availability

Scripts used for data analysis are available on Github (https://github.com/seethakris/HPCrewardpaper).

2.8 Supplementary

2.8.1 Supplementary figures

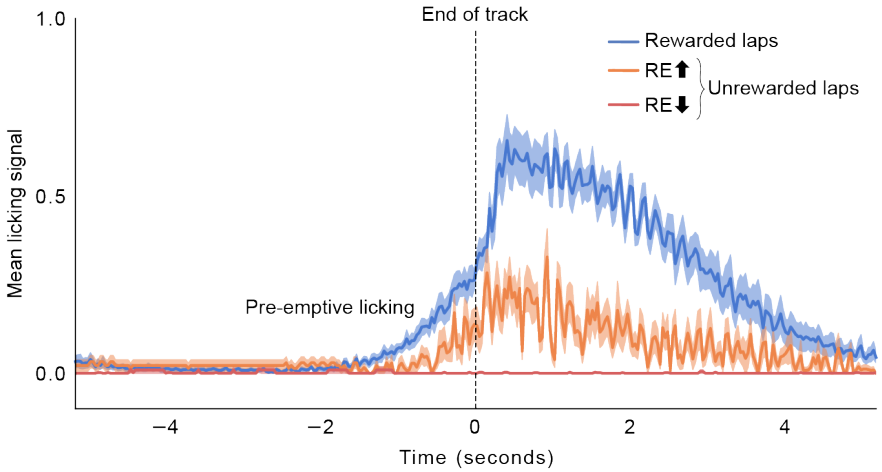

Figure 2.6: **Pre-emptive licking is displayed by mice for a few laps before a learned reward location in a familiar VR environment after reward is removed.** Mean number of licks around reward delivery (time = 0) in R (blue) and UR divided into laps with licking (REhigh, orange) and laps without (RElow , red). Number of licks were calculated for each mouse on each lap and were binarized as 1 or 0 depending on if the animal licked or not in the given time bin. In R, animals display preemptive licking in anticipation of the reward, which was present in REhigh and absent in RElow. Shading represents s.e.m. (n = 12 mice).

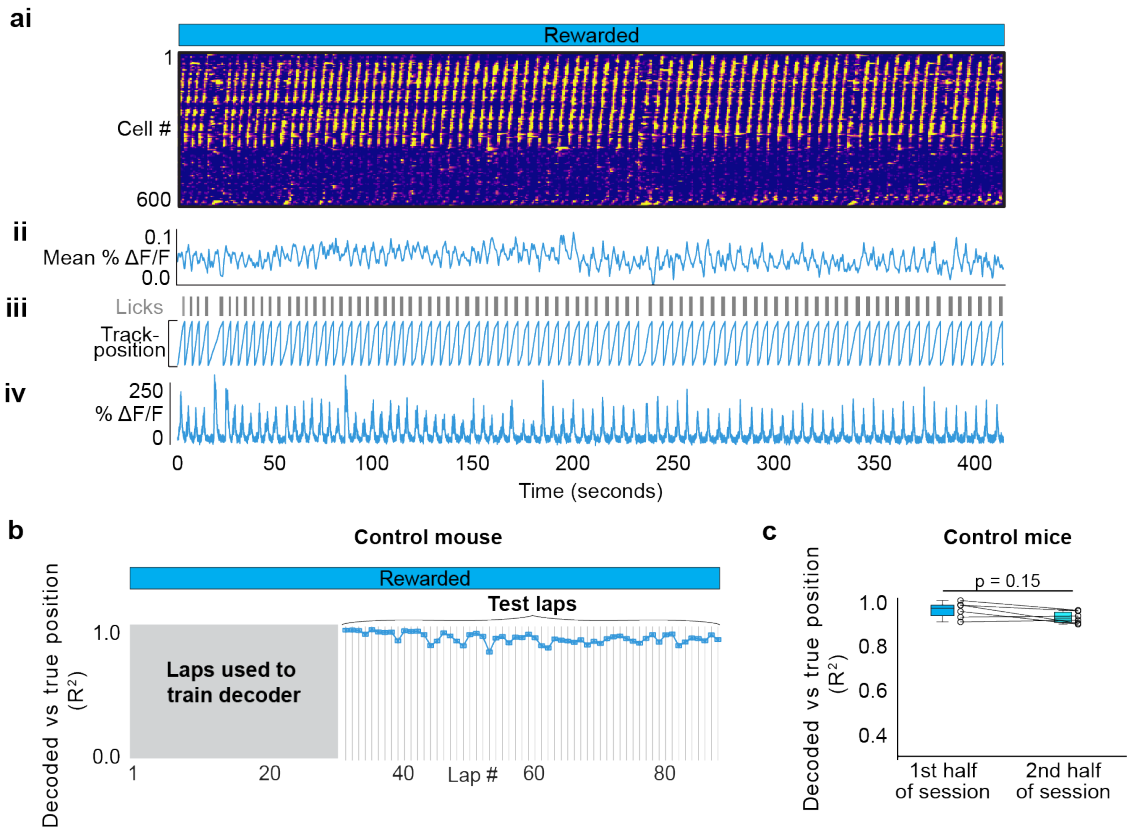

Figure 2.7: **Population activity remains stable with time. a,** i: Raster representation of population activity in 1 mouse traversing the rewarded environment for 15 minutes (a similar amount of time and number of laps over which experimental mice were switched between R and UR). ii: Mean activity of cells above, iii: mouse behavior, iv: example cell. Note the relative stability of the population activity compared to Fig 2.1 b. **b,** Bayesian decoder trained on activity on initial Rewarded laps to predict animal's position on the other laps. Decoder R^2 true and predicted position in each of the tested laps are shown. **c,** Tested laps were divided into two halves and boxplots display median R^2 of true vs predicted position for each mouse in each half of the session (n = 6 mice). Median: 1st half of session = 0.95, 2nd half of session = 0.90. P-value was calculated using a two-sided paired t-test.

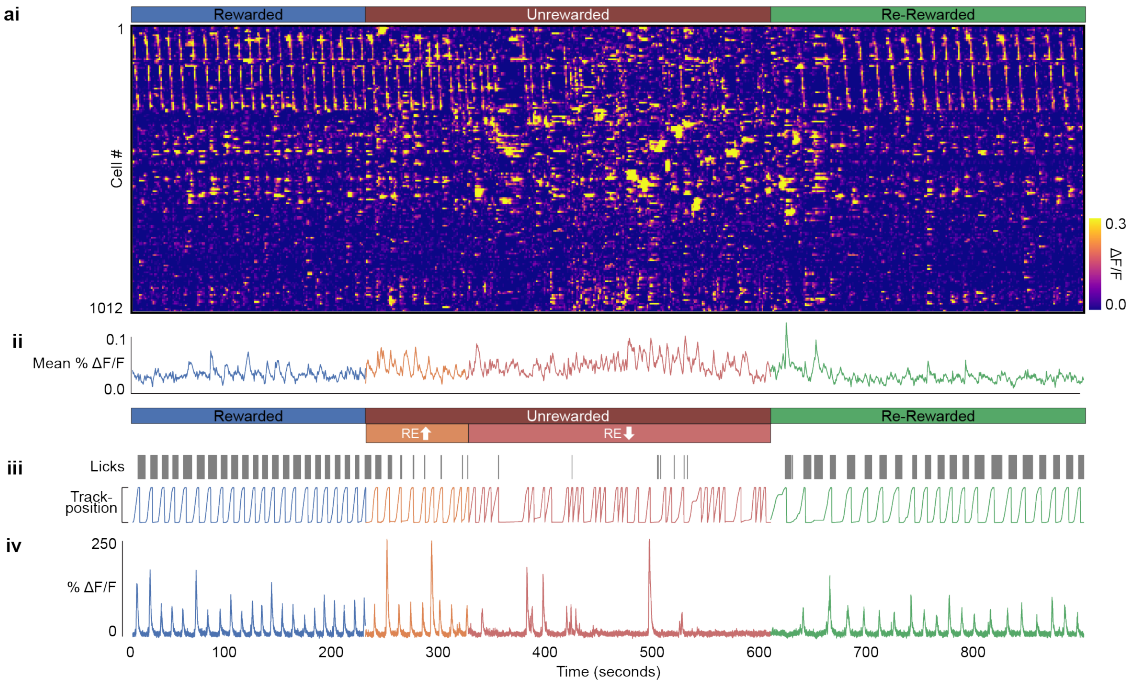

Figure 2.8: **Population activity without filtering laps for good running behavior.** Panels **a**i-v is the same dataset as Fig. 2.1c but without removing periods where the mouse was stationary. i: Rasterplot representing fluorescence changes ($\Delta F/F$) of cells across time. Cells (y-axis) are arranged with the most correlated cells next to each other. ii: Mean $\Delta F/F$ of the cells in (i). iii: Mouse licking behavior. iv: Mouse track position. v: $\Delta F/F$ from an example cell. Most laps look similar to the filtered version shown in Fig 2.1c because mice run in VR consistently even when reward is removed. Most stationary periods are found at the start of the track before the mouse begins its traversal of the environment. Unfiltered laps are shown in (iv).

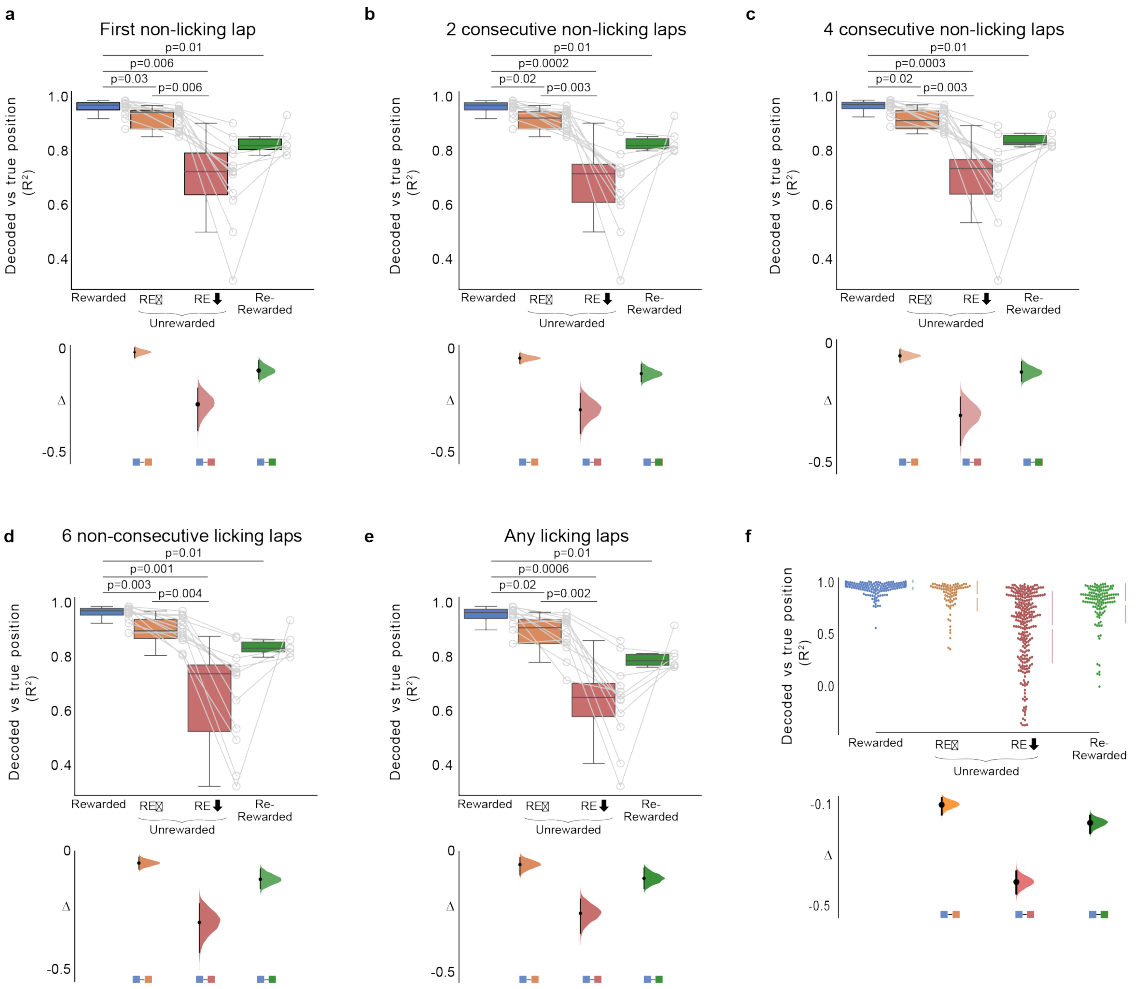

Figure 2.9: **Change in decoder performance in the unrewarded condition after licking stops by definition of when licking stops. a-e,** Boxplots show distribution of mean decoder R^2 between true versus predicted position for each mouse (circles) in the tested laps in R, UR, RR. The decoder was trained on initial laps in R and tested on remaining laps. UR laps are separated by before and after licking stops (REhigh, RElow). The definition of the lap at which licking stops varies in each panel as indicated in the title. P-values were obtained using a two-sided paired t-test. Bonferroni post-hoc was used for multiple comparison correction. **a-e,** Median: R = 0.96, RR = 0.80. **a,** Median: REhigh = 0.93, RElow = 0.69 **b,** REhigh = 0.91, RElow = 0.69 **c,** REhigh = 0.89, RElow = 0.70 **d,** REhigh = 0.87, RElow = 0.70 **e,** REhigh = 0.92, RElow = 0.70. For all further analysis, the lap when the animal stops licking was defined as the 2nd consecutive non-licking lap. (f) Decoder R^2 for each lap in each mouse (circles) in different conditions (Number of laps: R = 399, REhigh = 90, RElow = 244, RR = 121). Mean *pm* standard deviation is shown alongside (Mean (standard deviation): R = 0.97 (0.046), REhigh = 0.86 (0.14), RElow = 0.56 (0.34), RR = 0.79 (0.19). In all panels, Bootstrapped mean differences (Δ) with 95% CI (error bar) are shown at the bottom. X-axis indicates the comparisons made. In all panels, n = 12 mice in R and UR conditions and n = 6 mice in RR.

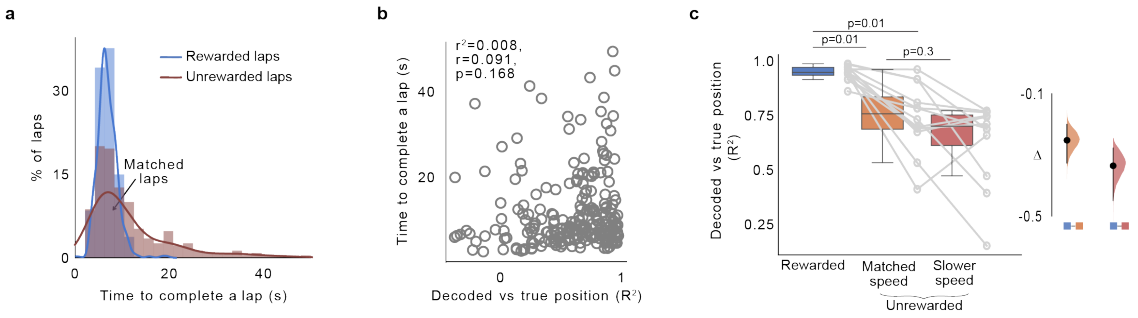

Figure 2.10: **Diminished decoder performance in the unrewarded condition is not due to changes in running behavior. a,** Histogram of lap speed defined as the time taken to complete a lap (in seconds) on the 200 cm track in R and UR (n = 12 mice, total laps in R = 399, UR = 334). Curves are kernel density estimates on the distribution. 70% of the laps in UR had lap speeds that matched lap speeds in R (matched speed laps = 233, slower speed laps = 101). Lap speed in seconds Mean [95% CI]: R = 7.34 [6.88 7.80], Matched speed = 7.4 [7.01 7.78], Slower speed = 20.00 [18.14 21.84] **b,** Scatter plot between lap speed and decoder R^2. Each circle is a lap (data pooled from all mice). R^2 was derived by fitting the data to a linear regression line $y = 10 + 2.3 * x$, r and p-value were derived from Pearson's correlation coefficient. **c,** (left) Boxplot shows distribution of decoder R2 in each mouse (circles, n = 12 mice) with running speed. (right) Bootstrapped mean differences (Δ) with 95% CI (error bar). X-axis indicates the comparisons made. Median: R = 0.96, Matched speed = 0.76 , Slower speed = 0.71. P-values were obtained using a two sided Wilcoxon signed rank test, Bonferroni post hoc was done to correct for multiple comparisons.

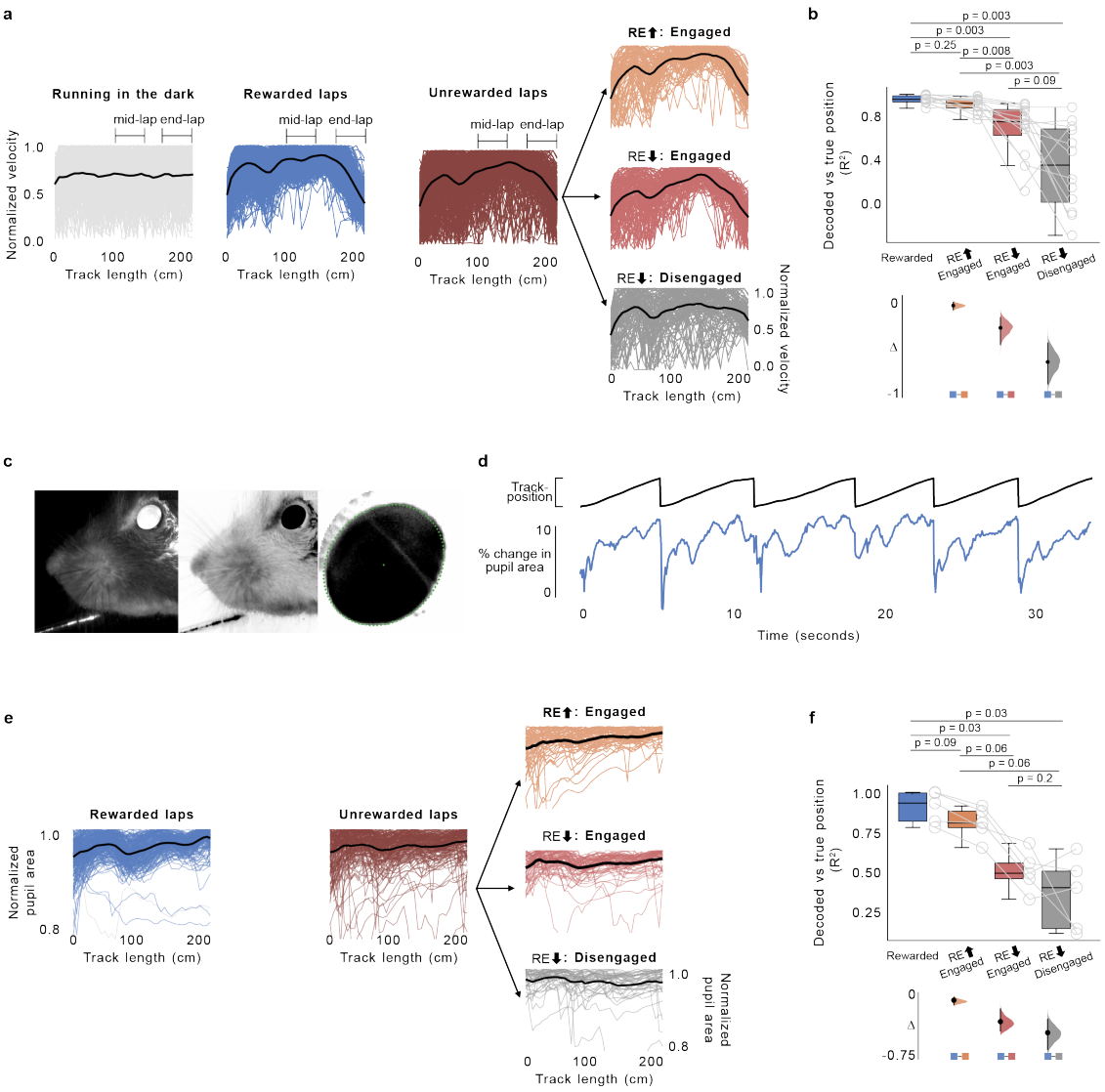

Figure 2.11: **Decoder fit when reward expectation is low is not dependent on the degree of engagement of the animal with the VR.** Two methods were used to calculate the engagement of animals with the VR in RElow laps; the amount of slowing down towards the end of the track (**a-b**) and pupil area across track length (**c-f**). **a,** Instantaneous velocity for each lap from 12 mice in R (n = 399 laps, blue traces) and UR (n = 334, brown traces) and 6 mice in Dark condition (n = 226, gray traces). The velocity on each lap was normalized to its peak. Mean velocity from all laps is shown in black. The degree of approach behavior at the end of the track was calculated as the ratio between lap velocity in the middle (100-150 cm) and end (175-200 cm) of the track as indicated above the traces in each condition. Engaged laps in each animal were then defined as laps where the ratio in RElow was greater than or equal to $mean \pm 1.5 * standarddeviation$ of the ratio in R (rest are disengaged laps).

Figure 2.11, continued: b, Boxplot shows distribution of decoder R^2 in each mouse (circles, n = 12 mice) with degree of engagement (P-values, two-sided Wilcoxon signed rank test). Bootstrapped mean differences (Δ) with 95% CI (error bar) are shown at the bottom. X-axis indicates the comparisons made.**c,** Frame from a video recording of the mouse's face (left), Inverted and intensity adjusted (middle), extracted pupil image circled in green (right). **d,** Example changes in pupil area (bottom) with track position (top) in one animal. **e,** Normalized pupil area from n = 5 mice in R (n = 237 laps, blue traces) and UR (n = 168 laps, brown traces). The Pearson correlation coefficient between the position binned pupil area and the mean position binned pupil area in the Rewarded condition for each mouse. Engaged laps in each animal were defined as laps where the correlation coefficient was greater than or equal to the mean correlation coefficient of laps in the Unrewarded condition (the remaining laps are defined as disengaged laps). **f,** Same as b but with the degree of engagement laps derived from pupil data (P-values, twosided paired t-test, n = 6 mice). Decoders in b, f were trained as in Fig. 2.1.

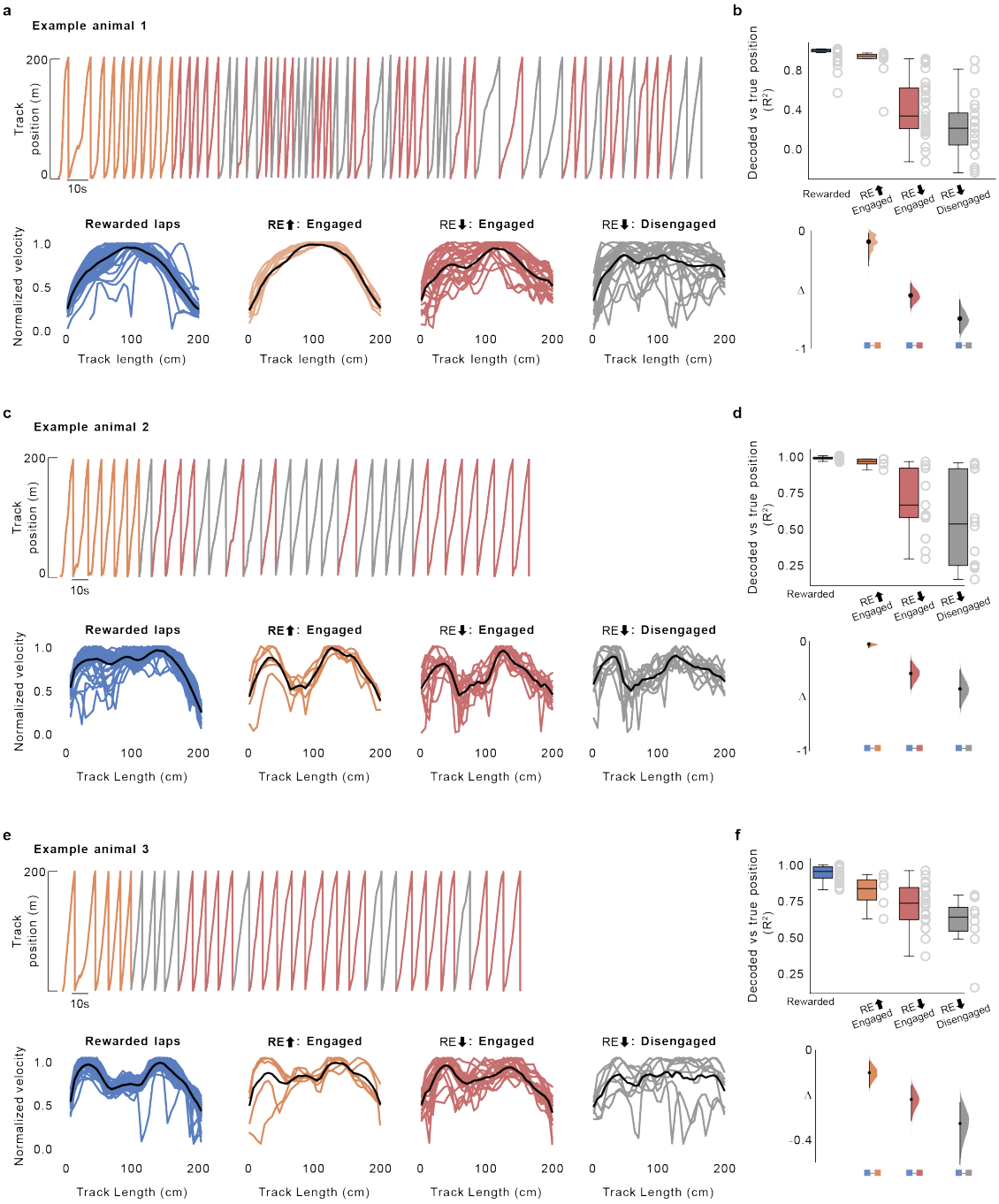

Figure 2.12: **Decoder performance and engagement in three example animals. a, c, e,** (Top) Animal's track position in the unrewarded condition. Laps are colored by degrees of engagement as calculated by the amount of slowing down towards the end of the track. (Bottom) Instantaneous velocity for each lap in the different conditions. The velocity on each lap was normalized to its peak. Mean velocity from all laps is shown in black for each condition.

Figure 2.12, continued: b, d, f, (Top) Boxplots show distribution of decoder R^2 in each lap (circles) for the different conditions. P-values were obtained using a Paired t-test, Bonferroni post hoc was done to correct for multiple comparisons. (Bottom) Bootstrapped mean differences (Δ) with 95% CI (error bar). X-axis indicates the comparisons made. Number of laps: Panel B, Rewarded: 19 REhigh Engaged: 9, RElow Engaged: 31, RElow Disengaged: 20. Panel D, Rewarded: 20 REhigh Engaged: 6, RElow Engaged: 13, RElow Disengaged: 12. Panel F, Rewarded: 20 REhigh Engaged: 6, RElow Engaged: 21, RElow Disengaged: 8

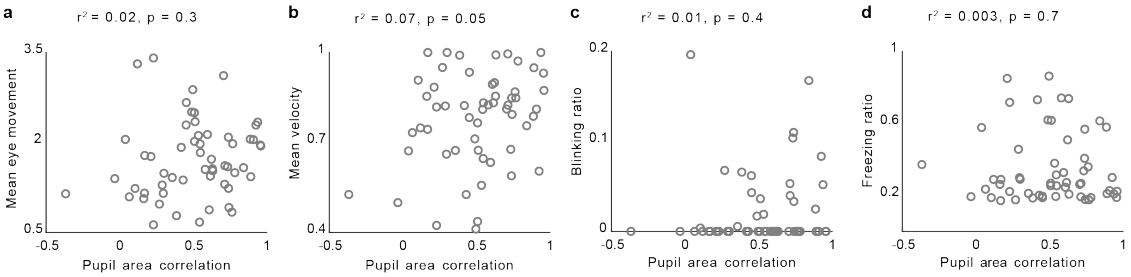

Figure 2.13: **Changes in behavior do not correlate with changes in pupil area.** Pupil area correlation was defined as the Pearson correlation coefficient between the mean position binned pupil area in R and the position binned pupil area of each lap in UR. **a,** Scatterplot between pupil area correlation and mean eye movement. **b,** Scatterplot between pupil area correlation and mean velocity normalized to max velocity. **c,** Scatterplot between pupil area correlation and blinking ratio. **d,** Scatterplot between pupil area correlation and freezing ratio. For all panels, each circle is a lap (n = 56 laps pooled from 5 mice). R^2 was derived by fitting the data to a linear regression line $y = 10 + 2.3 * x$, r and p-value were derived from Pearson's correlation coefficient.

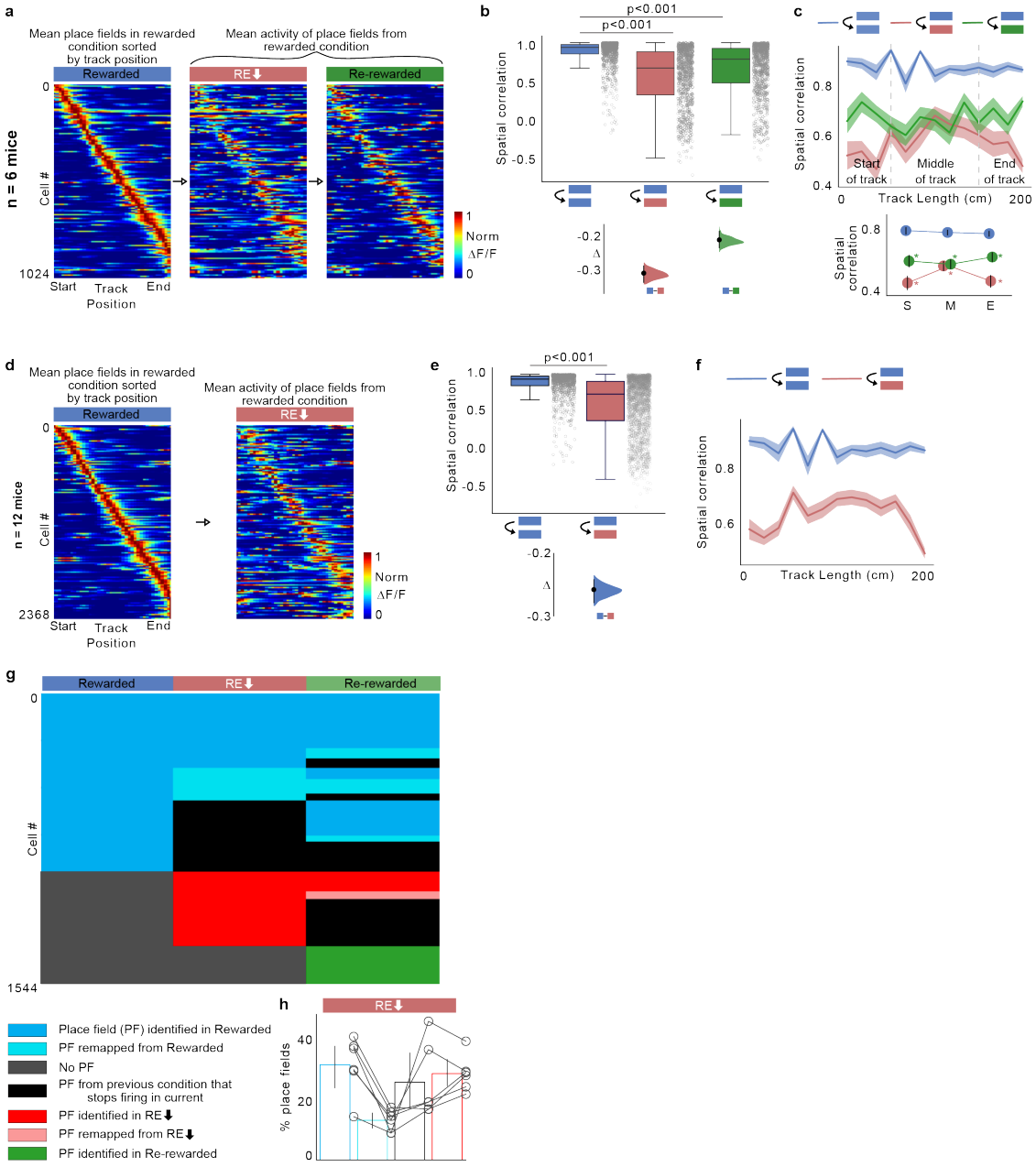

Figure 2.14: **Place cell dynamics in animals with engaged and disengaged laps. a,** Place fields defined in R plotted across all conditions in n = 6 mice. Activity of each place cell was normalized to peak in R and sorted by their center of mass along the track. **b,** Boxplots show distribution of place field spatial correlation for cells in (a) (dots) within R (blue) and between R and other conditions (n = 1024 place cells). P-values were obtained using a twosided paired t-test. (Bottom) Bootstrapped mean differences (Δ) with 95% CI (error bar). X-axis indicates the comparisons made. **c,** (Top) Same data, averaged by track position. Shading indicates s.e.m. (Bottom) Average correlation binned by track position indicated by gray lines in the top panel.

Figure 2.14, continued: S: Start of the track, M: Middle of the track, E: End of the track. * indicates significant p-values (two-sided paired t-test, $p < 0.01$) obtained by comparing R (blue) with other tasks at each position. **d-f,** .Same plots as **a-c** but with n = 12 mice and 2368 place cells. **g** Fate of place cells identified in different conditions (n = 6 mice). **h** Percentage of place cells by their fate in RElow in each animal (circles, n = 6 mice). Error bars indicate 95% confidence intervals. Percentage was calculated by number of cells in each fate type divided by the total number of unique place cells in R and RElow

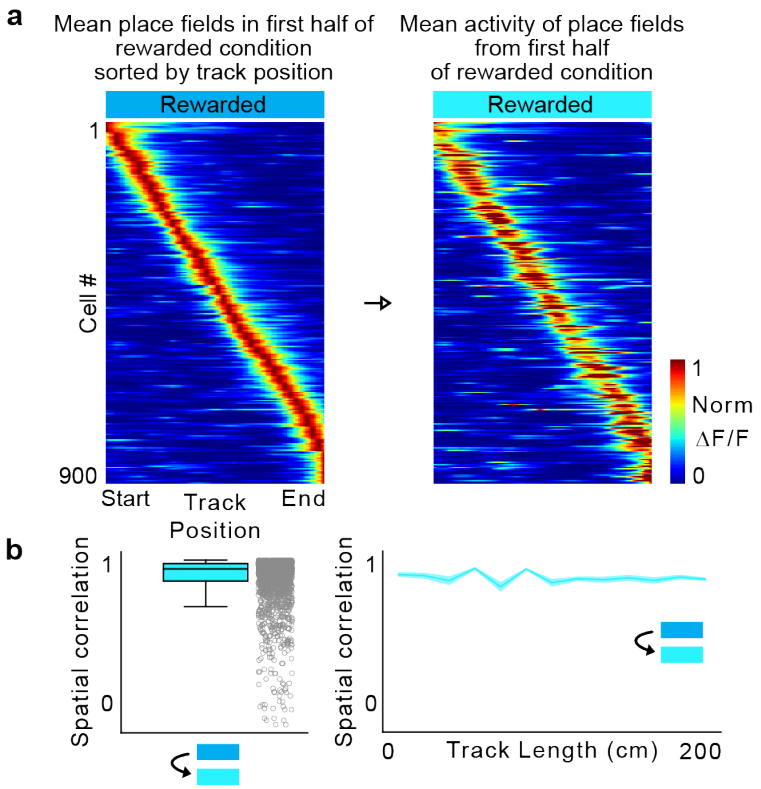

Figure 2.15: **Place fields across time in a rewarded condition.** Control mice (n = 6) were exposed only to the familiar rewarded condition for 15 minutes. The session was divided into two and place fields from the 2 halves were analyzed for changes in place field parameters. **a,** Place fields defined in the first half plotted across the two halves. Place cells were sorted by their center of mass and normalized to their peak in the first half. **b,** Boxplots show distribution of place field spatial correlation between the two halves for cells in **a** (circles).

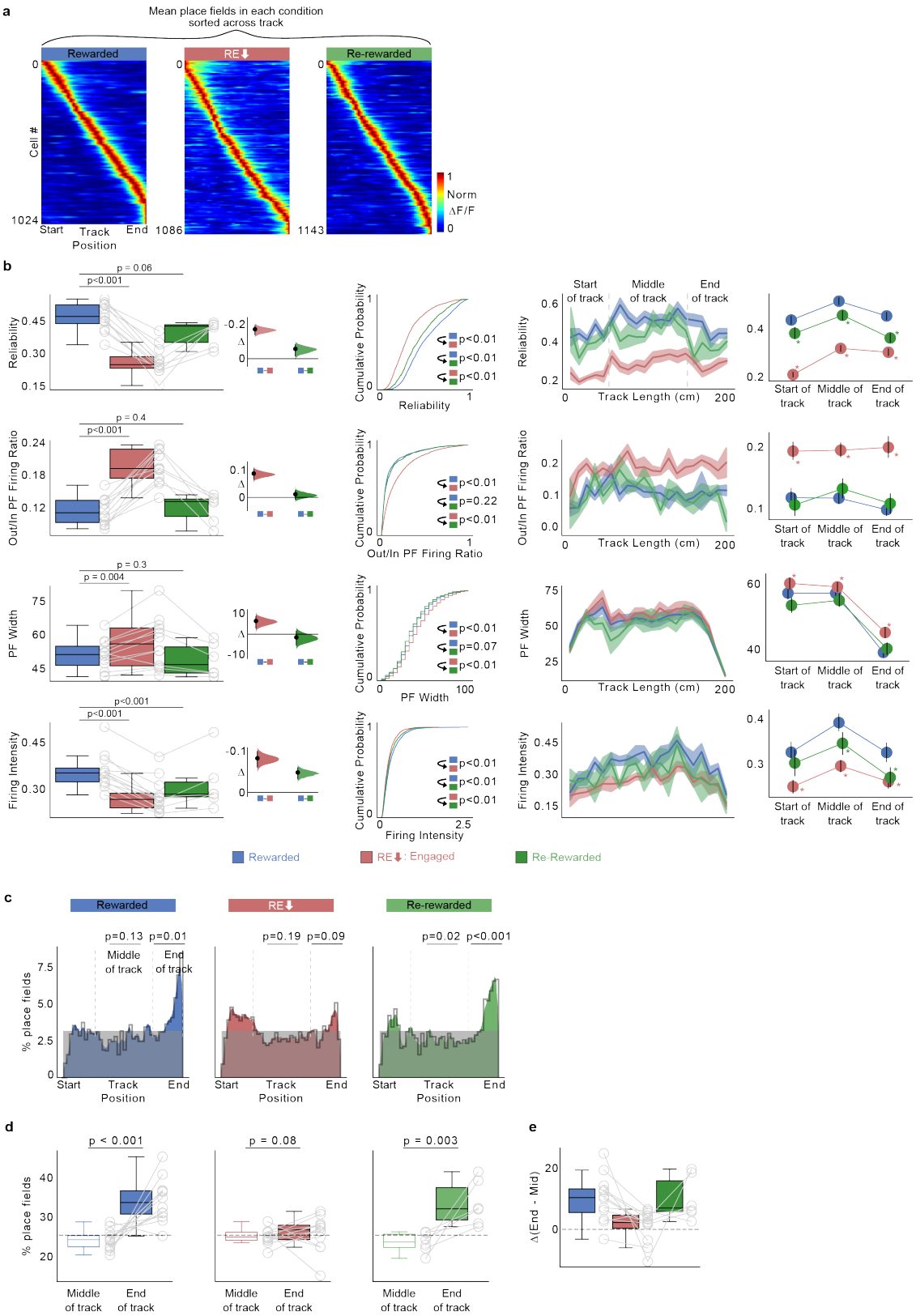

Figure 2.16: **Place field parameters in animals with engaged and disengaged laps**

Figure 2.16, continued: a, Place fields defined and sorted in each condition pooled from all mice (n = 6). Each cell's activity normalized to its peak and cells are sorted by their center of mass along the track. **b,** Place cell parameters in each condition are displayed as boxplot of average per animal (left), Bootstrapped mean differences (Δ) with 95% CI (left, inset), cumulative histogram (middle) and across track location (right). P-values were calculated using two sided paired t-test. Medians: Reliability - R = 0.48, RElow = 0.26, RR = 0.44. Out/In Field Firing - R = 0.10, RElow = 0.19, RR = 0.13. Place field width (cm) - R= 50.21, RElow = 54.96, RR = 45.71. Firing Intensity - R = 0.34, RElow = 0.26, RR = 0.28. All place field calculations in RElow condition were done on engaged and disengaged laps.**c,** Distribution of place field center of mass (COM) locations in each condition pooled from all mice (n = 12 in R and UR, n=6 in RR). Plots show observed density (gray line), uniform distribution (gray shade) and Gaussian distribution of place field density (color). P-values (two sided t-test) were obtained by calculating the place field distribution with the uniform distribution **d,** Percentage of place fields in the middle of the track versus end of the track in each animal (circles). **e,** Difference between end of track and middle of track place field percentages in each animal (circles). P-values were obtained using a two sided paired t-test. Dashed line in d and e indicates the percentage expected from a uniform distribution across the track. In all panels, n = 12 mice in R and RElow, n = 6 mice in RR. All place field calculations in RElow condition were done on Engaged and Disengaged laps

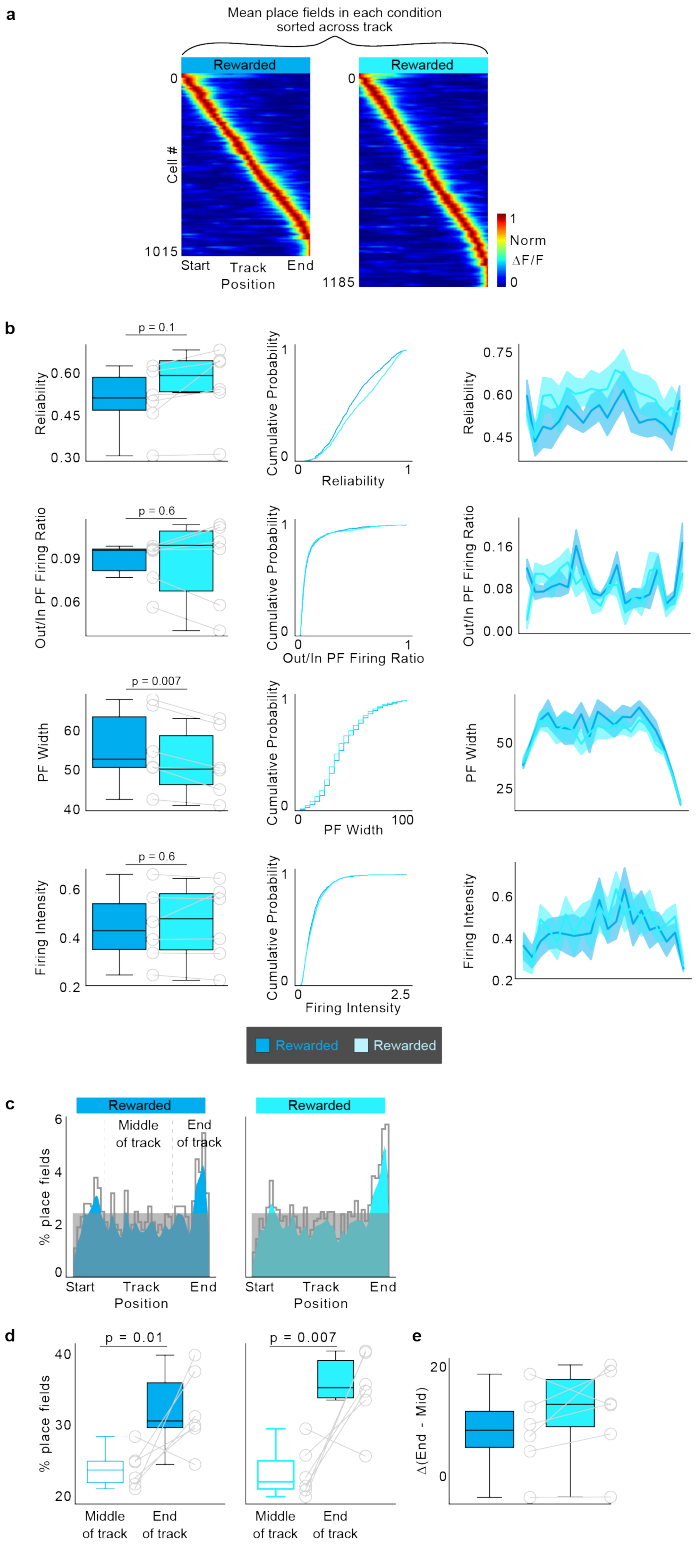

Figure 2.17: **Place field parameters in control animals**

Figure 2.17, continued: a, Place fields defined and sorted in two halves of the rewarded condition (n=6 mice). Each cell's activity normalized to its peak and cells are sorted by their center of mass along the track. **b,** Place cell parameters in each condition are displayed as boxplot of average per animal (left), cumulative histogram (middle) and across track location. Shading indicates s.e.m. (right). P-values were calculated using two sided paired t-test. Medians: Reliability - First half = 0.50, Second half = 0.58. Out/In Field Firing - First half = 0.09, Second half = 0.10. Place field width (cm) - First half = 52.03, Second half = 49.52. Firing Intensity - First half = 0.42, Second half = 0.47. **c,** Distribution of place field center of mass (COM) locations in the two halves pooled from all mice. Plots show observed density (gray line), uniform distribution (gray shade) and Gaussian distribution of place field density (color). **d,** Percentage of place fields in the middle of the track versus end of the track in each animal (circles, n=6 mice). P-values were obtained using two sided paired t-test. **e,** Difference between end of track and middle of track place field percentages in each animal (circles, n=6 mice).

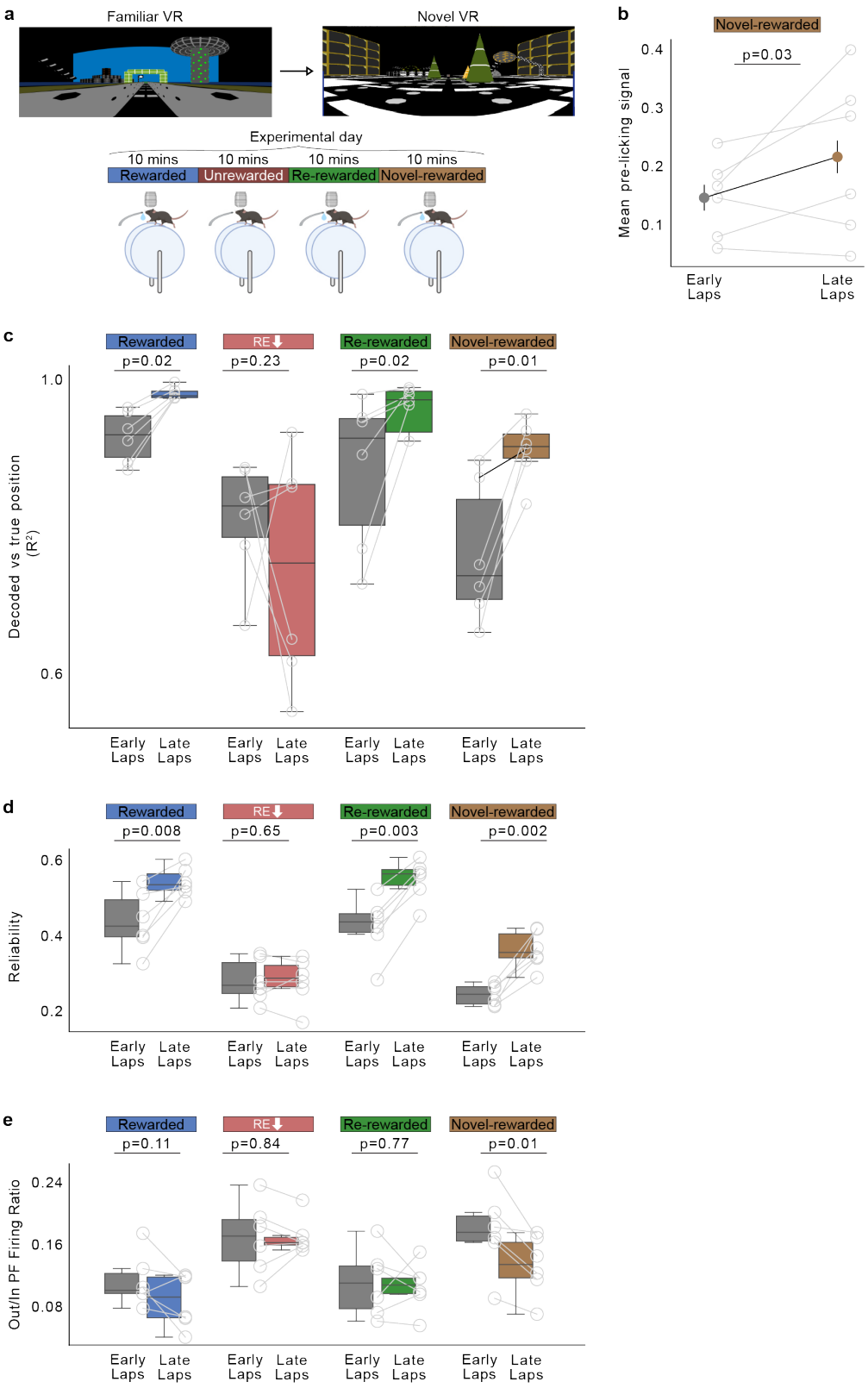

Figure 2.18: **Place field characteristics in a novel environment get better over time.**

Figure 2.18, continued: a, Experiment protocol (n = 6 mice). Bottom image created with BioRender.com. **b,** Average pre-emptive licking in early (first 12) versus late (last 12) laps in the novel-rewarded environment. Error bars indicate 95% CI. Gray circles indicate data from each animal. Licking was calculated similar to Supp Fig 2.6. **c,** Decoders were trained separately on each condition and were cross-validated. Boxplots display decoder R^2 calculated on the early and late laps in each condition and each mouse (gray circles). **d-e,** Boxplots of place cell reliability and out/in field firing ratio in early vs late laps in each session and in each animal (circles) . P-values were obtained using a two sided paired t-test. In all panels, n=6 mice were used.

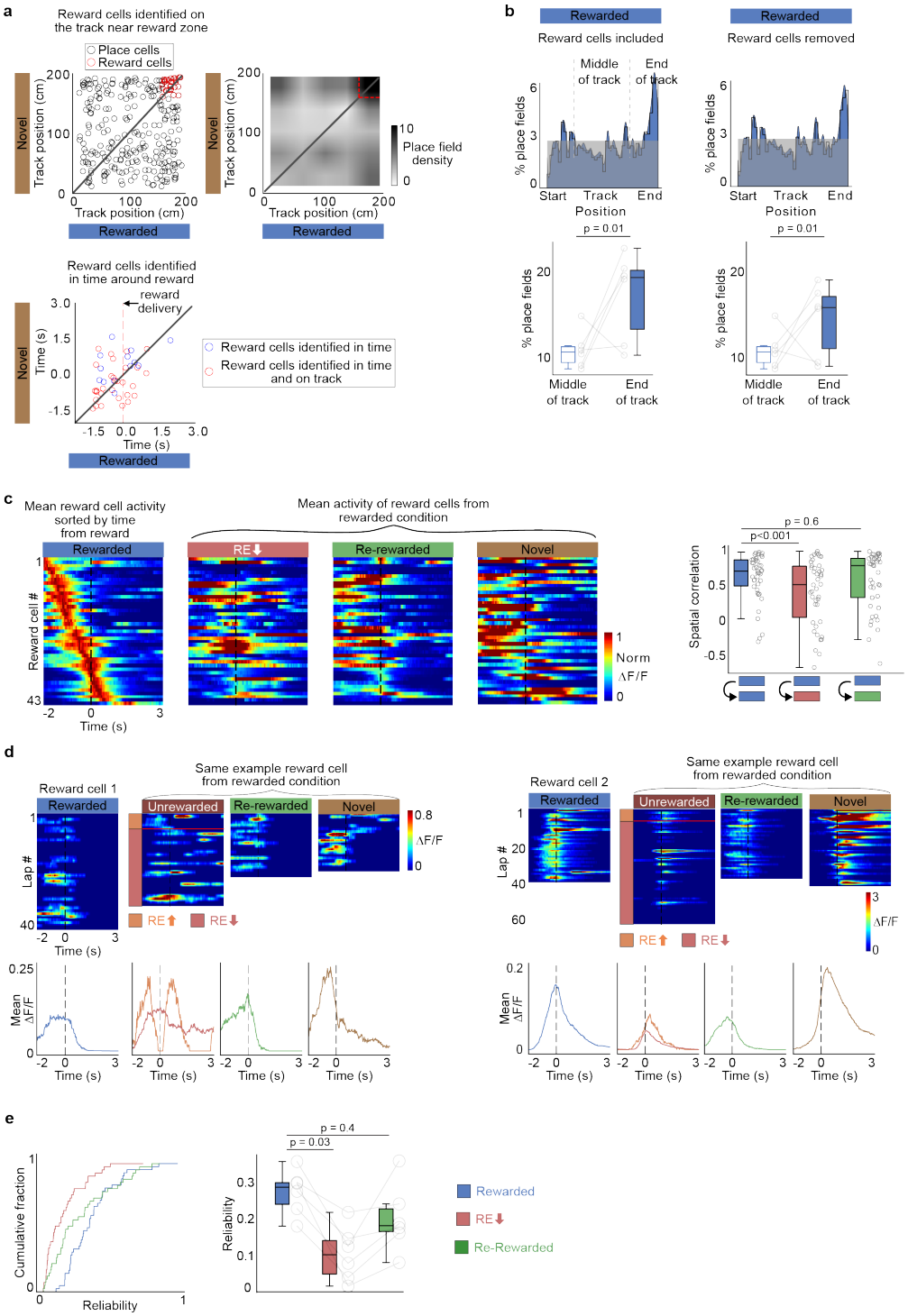

Figure 2.19: **Reward cell encoding is disrupted in the unrewarded condition. a,** (Top left), center of mass (COM) of all cells with place fields (circles) in both R and Novel rewarded conditions from 6 mice (n = 273 cells). In both environments, reward was given at the end of the track and cells that fired around the reward were considered reward cells (30 cells, red circles).

Figure 2.19, continued: **a,** (Top right), density of COMs between the two conditions, spatially binned and smoothed (width 25 cm). Red lines are drawn around the defined reward zone. (Bottom left), time of peak firing of cells from reward delivery. Cells that fired 1.5 seconds before and after reward delivery in both R and Novel conditions were also identified as reward cells (13 cells). Peak firing time of the cells that were identified on the track (top) are colored in red. **b,** (Top), distribution of place field center of mass (COM) in R with and without reward cells. Plots show observed density (gray line), uniform distribution (gray shade) and Gaussian distribution (color). (Bottom), percentage of place fields in the middle versus end of the track. P-values were obtained using a two sided paired t-test (n = 6 mice). **c,** (Left), mean activity of identified reward cells from time of reward delivery (dashed line). Cells (n = 43 reward cells) were sorted by their time of peak firing in R and plotted in the same order in the other conditions. Cells were normalized to their peak firing in R. (Right), boxplots show distribution of correlation coefficient of the same cells (dots) within R and between R and other conditions. P-values were obtained using a two sided paired t-test. **d,** Example of two reward cells. Their lap-by-lap activity is shown on top and average activity at the bottom. Dashed line indicates the time of reward delivery. Red line in UR indicates the lap when the animal stops licking. **e,** Trial-by-trial reliability of reward cells across conditions (See methods) as a cumulative distribution function (left, P-values: two tailed KS-Test) and average per animal (dots, right, n=6 mice). P-values for boxplot distributions in **c** and **e** were obtained using a two sided paired t-test.

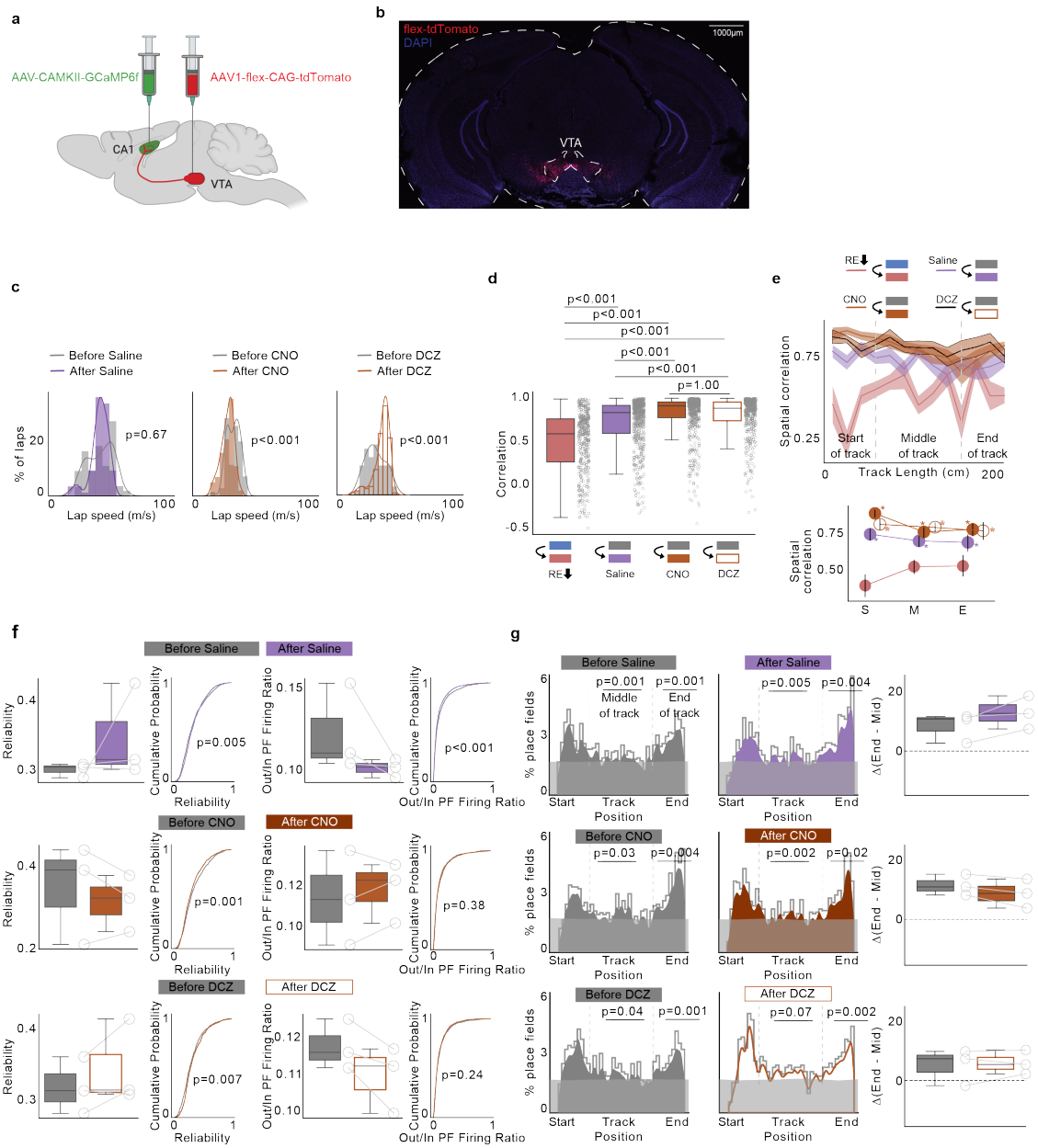

Figure 2.20: **Control mice expressing tdTomato in VTA neurons. a,** Schematic representation of injection procedure (image created with BioRender.com). Control animals (n = 3 mice) went through the exact same protocol as experimental animals. **b,** Representative coronal brain section from 1 of 3 mouse brains expressing tdTomato in VTA. **c,** Distribution of lap speed (m/s) in control animals before and after a manipulation. P-values were obtained using a two sided t-test. **d,** (Top) Boxplots show distribution of place field spatial correlation between activity of place cells, conditions correlated are displayed on the x-axis (circles). Place cells were defined in the former condition P-values were obtained using a two tailed KS-test. (Bottom) Bootstrapped mean differences (Δ) with 95% CI (error bar). X-axis indicates the comparisons made.

Figure 2.20, continued: **e,** (Top) Same data, averaged by track position. Shading indicates s.e.m. (Bottom) Average correlation binned by track position indicated by gray lines in the top panel. S: Start of the track, M: Middle of the track, E: End of the track. * indicates significant p-values (two tailed KS-Test, $p < 0.01$) obtained by comparing UR (red) with other tasks at each position. For **d, e,** Number of place cells: R/RElow. = 512, Before Saline/AfterSaline = 532, Before CNO/After CNO = 423, Before DCZ/After DCZ = 363. **f,** Place cell parameters (reliability - first two panels, out/in field firing ratio - last two panels) displayed as boxplot of average per animal and cumulative histogram (P-values, two tailed t-test). **g,** (left, middle) Distribution of place field center of mass (COM) locations in each condition pooled from all mice. Plots show observed density (gray line), uniform distribution (gray shade) and Gaussian distribution of place field density (color). P-values (two tailed t-test) were obtained by calculating the place field distribution with the uniform distribution. (right) Difference between end of track and middle of track place field percentages in each animal (circles, n=3 mice). Dashed line indicates the difference expected from a uniform distribution across the track.

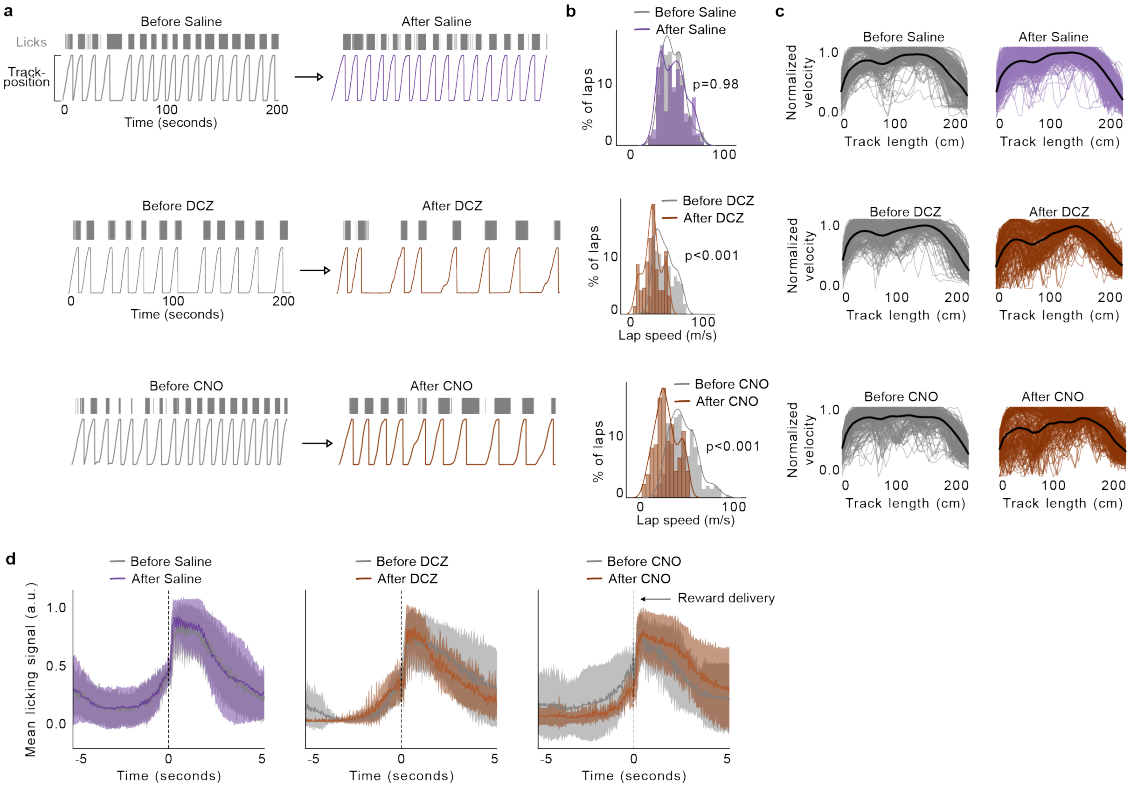

Figure 2.21: **DCZ and CNO administration decreases animals' running speed. a,** Behavior of an example animal. **b,** Distribution of lap speed (m/s) in all animals . Mice showed decrease in lap speed after administration of deschloroclozapine (DCZ) and clozapine-N-oxide (CNO) (n = 5 mice, Saline; n = 6 mice, DCZ, CNO, p-values obtained using two tailed t-test). **c,** Instantaneous velocity for each lap calculated similar to Fig 2.2. **d,** Mean number of licks around reward delivery (time = 0) in each condition. Licking was calculated similar to Supp Fig 2.6. Shading represents s.e.m.

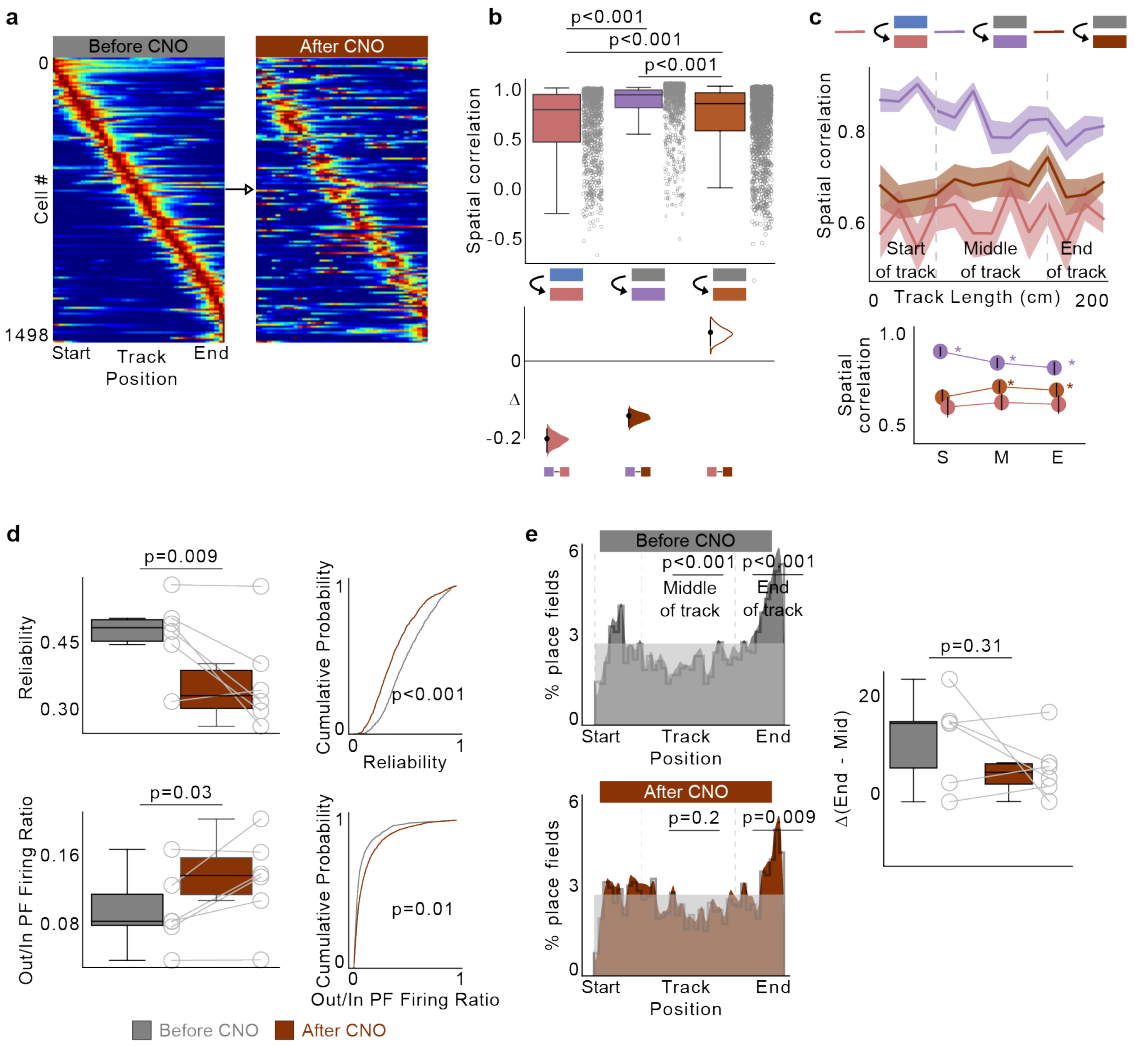

Figure 2.22: **Bilateral inactivation of VTA using CNO. a,** Place fields defined in the Before CNO and plotted across conditions. Activity of each place cell was normalized to peak in the Before conditions and sorted by their center of mass along the track. **b,** (Top) Boxplots show distribution of place field spatial correlation between activity of place cells (circles) in Rewarded/RElow (left), Before Saline/AfterSaline (middle) and Before CNO/After CNO (right, n=1498 place cells). Place cells were defined in the former condition. Pvalues were obtained using two tailed KS-test. (Bottom) Bootstrapped mean differences (Δ) with 95% CI (error bar). X-axis indicates the comparisons made. **c,** top) Same data, averaged by track position. Shading indicates s.e.m. (bottom) Average correlation binned by track position indicated by gray lines in the top panel. S: Start of the track, M: Middle of the track, E: End of the track. * indicates significant p-values (two tailed KS-test, $p < 0.01$) obtained by comparing UR (red) with other tasks at each position. **d,** Place cell parameters in each condition are displayed as boxplot of average per animal (left, n=6 mice) and cumulative histogram (right). P-values were obtained using two tailed paired t-test.

Figure 2.22, continued: e, (left) Distribution of place field center of mass (COM) locations in each condition pooled from all mice. Plots show observed density (gray line), uniform distribution (gray shade) and Gaussian distribution of place field density (color). P-values (two tailed t-test) were obtained by calculating the place field distribution with the uniform distribution.(right) Difference between end of track and middle of track place field percentages in each animal (circles, n=6 mice). Dashed line indicates the difference expected from a uniform distribution across the track. P-values were calculated using a two tailed Wilcoxon signed rank test

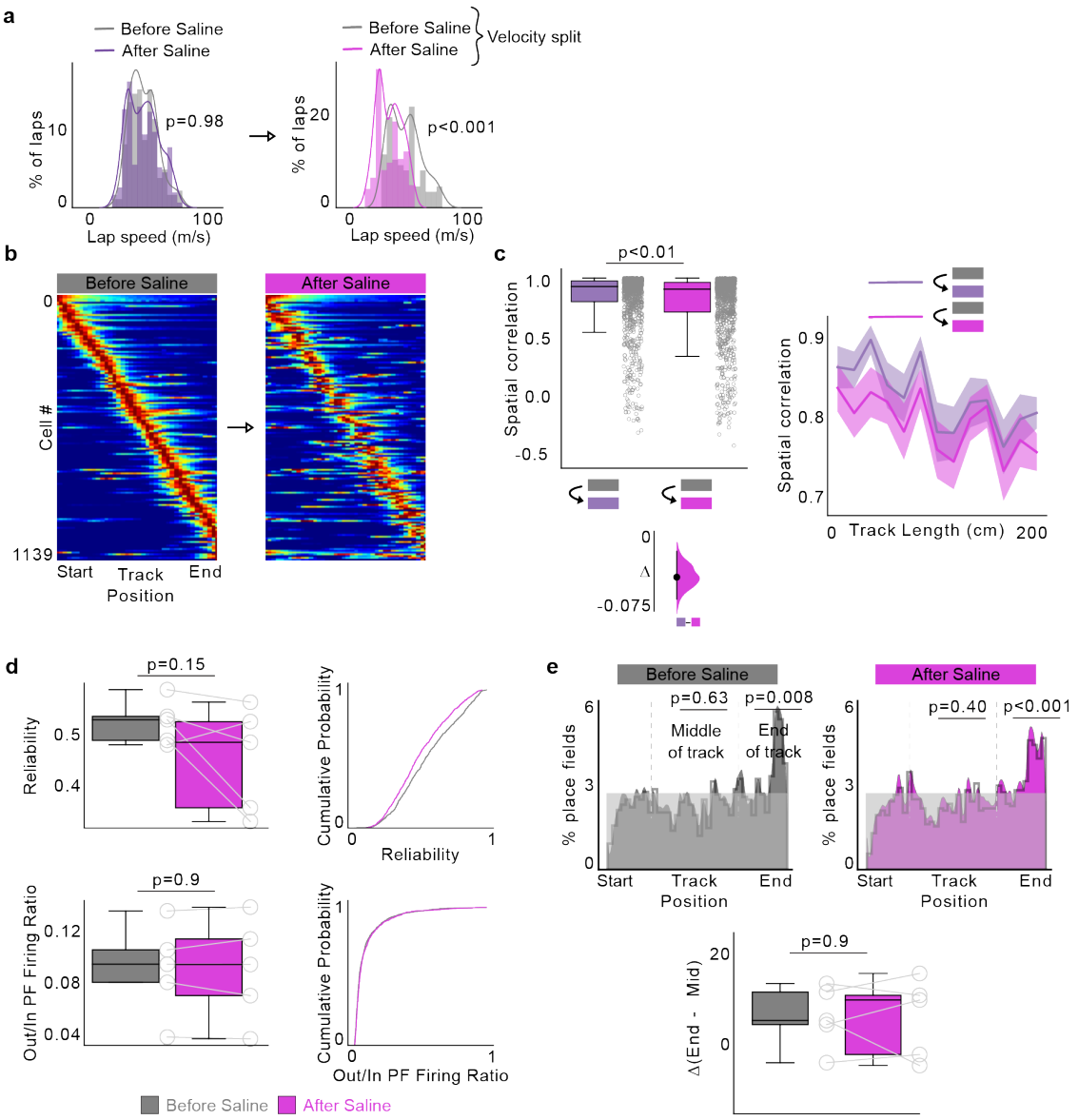

Figure 2.23: **Place cell parameters related to lap speed in Saline condition. a,** Distribution of lap speed (m/s) in all animals (n=5 mice). Original (left) After separating laps by faster laps (in Before Saline) and slower laps (in After Saline). Faster laps were > 60th percentile and slower laps were > 40th percentile mean lap speed. Mean lap speed (ms) [95% CI]: Original: Before Saline 42.74 [41.12 44.36], After Saline 42.75 [41.34 44.17], After velocity split: Before Saline 47.30 [44.69 49.57], After Saline 35.03 [33.46 36.60]. **b,** Place fields defined in the Before condition and plotted across conditions. Activity of each place cell was normalized to peak in the Before condition and sorted by their COM along the track. **c,** Boxplots show distribution of place field spatial correlation between (circles) Before Saline/AfterSaline, original (left) and after velocity split (right), n=1139 place cells.

Figure 2.23, continued: P-values were obtained using a two tailed KS-Test. (Bottom) Bootstrapped mean differences (Δ) with 95% CI (error bar). X-axis indicates the comparisons made. (right) Same data, averaged by track position. Shading indicates s.e.m. **d,** Place cell parameters in each condition are displayed as boxplot of average per animal (left, n=5 mice) and cumulative histogram (right). P-values were obtained using two tailed paired t-test. Medians: Reliability - Before Saline = 0.52, After Saline = 0.48, Out/In Field Firing - Before Saline = 0.09, After Saline = 0.09, Place field width (cm) - Before Saline = 61.07, After Saline = 54.15, Firing Intensity - Before Saline = 0.03, After Saline = 0.03. **e,** (top) Distribution of place field center of mass (COM) locations in each condition pooled from all mice. Plots show observed density (gray line), uniform distribution (gray shade) and Gaussian distribution of place field density (color). P-values (two tailed t-test) were obtained by calculating the place field distribution with the uniform distribution. (bottom) Difference between end of track and middle of track place field percentages in each animal (circles, n=5 mice). Medians: Before Saline = 5.59, After Saline = 10.12. Dashed line indicates the difference expected from a uniform distribution across the track. P-values were calculated using a two tailed Wilcoxon signed rank test.

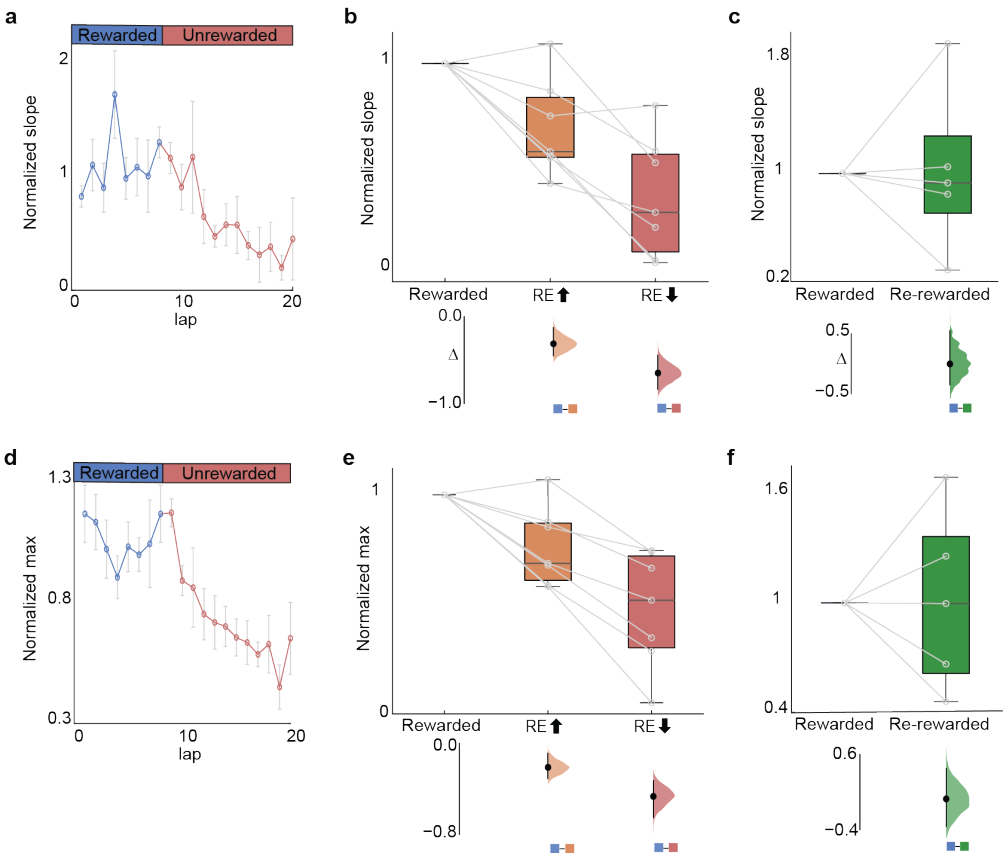

Figure 2.24: **Slope and Max of VTA ramps depend on reward expectation. a,** Mean slope for laps in the Rewarded and Unrewarded conditions for all axons, error bars represent s.e.m (7 axons in 6 mice). **b,** Boxplot shows distribution of mean slope in each axon within different conditions (n = 7 axons, Mean: slope: R = 1.00 , REhigh = 0.69 , RElow = 0.35). P-values were obtained using a two-sided paired t-test, with Bonferroni post hoc performed to correct for multiple comparisons. Bootstrapped mean differences (Δ) with 95% CI (error bar) are shown at the bottom. X-axis indicates the comparisons made. **c,** Boxplot shows distribution of mean slope*max in each axon (circles, n = 5 axons in 5 mice) within R and RR conditions (circles, n = 5 axons, Mean: slope: R = 1.00 , RR = 1.01. P-values were obtained using a two-sided paired t-test. (Bottom) Bootstrapped mean differences (Δ) with 95% CI (error bar). X-axis indicates the comparisons made. **d,** Mean max for laps in the Rewarded and Unrewarded conditions for all axons, error bars represent s.e.m (7 axons in 6 mice). **e,** Boxplot shows distribution of mean max in each axon within different conditions (circles, n=7 axons, Mean : max: R = 1.00, REhigh = 0.79, RElow = 0.53). P-values were obtained using a two-sided paired t-test, with Bonferroni post hoc was done to correct for multiple comparisons. Bootstrapped mean differences (Δ) with 95% CI (error bar) are shown at the bottom. X-axis indicates the comparisons made. (F) Boxplot shows distribution of mean max value of each axon R and RR conditions (circles, n = 5 axons, Mean: max: R = 1.00, RR = 1.01). P-values were obtained using a two-sided paired t-test. (bottom) Bootstrapped mean differences (Δ) with 95% CI (error bar). X-axis indicates the comparisons made.

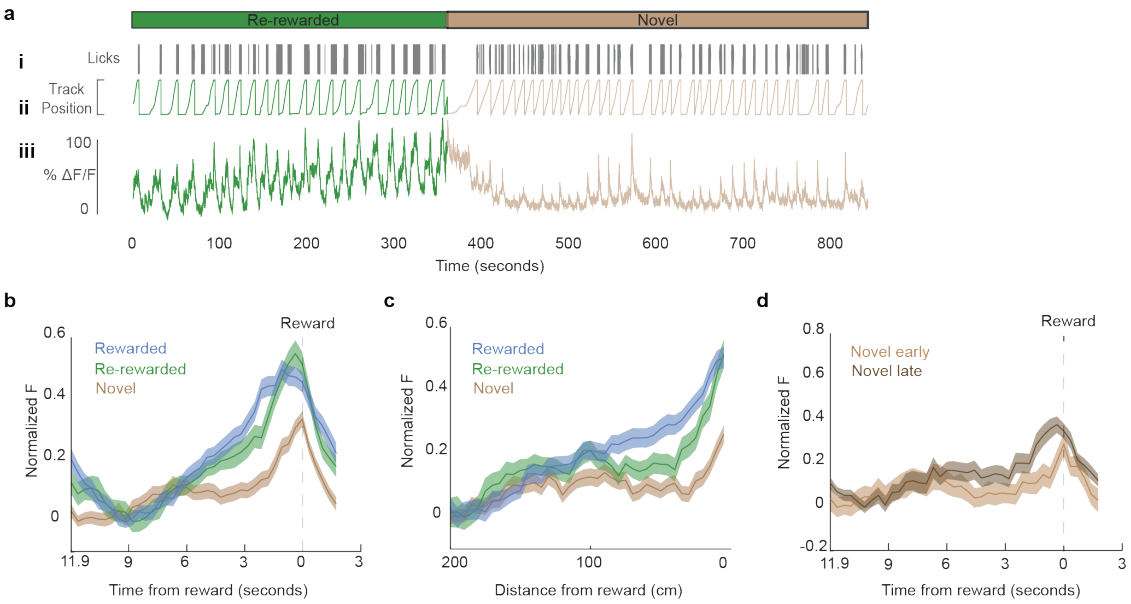

Figure 2.25: **VTA activity is shaped by continued reward delivery in Novel environments. a,** Example mouse. i: Mouse licking behavior. ii: Mouse track position. iii: $\Delta F/F$ from an example ROI. **b,** Fluorescent time binned activity of axons (5 axons in 5 mice) in the R (blue), RR (green), and Novel (brown) experimental conditions averaged by time to reward. **c,** Same data, averaged by position. **d,** Novel time binned fluorescent activity divided into early (light green) and late laps (dark green) and averaged by time to reward. Shaded area represents s.e.m

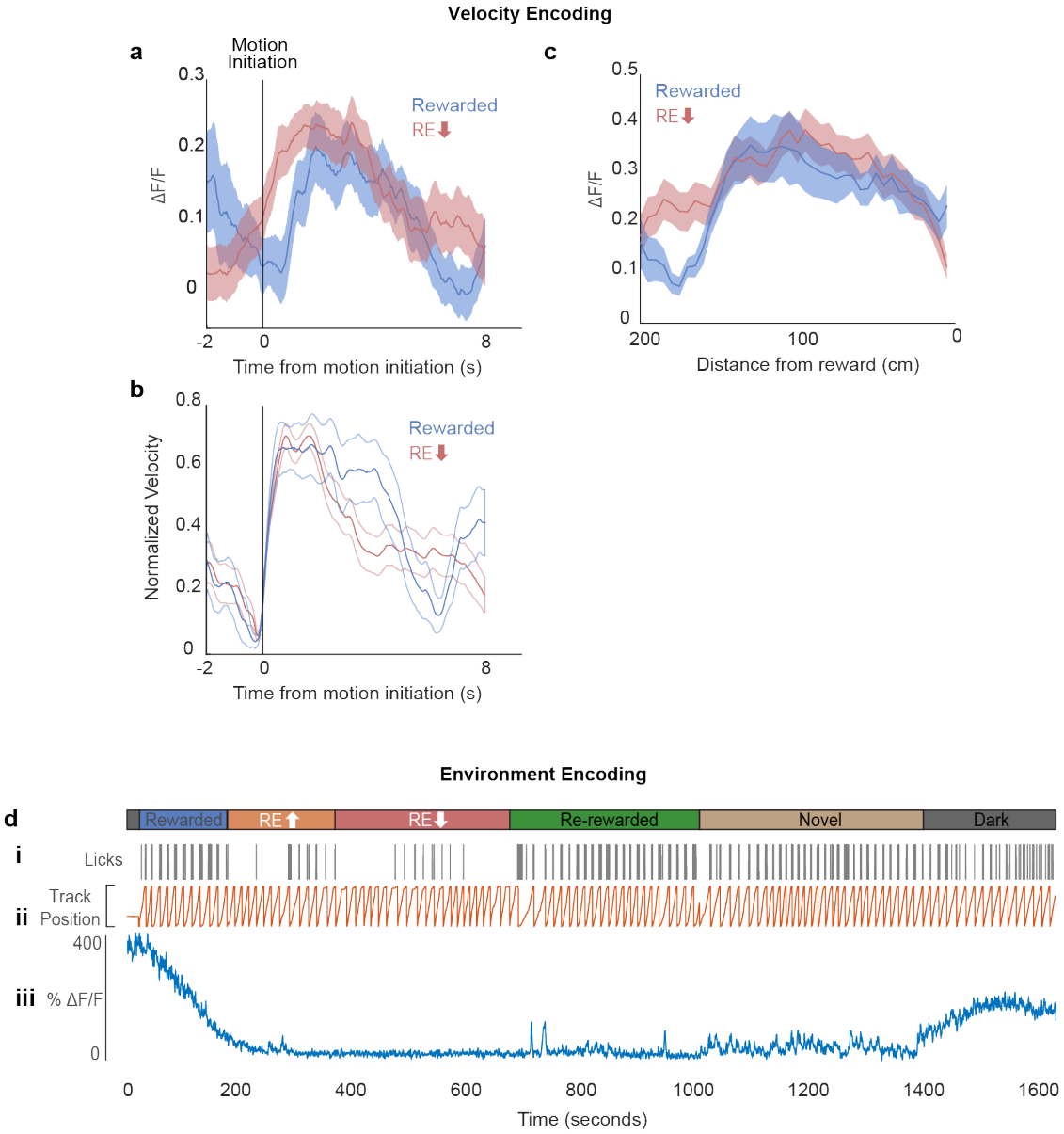

Figure 2.26: **Heterogeneity in VTA DA inputs to dCA1. a,** Fluorescent activity of VTA axon in the Rewarded (blue) and RElow (red) experimental conditions aligned to initiation of motion and averaged by time from motion initiation. Shaded areas represent s.e.m. **b,** Velocity of mouse in the Rewarded (blue) and RElow (red) experimental conditions aligned to initiation of motion, averaged by time from motion initiation and normalized by the max velocity for that motion epoch. **c,** Same data as **a**, averaged by position along track. Shaded areas represent s.e.m. **d,** Example of environment specific activity in axon. i: Mouse licking behavior. ii: Mouse track position. iii: $\Delta F/F$ from an example ROI.

CHAPTER 3

DISTINCT SETS OF DOPAMINERGIC INPUTS IN HIPPOCAMPAL CA1 TRANSMIT CONTRASTING SIGNALS DURING BEHAVIOR IN A CHANGING WORLD

3.1 Abstract

Dopaminergic activity within the hippocampus plays a pivotal role in shaping synaptic plasticity, influencing the activity of hippocampal neurons, and impacting the processes involved in learning and memory. Traditionally, these effects were attributed to the release of dopamine from sparse projections originating in the ventral tegmental area (VTA) and extending to the hippocampus. However, recent discoveries have unveiled dopamine is also released from inputs originating in the locus coeruleus (LC). To dissect the impacts of both VTA and LC dopaminergic circuits on hippocampal function and memory, a thorough examination of how these pathways might divergently operate during behavior and learning is necessary. We therefore utilized 2-photon microscopy to functionally capture the activity of VTA and LC axons within the CA1 region of the dorsal hippocampus in mice that were head-fixed and navigating linear paths within virtual reality (VR) environments. Within familiar environments, as mice approached previously learned rewarded locations, VTA axons in CA1 exhibited a gradual ramping-up of activity, peaking at the reward location. In contrast, LC axons in CA1 displayed a correlation with the animals' running speed and a pre-movement signal, devoid of the ramping-to-reward dynamics observed in VTA axons. A marked divergence emerged in novel VR environments. LC axon activity sharply and persistently increased for over a minute, while the previously observed VTA axon ramping-to-reward dynamics disappeared. In conclusion, these findings highlight distinct roles of VTA and LC dopaminergic inputs in the dorsal CA1 hippocampal region. These inputs encode unique information, likely contributing to differential modulation of hippocampal activity

during behavior and learning.

3.2 Introduction

Within the hippocampus there are pyramidal neurons known as place cells that selectively fire action potentials at specific locations in an environment (J. O'Keefe and Dostrovsky 1971). Together, populations of these neurons are thought to serve as the neural basis of a cognitive map, or an internal representation of an external environment, allowing animals to acquire, store, code, and recall information about environments (John O'Keefe and Nadel 1978). In support of this idea, place cells flexibly encode both external environmental cues and internal contextual variables, as they are modulated by odors(Save, Nerad, and Bruno Poucet 2000; S. Zhang and Denise Manahan-Vaughan 2015), colors (Leutgeb 2005), novelty (Larkin et al. 2014), time (Eichenbaum 2017), engagement (Pettit, Yuan, and Harvey 2022), and reward expectation (Krishnan et al. 2022). Changing object or reward locations causes some individual place cells to remap (Bourboulou et al. 2019; Gauthier and Tank 2018), or change their firing locations, while exposure to a novel environment causes the entire population of place cells to remap (Dong, Madar, and M. E. J. Sheffield 2021; Mark E.J. Sheffield, Adoff, and Daniel A. Dombeck 2017). It is thought that neuromodulatory inputs help promote the plasticity required for this flexible encoding of place cells(Duszkiewicz et al. 2019), however, the precise circuit mechanisms driving these processes is not well understood.

Dopaminergic activity in the dorsal hippocampus has been shown to play a wide range of roles in learning and memory, impacting formation and persistence of spatial memories (Silva et al. 2012), reward-location associations (Retailleau and G. Morris 2018)), aversive conditioning (Tsetsenis et al. 2019), and the encoding of novel environments (N. Hansen and D. Manahan-Vaughan 2014; Lemon and D. Manahan-Vaughan 2012; S. Li et al. 2003). In support of these findings, hippocampal dopamine can bidirectionally alter synaptic plasticity (Huang and Kandel n.d.; Hagena and Denise Manahan-Vaughan 2013; N. Hansen and D.

Manahan-Vaughan 2014; Chu et al. 2011) and cell excitability (Edelmann and Lessmann 2018) and influence the formation and stability of hippocampal place cells (Kentros et al. 2004; Retailleau and G. Morris 2018)(Morris 2018, kentros 2004). These effects were originally attributed to release of dopamine (DA) from inputs from the ventral tegmental area (VTA), a midbrain region that is part of the brains reward circuitry. VTA DA inputs to the dorsal hippocampus mainly innervate stratum oriens (Takeuchi et al. 2016; Adeniyi, Shrestha, and Ogundele 2020; Adeyelu and Ogundele 2023), and their activity bidirectionally modulates Schaffer Collateral synapses (Rosen, Cheung, and Siegelbaum 2015), enhances persistence of reward-location associations (McNamara et al. 2014), and drives place preference (Mamad et al. 2017). Their activity also biases place fields to a location (Mamad et al. 2017), improves place field stability across days (McNamara et al. 2014), and drives reward expectation dependent enhancement of place field quality (Krishnan et al. 2022). However, VTA DA inputs to dCA1 are relatively sparse (Takeuchi et al. 2016; Wagatsuma et al. 2018; Adeniyi, Shrestha, and Ogundele 2020; Adeyelu and Ogundele 2023) and it has recently been shown that DA is also released into the hippocampus by inputs from the locus coeruleus (LC) (Kempadoo et al. 2016; Takeuchi et al. 2016), a brainstem nucleus well known for its roles in arousal and attention (Aston-Jones and Bloom 1981; McCarley and Hobson 1975). Many of the effects of DA modulation of the hippocampus have now been attributed to LC inputs as their activity enhances the strength of Schaffer Collateral synapses (Takeuchi et al. 2016), improves memory retention (Kempadoo et al. 2016), improves place field stability across days (Wagatsuma et al. 2018), and can bias place fields to a location when paired with a reward (Kaufman, Geiller, and Losonczy 2020) through DA mechanisms. Although many of the effects of LC and VTA are overlapping potentially indicating shared mechanisms of action, they are believed to play different roles in spatial learning and memory (Duszkiewicz et al. 2019). LC inputs influence the encoding of novel environments (Kempadoo et al. 2016; Wagatsuma et al. 2018), while VTA DA inputs increase persistence of reward context as-

sociation (McNamara et al. 2014) and can bias place preference (Mamad et al. 2017). It is possible that these differences arise because of the differences in activity observed between LC and VTA DA neurons. Therefore, characterizing the encoding properties of LC and VTA inputs directly in the hippocampus during navigation and spatial learning would provide important insights into the specific roles of these distinct DA inputs.

Recent findings indicate considerable heterogeneity in the activity of VTA (Engelhard et al. 2019) and LC (Uematsu et al. 2017; Noei et al. 2022; Chandler, Gao, and Waterhouse 2014) neurons, highlighting the need for projection specific recordings. Therefore, we functionally imaged VTA DA and LC axons in dCA1 of mice as they navigated familiar and novel virtual reality (VR) environments for rewards. We observed distinct encoding properties between these sets of inputs during navigation and in response to novel environments. VTA DA axons ramped in activity during approach of a learned rewarded location, while LC axon activity did not show ramping-to-reward signals and instead predicted motion onset and correlated with animal velocity. Following exposure to a novel environment, VTA axon ramping-to-reward signals greatly reduced but LC axon activity sharply increased. These findings support distinct roles for VTA and LC inputs to the hippocampus in spatial navigation of rewarded and novel environments.

3.3 Results

To record the activity of dopaminergic inputs to the dorsal hippocampus, we expressed axon-GCaMP6s or axon-GCaMP7b in LC or VTA neurons of different mice. We utilized the NET-cre mouse line (Wagatsuma et al. 2018) to restrict expression to norepinergic LC neurons, and the DAT-Cre line (Zhuang et al. 2005) to restrict expression to dopaminergic VTA neurons (Fig 3.1B). Mice were then headfixed and trained to run a linear virtual reality (VR) track for water rewards delivered at the end of the track (Fig 3.1A). Following reward delivery, mice were teleported to the beginning of the track and allowed to complete another

lap. On experiment day, mice navigated the familiar, rewarded VR environment for 10 min while 2-photon microscopy was used to image the calcium activity of LC (90 axons from 22 imaging sites in 16 mice) or VTA (7 axons from 7 imaging sites in 7 mice) axons in the dorsal CA1 (Fig 3.1C). Based off the z-axis depth of the recording planes, and the presence of increased autofluorescence in stratum pyramidal, we determined all 7 VTA axons were in *Stratum Oriens*, while for LC recordings, 18 sessions(81 axons in 11 mice) occurred in *Stratum Oriens* and 5 sessions (9 axons in 5 mice) in *Stratum Pyramidalis*. Example VTA (left, orange) and LC (right, blue) axon calcium activity aligned to the animal's behavior are shown in Fig 3.1D. Axons from both brain regions showed periodic activity linked to the animals' exploration of the VR environment.

3.3.1 Distinct activity dynamics in VTA and LC inputs during rewarded navigation of a familiar environment

To examine axon activity further, we first looked at the mean activity of axons as a function of track position (Fig 3.1E). As previously reported (Krishnan Heer), these VTA DA axons increase activity along the track, peaking at the reward location at the end of the track. In contrast, LC input activity remains relatively constant across all positions along the track (Fig 3.1Eii). To examine if this difference could be due to the lower sample size of VTA axons compared to LC axons, the LC axons were down-sampled to match the VTA sample size (n = 7) and the slope and intercepts of the down-sampled data was found. This was repeated 1000 times and did not generate any LC datapoints that overlap with VTA data demonstrating the difference in relationship between position and activity was not due to the different sample sizes (Fig 3.1Eiii). We also examined the position related activity of individual VTA and LC axons and observed a positive relationship between position and activity in 85.7% of VTA axons (6/7) but only 27.8% of LC axons (25/90) while 41.1% of LC axons (37/90) had a negative relationship between position and activity (Fig 3.1E.iv.).

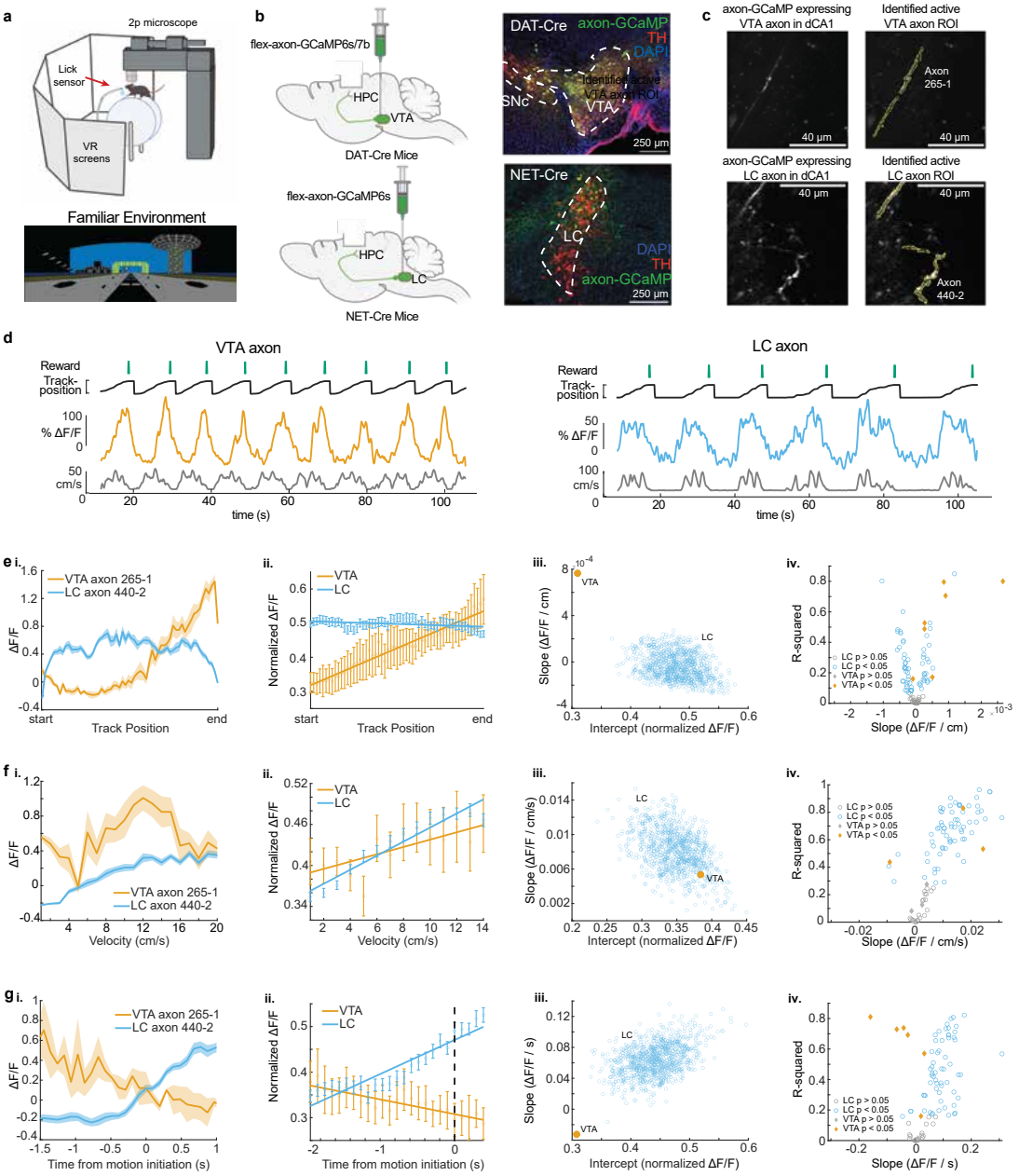

Figure 3.1: **Distinct activity dynamics in VTA and LC axons during navigation of familiar environments a,** Experimental setup (top), created with BioRender.com. Example virtual reality environment. **b,** Schematic representation of injection procedure (left). Representative coronal brain sections immunostained for Tyrosine Hydroxolase (TH) from a DAT-Cre mouse showing overlapping expression of axon-GCaMP (green) and TH (red) in VTA neurons (top) and from a NET-Cre mouse showing overlapping expression of axon-GCaMP(green and TH (red) in LC neurons (bottom).

Figure 3.1, continued: c,. Example CA1 field of view of VTA axons (top) and LC axons (bottom). Extracted regions of interest used for example VTA and LC activity throughout the figure. **d,** Example DAT-Cre mouse (left) and NET-Cre mouse (right) with aligned reward delivery (top, green), mouse track position (black), $\Delta F/F$ from example roi (VTA-orange, LC-blue), and mouse velocity (bottom, gray). **e, i,** Position binned $\Delta F/F\pm$ s.e.m in example VTA (orange) and LC (blue) ROIs during navigation of the familiar rewarded environment. **ii,** Population average position binned $\Delta F/F\pm$ s.e.m. in VTA ROIs (orange, n = 7 ROIs in 7 mice) and LC ROIs (blue, n = 90 ROIs from 27 sessions in x mice) . Linear regression analysis (on all data points, not means) shows that the population of VTA ROIs increase activity during approach of the end of the track while the population of LC ROIs have consistent activity throughout all positions. Linear regression, F test, VTA, $P < 1e{-}21$, LC, $P < 0.01$. **iii,** The LC data set was resampled 1000x using n = 7 axons to match the number of VTA Rois and the slope and intercept of the regression line were measured each time (blue dots). The VTA slope is steeper than all LC slopes indicating a stronger positive relationship between position and activity for VTA inputs. **iv**, Linear regression of position binned activity of individual VTA (orange diamonds), and LC (blue, circles) axons. The majority (4/7) of VTA axons show a significant positive relationship with position while LC axons show both a positive (25/90) and negative (37/90) relationship. **F, i,** Same example ROIs as (d) binned by velocity. **ii,** Same data as (d, ii,) binned by velocity. Linear regression shows that the population of VTA and LC ROIs have a significant relationship with velocity. Linear regression, F test, VTA, $P < 0.05$, LC,$P < 1e-68$. **iii,** Resampling shows the VTA slope and intercept is within the resampled LC slopes and intercepts indicating similar relationships with velocity. **iv,** Linear regression of individual VTA and LC axons shows the majority (65/90) of LC axons have a significant positive relationship with velocity while only 2 VTA axons show this relationship. **g,** Same example ROIs as (d) aligned to motion onset. **ii,** Same data as (d, ii,) aligned to motion onset. Linear regression shows that the population of VTA axons have a negative slope prior to motion onset while LC axons have positive slope. Linear regression, F test, VTA, $P < 0.01$, LC, $P < 1e-65$. **iii,** Resampling shows the VTA slope is negative while all resampled LC slopes are positive. **iv,** Linear regression of individual VTA and LC axons shows the majority (58/90) of LC axons have a significant positive slope prior to motion onset while the majority (4/7) of VTA axons have a negative slope.

Next, we investigate the mean activity of these axons at different velocities. The population mean of both VTA and LC axons increased as velocity increased (Fig 3.1F). This is consistent with the findings that LC inputs to dCA1 encode velocity (Kaufman, Geiller, and Losonczy 2020) and the findings that highlight kinematic encoding in DA VTA neurons (Engelhard et al. 2019). Again, to account for differences in sample size, we down sampled the LC axons 1000 times and found the slope and y-intercept of each sampling. The overlap of the VTA and LC slopes and intercepts confirms we cannot conclude any differences in

velocity related activity in the VTA and LC axon populations (Fig 3.1Fiii). However, when we examine this activity in individual VTA and LC axons we observe a positive relationship between velocity and activity in the majority, 72.2%, of LC axons (65/90) but only 28.6% (2/7) of VTA axons showed a positive relationship with velocity. (Fig 3.1F.iv). The strong velocity correlated activity in a small subset of VTA DA axons may indicate heterogeneity in the activity of these inputs similar to what is observed in VTA DA cell bodies (Engelhard et al. 2019).

Finally, we examined the activity of LC and VTA axons during rest and the transition to movement. The population of LC axons ramped up in activity during the 2s leading up to motion onset (Fig 3.1G). This is consistent with reports of activity of LC axons in cortical areas (Reimer et al. 2016) showing LC activity prior to motion onset. In contrast, VTA axons show decreasing activity during the 2 s leading up to motion onset (Fig 3.1G). This ramping down in VTA axon activity is likely due to most (x%) periods of immobility occurring between reward delivery and the start of the next lap, during which we previously demonstrated reward related activity ramps down in VTA axons (Krishnan et al. 2022). These differences in activity are not an artifact of lower sample size of VTA axons as shown by down-sampling the LC axon activity 1000 times and measuring the slopes and intercepts of the down-sampled data did not generate any data points that overlapped with the VTA slope and intercept (Fig 3.1G.iii). In further support of distinct activity profiles leading up to motion onset, we found that the majority (4/7) of VTA axons decreased in activity leading up to motion onset but only 3/90 LC axons decreased in activity, while the majority, (58/90), of LC axons increased in activity leading up to motion onset (Fig 3.1G.iv). Together, this analysis demonstrates overlapping but distinct activity in VTA and LC neurons during spatial navigation with VTA axons showing strong activity correlated with position related to reward location and some velocity correlated activity, while LC axons demonstrate activity correlated to velocity and time to motion onset.

3.3.2 Environmental Novelty induces activity in LC but not VTA inputs

Following 10 minutes in the familiar environment, mice were teleported to a novel VR environment of the same track length, with a reward at the same position at the end of the track. Following teleportation, we found the running speed of mice decreases (Fig 3.2A) and they spend less time immobile (Fig 3.2A), demonstrating mice recognize they are navigating a novel environment.

We aligned VTA and LC axon activity to the switch to the novel environment and investigated changes in activity due to exposure to novelty. To test whether the mean axon activity is significantly elevated or lowered, we defined a baseline in which to compare to by generating 1000 shuffles of the axon traces across the entire recording sessions, downsampling the shuffled data 1000 times to match the VTA (n = 7) and LC (n = 90) sample sizes, and calculating the mean and 95% CI of the shuffled data. After teleportation, the periodic activity observed in the mean of VTA axons, likely reflecting ramping-to-reward signals in each individual axon, decreases dramatically (Fig 3.2B). This is evident in the traces of most of the individual VTA axons showing a loss of the ramping-to-reward signal, as we have previously shown (Krishnan et al. 2022) (Fig 3.2C).

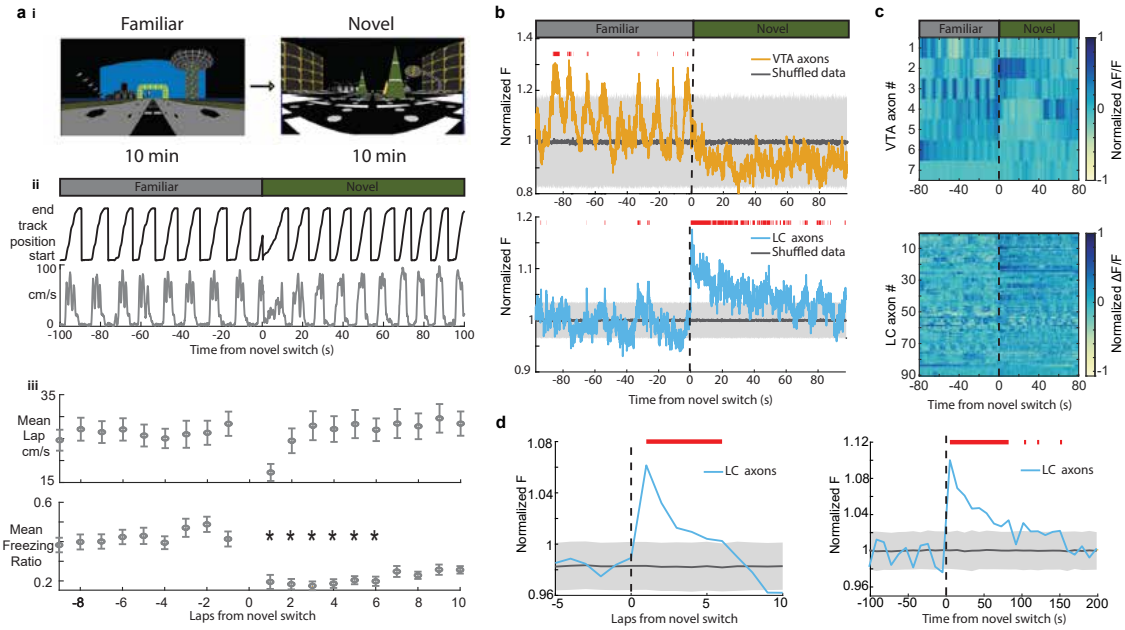

Figure 3.2: **Strong environmental novelty induced activity in LC but not VTA inputs to dCA1 a, i,** Experimental Paradigm. **ii,** Behavior from example mouse during the transition from the familiar VR environment to a novel VR environment showing the animals track position (top, black) and velocity (bottom, gray). **iii,** The average running velocity ± s.e.m. of all mice during the transition to a novel VR environment (top). The average freezing ratio of all mice ± s.e.m., calculated as the time spent immobile (velocity < 5cm/s) divided by the total lap time. Each lap was compared to the first lap in F using a one-way ANOVA with Tukey HSD post hoc test. * $P < 0.05$ **b,** Mean normalized F of all VTA ROIs (top, n = 7) and LC ROIs (bottom, n = 90) aligned to the switch to the novel environment. To define a baseline and 95% CI (gray shaded region), 1000 shuffles were created from the calcium traces and down sampled to match the sample size and averaged. This was repeated 1000 times and the mean and 95% CI of this shuffled data was determined for each frame. Red lines indicate periods where two or more consecutive frames passed above the % CI of the shuffled baseline. **c,** Normalized $\Delta F/F$ activity of all VTA ROIs (top) and LC ROIs (bottom) aligned to the switch to the novel VR environment. **d,** The normalized fluorescence of all LC ROIs binned by lap (left) or into 50 frame bins (right). The baseline and 95% CI (gray shaded region) was defined using the same method as in (b) Red lines indicate bins above the baseline 95% CI.

Strikingly, LC axons show a dramatic increase in mean activity that remains elevated for $>$ 1 minute following exposure to the novel environment (Fig 3.2B) similar with findings that LC cell body activity is elevated for minutes following exposure to environmental novelty (Takeuchi et al. 2016). This increase in activity can be seen in many, but not all the individual

LC axons (Fig 3.2C). To further characterize this activity, we found the mean population activity for each lap and separately for 10s bins leading up to and following exposure to the novel environment. This method shows that LC activity is significantly elevated above baseline for 6 consecutive laps and 90s following exposure to the novel environment (Fig 3.2D). These findings demonstrate that LC inputs signal environmental novelty, supporting a role for these inputs in novelty encoding in the hippocampus.

3.3.3 Novelty-induced changes in behavior explains the late but not early increases in LC activity

It is possible that the change in behavior in the novel environment could explain the increase in LC activity in the novel environment, as LC activity is related to behavior (Fig. 3.1). For instance, LC axons show elevated activity during motion versus rest. Therefore, an increase in the time spent in motion upon exposure to the novel environment could lead to an increase in LC activity. To account for the differences in behavior between the two environments we removed any periods where the mice were immobile to isolate the effects of novelty without confounds due to differences in behavior (Fig 3A). We found that LC axon activity is elevated for 2 laps, or 40s, in the novel environment (Fig 3.3B-E). This indicates that there are two separate components that drive LC axon activity during the initial exposure to the novel environment. One, a shorter purely novelty-induced increase in activity which occurs during the first 2 laps, or about 40s, in the novel environment. Two, a behavior-induced increase in LC activity that extends beyond the increase in the novelty-induced activity for laps or 90s. If the novelty-induced signal is an additional signal riding on top of the behavior correlated signals - position , velocity, and motion onset – we would expect a disruption to these behavior correlations.

Indeed, the slopes of the position binned, velocity binned, and motion onset aligned data are all significantly more negative in the first lap in the novel environment than the final laps

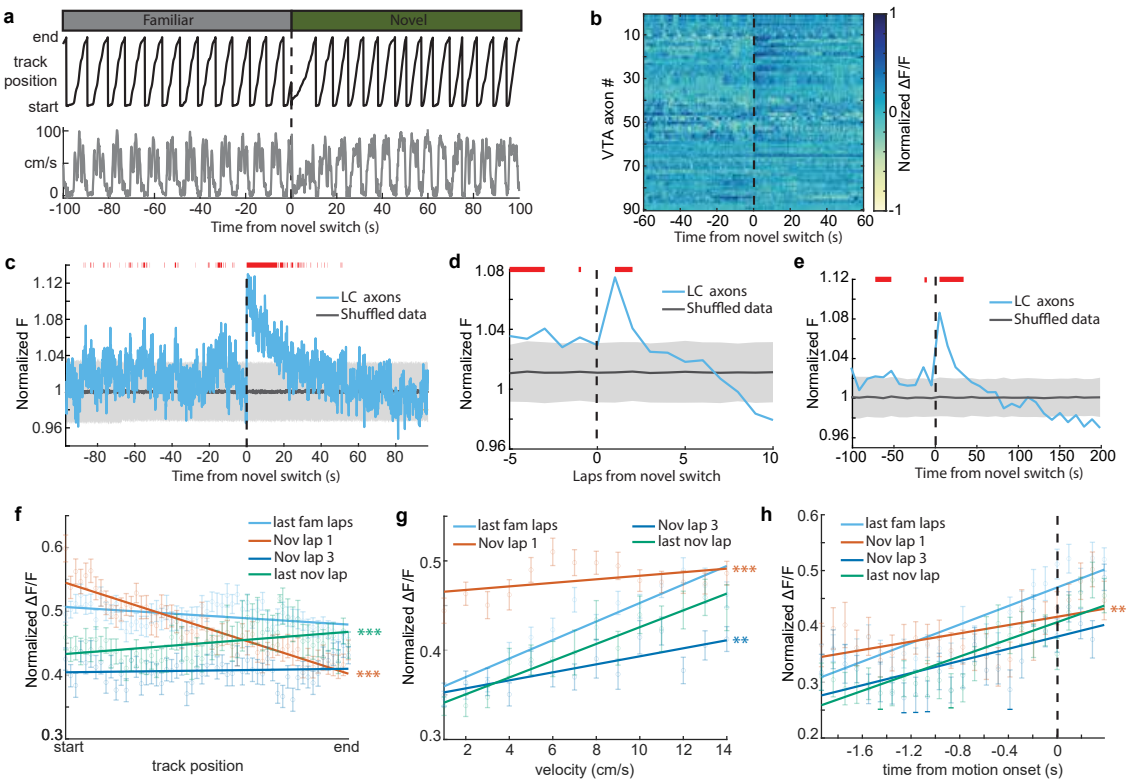

Figure 3.3: **Novelty-induced changes in behavior explain the late but not early increases in LC activity a,** Good behavior from example mouse following removal of freezing periods (velocity < 0.2 cm/s) during the transition from the familiar to a novel VR environment showing the animals track position (top, black) and velocity (bottom, gray). **b,** Normalized $\Delta F/F$ activity of all LC ROIs aligned to the switch to the novel VR environment following removal of freezing periods. **c,** Mean normalized F of all VTA ROIs (top, n = 7) and LC ROIs (bottom, n = 90) aligned to the switch to the novel environment. To define a baseline and 95% CI (gray shaded region), 1000 shuffles were created from the calcium traces and down sampled to match the sample size and averaged. This was repeated 1000 times and the mean and 95% CI of this shuffled data was determined for each frame. Red lines indicate periods where two or more consecutive frames passed above the 95% CI of the shuffled baseline. **d,e,**. The normalized F of all LC ROIs binned by lap (d) or into 50 frame bins (e). The baseline and 95% CI (gray shaded region) was defined using the same method as in (c). Red lines indicate bins above the baseline 95% CI. **f-h,** Population average position binned (f), velocity binned (g), and motion onset aligned (h) $\Delta F/F \pm$ s.e.m. in LC ROIs (n = 90) in the final laps of the familiar environment (light blue), and the first (orange), third (dark blue), and final laps (green) of the novel environment. Linear regression, F test, position binned (f) fam last, $P < 1e-4$, nov 1, $P < 1e-68$, nov 3, $P = 0.48$, nov last, $P < 0.001$; velocity binned (g) fam last, $P < 1e-31$, nov 1, $P < 0.05$, nov 3, $P < 1e-5$, nov last, $P < 1e-13$; motion onset aligned (h) fam last, $P < 1e-29$, nov 1, $P < 0.001$, nov 3, $P < 1e-9$, nov last, $P < 1e-18$. The slope of each lap was compared to the final familiar laps using a one-way ANOCOVA with Tukey HSD post hoc test. * $P < 0.01$, ** $P < 0.001$, *** $P < 1e-4$.

of the familiar environment (Fig 3.3F-H). This is consistent with a decaying novelty signal that peaks at the start of the first lap and rides on top of these other signals. This produces an elevation in activity at positions near the start of the first lap that is lower at positions near the end of the first lap, causing a negative slope relationship between position and LC axon activity on the first lap (Fig. 3.3F; orange line). Further, low velocities occur at the start of each lap compared to the end of the lap. Because the novelty signal is highest when animals are running slowest, the novelty signal flattens the velocity-LC activity relationship (Fig. 3.3G; orange line). Lastly, rest periods typically occur at the start of the track. Therefore, motion onset encoding on the first lap in the novel environment occurs when the novelty signal is highest, again, flattening the relationship (Fig. 3.3G; orange line). By the third lap in the novel environment, once the novelty signal has disappeared, the relationships seen in the position binned and motion onset aligned data are no longer different than the relationship in the familiar laps (Fig 3.3F,H). Although the relationship between velocity and activity is different in the third novel lap than that of the final familiar laps, this relationship returns to the familiar relationship by the final lap in the novel environment (Fig 3G). Interestingly, the slope is significantly increased in the final lap of the novel environment (Fig 3.3F), potentially indicating the development of activity at the novel reward location as seen by Kaufman et. al. Altogether, examining the lap-by-lap dynamics of the position, velocity, and motion indicates that novelty induces increased activity in the first lap of the novel environment while a change in behavior leads to increased activity throughout additional exploration of the novel environment.

3.4 Discussion

During spatial navigation in the familiar environment, VTA DA inputs activity was strongly modulated by position relative to reward, ramping up as mice approached the end of the track where reward was located. We have previously shown that this activity is dependent

on the history of reward delivery and reflects the animals' reward expectation (Krishnan et al. 2022). VTA axons also showed decreasing activity during rest prior to motion onset. However, most pauses occurred immediately following reward delivery. Therefore, decreasing VTA axon activity during rest is likely due to decreasing reward-related activity following reward delivery. In other words, the decaying reward-related activity is bleeding into the rest period. To test this, we could examine VTA axon activity during rest and prior to motion onset during rest periods where reward-related activity is absent. These would include rest periods that occur at locations other than the end/start of a lap, in unrewarded laps, and in the novel environment. This will be the focus of future analysis to determine whether VTA axons have any relationship with rest and motion onset.

VTA axons also showed activity modulated by velocity. This relationship was largely due to the activity of two VTA axons that were strongly modulated by velocity, suggesting that there may be heterogeneity in the population of VTA axons. This is consistent with findings demonstrating heterogeneous encoding of behavioral variables in VTA DA cell bodies, including activity related to rewards and kinematics (Engelhard et al. 2019). However, the apparent velocity encoding axons we report here could be due to the strongly stereotyped behavior that is observed in our well-trained mice. This creates a high correlation between velocity and track position. In this case, axons that encode position would also show a correlation with velocity. To determine if some VTA axons do really encode velocity, we will analyze velocity related activity in the unrewarded laps and in the novel environment when reward-related activity is absent in these axons.

LC axons showed no position encoding. Instead, they were modulated by velocity and ramped up in activity prior to motion initiation, consistent with recordings of LC axons in dCA1 (Kaufman, Geiller, and Losonczy 2020) and in the cortex (Reimer et al. 2016), respectively. An important question is how is this LC axon activity impacting hippocampal neurons during navigation in a familiar environment? It is possible that LC axons during

navigation provide increases in excitability that promotes place cell activity as both dopamine and norepinephrine in the hippocampus can impact cell excitability (Segal, Markram, and Richter-Levin 1991; Edelmann and Lessmann 2011; Edelmann and Lessmann 2018). Additionally, place cells are flexible during spatial navigation with new place fields forming in familiar environments (Mark E.J. Sheffield, Adoff, and Daniel A. Dombeck 2017; Dong, Madar, and M. E. J. Sheffield 2021)and shifting position with time/experience (Dong, Madar, and M. E. J. Sheffield 2021). Place fields can also shift to follow changing reward (Gauthier and Tank 2018)and object locations (Bourboulou et al. 2019). The combination of elevated LC input and excitatory input activity during spatial navigation may allow place cells to adapt to relevant stimuli by promoting plasticity of specific inputs (Kaufman, Geiller, and Losonczy 2020; Redondo and R. G. M. Morris 2011). In other words, LC inputs could allow the hippocampus to be flexible during navigation through their impacts on synaptic plasticity (Takeuchi et al. 2016; Yamasaki and Takeuchi 2017; Duszkiewicz et al. 2019). Further experiments should be conducted to investigate the impact of LC input activity on place cells in the dorsal hippocampus during navigation of a familiar and unchanging environment.

Exposure to environmental novelty leads to an increase in dopamine in the dorsal hippocampus (Ihalainen, Riekkinen Jr, and Feenstra 1999) and promotes synaptic plasticity (S. Li et al. 2003; Hagena and Denise Manahan-Vaughan 2012), hippocampal replay (McNamara et al. 2014; Dupret et al. 2010) and memory persistence (S. Li et al. 2003; Cohen, Bolstad, and A. K. Lee 2017). In our experiment, exposure to a novel environment caused an increase in LC axon activity but not in VTA DA axon activity, supporting findings that novel experiences induce activity of LC neurons (Takeuchi et al. 2016). The activity of LC neurons in turn increases hippocampal neuron activity (Wagatsuma et al. 2018), increases efficacy of Schaffer Colateral synapses (Takeuchi et al. 2016), stabilizes place cells across days (Wagatsuma et al. 2018) and memory persistence (Wagatsuma et al. 2018; Takeuchi et al. 2016; Chowdhury et al. 2022) persistence through dopamine receptor dependent mecha-

nisms. Importantly, while LC inputs to CA1 have been shown to cause an increase in activity (Wagatsuma et al. 2018; Chowdhury et al. 2022), shape overrepresentation of novel reward locations (Kaufman, Geiller, and Losonczy 2020), and memory linking (Chowdhury et al. 2022), in dCA1 they do not play a role in the formation of contextual memories (Chowdhury et al. 2022) or stable place cell maps across days (Wagatsuma et al. 2018) in dCA1. However, these experiments have only investigated the role of LC inputs to dCA1 in stability across days. It is possible this novelty induced activity in LC dCA1 impacts the formation of instant or delayed place field formation observed in novel environments (Dong, Madar, and M. E. J. Sheffield 2021). Additionally, their activity may play a role in dynamics that occur across trials, such as the backward shifting of place fields (Dong, Madar, and M. E. J. Sheffield 2021). Further experiments should be conducted to investigate the role of LC inputs to dCA1 on the trial-by-trial dynamics of new place fields in novel environments to determine the role of the novelty signal we report here.

While LC neurons have been shown to impact novelty encoding through dopaminergic mechanisms (Wagatsuma et al. 2018; Takeuchi et al. 2016; Chowdhury et al. 2022), this does not exclude the possiblity that they also release norepinephrine during exposure to novelty and exploration of a familiar environment. Indeed, hippocampal levels of norepinephrine also increase during exposure to environmental novelty (Lima et al. 2019; Moreno-Castilla et al. 2017). How this norepinephrine release during novelty exposure effects hippocampal function is not well understood. Additionally, it is not known whether norepinephrine and dopamine are release from the same LC inputs or from distinct sets of LC inputs. Dopamine is in the synthesis pathway of norepinephrine and is loaded into vesicles where it is then converted to norepinephrine by dopamine β-hydroxylase in LC neurons. It is possible that high levels of activity of LC inputs, like those occurring during exposure to novelty, lead to release of vesicles before dopamine can be converted thus leading to the release of dopamine. However, low levels of LC activation, like those observed during familiar environment exploration, may

provide time for dopamine to be converted and thus lead to the release of norepinephrine. Further experiments investigating the dynamics of dopamine conversion and release in LC inputs to the hippocampus should be conducted to test this hypothesis.

The findings that VTA DA axons show novelty induced activity is in contrast with several studies showing novelty induced activity in VTA DA cell bodies (Takeuchi et al. 2016; Duszkiewicz et al. 2019; Lisman and Grace 2005), indicating potential heterogeneity in VTA neurons response to novelty (Engelhard et al. 2019). It is possible that some VTA DA inputs to dCA1 respond to novel environements, and the small number of axons recorded here are not representative of the whole population. Perhaps more likely, this lack of a novelty response is due to differences in experimental design. Here, mice learned to approach a location for reward which has been shown to lead to ramping activity in dopaminergic VTA neurons (Howe et al. 2013; Krishnan et al. 2022; Kim et al. 2020; London et al. 2018; Jeong et al. 2022). When mice were switched to the novel environment they had no expectation of reward, therefore, the ramping activity was absent, leading to a decrease in activity that could obscure novelty induced activity.

The distinct activity dynamics exhibited by LC and VTA DA axons during spatial navigation of familiar and novel environments underscore their distinct contributions to hippocampal dependent learning and memory processes. Notably, these findings reinforce the notion that VTA DA inputs play a pivotal role in the ongoing maintenance and updating of associations between expected rewards and the locations that lead to them, while LC axons appear to be integral to the process of encoding memories of entirely new environments.

3.5 Methods

3.5.1 Subjects

All experimental and surgical procedures were in accordance with the University of Chicago Animal Care and Use Committee guidelines. For this study, we used 10–20 week-old male Slc6a3Cre+/- (DAT-Cre+/-) mice and Slc6a2 Cre+/- (NET-Cre+/-)(23–33 g). Male mice were used over female mice due to the size and weight of the headplates (9.1 mm × 31.7 mm, 2 g) which were difficult to firmly attach on smaller female skulls. Mice were individually housed in a reverse 12 h light/dark cycle at 72 °F and 47% humidity, and behavioral experiments were conducted during the animal's dark cycle.

3.5.2 Mouse surgery and viral injections

Mice were anesthetized (1–2% isoflurane) and injected with 0.5 ml of saline (intraperitoneal injection) and 0.5 ml of Meloxicam (1–2 mg/kg, subcutaneous injection) before being weighed and mounted onto a stereotaxic surgical station (David Kopf Instruments). A small craniotomy (1–1.5 mm diameter) was made over the ventral tegmental area (VTA) (± 0.5 mm lateral, 3.1mm caudal of Bregma) of DAT-Cre+/- mice or over the locus coeruleus (LC) (± 0.875 mm lateral, -5.45 mm caudal of Bregma). The genetically-encoded calcium indicator, pAAV-hsyn-Flex-Axon-GCaMP6s (pAAV-hSynapsin1-FLEx-axon-GCaMP6s was a gift from Lin Tian (Addgene viral prep # 112010-AAV5 ; http://n2t.net/addgene:112010 ; RRID:Addgene 112010) was injected into the VTA of DAT-Cre+/- mice (200 nL at a depth of 4.4 mm below the surface of the dura) or the LC of NET-Cre+/- mice (200 nL at a depth of 3.65 mm below Bregma). For a subset (4/7) of VTA recordings, a different GCaMP variant, pAAV-Ef1A-Flex-Axon-GCaMP7b, was injected due to the difficulty finding and recording VTA axons in dCA1 (pAAV-Ef1a-Flex-Axon-GCaMP7b (pAAV-Ef1a-Flex-Axon-GCaMP7b was a gift from Rylan Larsen - Addgene plasmid # 135419; http://n2t.net/addgene:135419;

RRID: Addgene 135419). Following injections, the site was covered up using dental cement (Metabond, Parkell Corporation) and a metal head-plate (9.1 mm × 31.7 mm, Atlas Tool and Die Works) was also attached to the skull with the cement. Mice were separated into individual cages and water restriction began 3 weeks later (0.8–1.0 ml per day). Mice then underwent surgery to implant a hippocampal window as previously described75. Following implantation, the headplate was reattached with the addition of a head-ring cemented on top of the head-plate which was used to house the microscope objective and block out ambient light. Post-surgery mice were given 2–3 ml of water/day for 3 days to enhance recovery before returning to the reduced water schedule (0.8–1.0 ml/day).

3.5.3 Behavior and virtual reality

Our virtual reality (VR) and treadmill setup was designed similar to previously described setups44,76. The virtual environments that the mice navigated through were created using VIRMEn77. 2 m (DAT-Cre mice) or 3 m (NET-Cre mice) linear tracks rich in visual cues were created that evoked numerous place fields in mice as they moved along the track at all locations (Fig. x)78. Mice were head restrained with their limbs comfortably resting on a freely rotating styrofoam wheel ('treadmill'). Movement of the wheel caused movement in VR by using a rotatory encoder to detect treadmill rotations and feed this information into our VR computer, as in refs. 46, 77. Mice received a water reward (4 µL) through a waterspout upon completing each traversal of the track (a lap), which was associated with a clicking sound from the solenoid. Licking was monitored by a capacitive sensor attached to the waterspout. Upon receiving the water reward, a short VR pause of 1.5 s was implemented to allow for water consumption and to help distinguish laps from one another rather than them being continuous. Mice were then virtually teleported back to the beginning of the track and could begin a new traversal. Mouse behavior (running velocity, track position, reward delivery, and licking) was collected using a PicoScope Oscilloscope (PICO4824, Pico

Technology, v6.13.2). Pupil tracking was done through the imaging software (Scanbox v4.1, Neurolabware) at 15 frames per sec, using Allied Vision Mako U-130b camera with a 25 mm lens and a 750 nm longpass IR filter. IR illumination from the objective was used to illuminate the pupil for tracking. Behavioral training to navigate the virtual environment began 4–7 days after window implantation (30 min per day) and continued until mice reached >2 laps per minute, which took 10–14 days (although some mice never reached this threshold). Mice that reached this behavioral threshold were imaged the following day.

3.5.4 Two-photon imaging

Imaging was done using a laser scanning two-photon microscope (Neurolabware). Using a 8 kHz resonant scanner, images were collected at a frame rate of 30 Hz with bidirectional scanning through a 16x/0.8 NA/3 mm WD water immersion objective (MRP07220, Nikon). GCaMP6s and GCaMP7b were excited at 920 nm with a femtosecondpulsed two photon laser (Insight DS + Dual, Spectra-Physics) and emitted fluorescence was collected using a GaAsP PMT (H11706, Hamamatsu). The average power of the laser measured at the objective ranged between 50–80 mW. A single imaging field of view (FOV) between 400–700 µm equally in the x/y direction was positioned to collect data from as many VTA or LC axons as possible. Time-series images were collected from 3-5 planes spaced 2 um apart using an electric lens to ensure axons remained in a field of view and reduce power going to an individual plane. Images were collected using Scanbox (v4.1, Neurolabware) and the PicoScope Oscilloscope (PICO4824, Pico Technology, v6.13.2) was used to synchronize frame acquisition timing with behavior.

3.5.5 Imaging sessions

The familiar environment was the same environment that the animals trained in. The experiment protocol for single day imaging sessions is shown in Fig. x. Each trial lasted

8–12 min and was always presented in the same order. Mice were exposed to the familiar rewarded environment for 10 minutes, then were immediately teleported to the start of a novel rewarded VR environment and allowed to navigate for 10 minutes. Mice on average ran 19 ± 3.8 (mean ± 95% CI) laps in the familiar environment, at which point they were teleported to the novel environment and imaging continued for 30 ± 5.4 laps. The Novel-rewarded environment (N) had distinct visual cues, colors and visual textures, but the same dimensions (2 or 3 m linear track) and reward location (end of the track) as the familiar environment. Imaging sessions with large amounts of drift or bleaching were excluded from analysis (6 sessions for NET mice, 6 sessions for LC Mice).

3.5.6 Histology and brain slices imaging

We checked the expression axon-GCaMP to confirm expression was restricted to the VTA of DAT-Cre mice and the LC of NET-Cre Mice were anesthetized with isoflurane and perfused with 10 ml phosphate-buffered saline (PBS) followed by 20 mL 4% paraformaldehyde in PBS. The brains were removed and immersed in 30% sucrose solution overnight before being sectioned at 30 µm-thickness on a cryostat. Brain slices were collected into well plates containing PBS. Slices were washed 5 times with PBS for 5 min then were blocked in 1% Bovine Serum Albumin, 10% Normal goat serum, 0.1% Triton X-100 for 2 h. Brain slices were then incubated with 1:500 rabbit-α-TH (MAB318, Sigma Aldrich) and 1:500 mouse-α-GFP (x)in blocking solution at 4 . After 48 h, the slices were incubated with 1:1000 goat-α-rabbit Alexa Fluor 647nm secondary antibody (A32731, ThermoFisher) and 1:1000 goat-α-mouse Alexa Fluor 488nm (x) for 2 h. Brain slices were then collected on glass slides and mounted with a mounting media with DAPI (SouthernBiotech DAPI-Fluoromount-G Clear Mounting Media, 010020). The whole-brain slices were imaged under $\times$10 and x40 with a Caliber I.D. RS-G4 Large Format Laser Scanning Confocal microscope from the Integrated Light Microscopy Core at the University of Chicago.

3.5.7 Image processing and ROI selection

Time-series images were preprocessed using Suite2p (v0.10.1)79. Movement artifacts were removed using rigid and non-rigid transformations and assessed to ensure absence of drifts in the z-direction. Datasets with visible z-drifts were discarded (x). For axon imaging, ROIs were first defined using Suite2p and manually inspected for accuracy. ROIs were then hand drawn over all segments of Suite2p defined active axons using ImageJ to ensure all axon segments were included for analysis. Fluorescent activity for each ROI was extracted and highly correlated ROIs (Pearson correlation coefficient ≥ 0.7) were combined and their fluorescent activity was extracted. To be included Baseline corrected $\delta F/F$ traces across time were then generated for each ROI using both a small window of 300 frames for lap by lap analysis, and a larger sliding window of 2000 frames to avoid flattening slow signals for novelty response analysis. Additional ROIs were drawn over autofluorescent structures that were not identified by suite2p. These "blebs" were processed in the same way as axon ROIs and used as controls to check for imaging and motion artifacts.

To remove low signal to noise axons, we defined the SNR of each ROI using the power spectrum of their fluorescent activity similar to (Reimer et al. 2016). For frequencies above 1Hz, the power was defined as noise because this sits outside of the range of frequencies possible for GCaMP6s fluorescence. The SNR ratio was then defined as the ratio of the peak power between 0.5 Hz and 1Hz over the average power between 1 Hz and 3 Hz. The SNR of "blebs" was also determined and any axon with a SNR greater than 1.5 std from the mean of the "blebs" SNR was used for analysis (110/231 LC ROIs, 7/7 VTA ROIs).

Additionally, it was observed that a subset of axon ROIs would greatly increase fluorescence at seemingly random timepoints and remain elevated for the rest of the trial. This activity could be due to the axons being unhealthy and filling with calcium. Therefore, we identified these axons using the *cusum* function in matlab to detect changes in mean activity that remained elevated for at least 2000 frames or at least 500 frames if they were still ele-

vated at the end of the recording session and removed them from analysis(20/110 LC ROIs, 0/7 VTA ROIs).

3.5.8 Behavioral Analysis

Mouse velocity was calculated as the change in VR position divided by the sampling rate and smoothed using a Savitzky-Golay filter with a 7 frame window and 5 degree polynomial. To find the lap mean velocity, periods where the mice were immobile (velocity $<$ x cm/s) were removed and the average velocity during the remaining frames was calculated. The lap mean freezing ratio was calculated as the number of frames spent immobile (velocity $<$ 0.2 cm/s) divided by the total number of frames for each lap.

3.5.9 Axon Imaging Analysis

For the three measures below, to avoid weighting axons with a high SNR more than others each ROI was normalized by $\delta F/F\breve{}\delta F/Fmin)/(\delta F/Fmax\breve{}\delta F/Fmin)$ where $\delta F/Fmin$ is the 1st quantile and $\delta F/Fmax$ was the 99 quantile for each ROI. The 1st and 99th quantiles were used in order to avoid normalize to noisy outlier data points.

3.5.10 Position binned fluorescence

To find the position binned fluorescent activity of each ROI, the track was divided into 5 cm bins. For each lap, the average fluorescence in each bin was calculated for each ROI. The position binned fluorescence was then averaged across all laps in each environment to find the mean position binned activity in the familiar and novel environments.

3.5.11 Velocity binned fluorescent activity

To find the velocity binned fluorescent activity for each ROI, the velocity was divided into 1 cm/s bins from 1 to 30 cm/s. Velocities above this 14 cm/s were excluded from figures because not all mice ran faster than 14 cm/s. For each lap, the ROIs average fluorescence in each velocity bin was calculated and then averaged across all laps in each environment to find the velocity binned activity in the familiar and novel environments.

3.5.12 Motion initiation aligned fluorescence

Periods where mice were immobile (velocity < 5 cm/s) for at least 1.5s then proceed to run (velocity $\geq$ 5cm/s) for at least 3s were identified. The fluorescent activity for ROIs for these periods was aligned to the frame mice began running (velocity crossed above 5cm/s). The average aligned fluorescent activity of each ROI was then determined for each environment.

3.5.13 Linear regression analysis

To assess dynamics between each of the above measures and calcium activity of LC and VTA axons, we performed linear regression on the population's familiar environment data and significance was assessed with an F test. To compare the dynamics between LC and VTA axons, we performed exact testing based on Monte-Carlo resampling (1000 resamples with sample size matching the lower sample size condition) as detailed in legends (Fig 3.1E).

To assess the changing position and velocity encoding of LC axons following exposure to a novel environment, we performed linear regression on the population fluorescence data of the average of the last 4 laps in the familiar environment, and each of the first three laps in the novel environment for each measure. The significance for the fit of each line was assessed with an F test, and an ANCOVA was conducted to test for differences in slope between the four laps. The same process was conducted for the motion initiation dynamics, but only using ROIs in mice who paused within the first 2 laps and 30s following exposure to the

novel environment.

3.5.14 Novel response analysis

To examine the response of LC and VTA axons to the novel VR environment, the fluorescence data was normalized by the mean for each ROIs and aligned to the frame where the mice were switched to the novel environment and the mean normalized F for LC and VTA ROIs at each time point was calculated. Baseline fluorescent activity was then calculated for LC and VTA ROIs separately by generating 1000 shuffled traces of the ROIs calcium activity and subsampling down to the sample size (90 for LC; 7 for VTA) 1000 times and finding the mean of the subsampled shuffles. The mean and 95% CI of all 1000 subsamples was found and the mean activity of LC and VTA ROIs was considered significantly elevated when it passed above the 95% CI of the shuffled data. The same process was repeated to define a baseline for the time binned data (fluorescent activity divided into 50 frame bins) and the lap binned data (mean activity for each lap).

Additionally, to account for changes in behavior between the familiar and novel environments, periods where the animals were immobile (velocity $\leq$ 0.2 cm/s) were removed and running periods were concatenated together and aligned to the switch to the novel environment. Here, we again defined a baseline for the time mean traces, time binned activity, and the lap binned activity using the above bootstrapping approach.

3.5.15 Figure graphics

All figure graphics including Fig 3.1A-B were created using BioRender.com.

3.5.16 Code availability

Scripts used for data analysis are available on Github (x)

CHAPTER 4

CONCLUSION AND FUTURE DIRECTIONS

4.1 Summary of Findings

Chapter 2: Reward expectation extinction restructures and degrades CA1 spatial maps through loss of a dopaminergic reward proximity signal

1. When reward expectation is extinguished in mice, they remain egaged with their environment, but over-representation of rewards vanishes, place field remapping throughout the environment increases, and place field trial-to-trial reliability decreases.

2. Ventral tegmental area (VTA) dopaminergic axons in dorsal CA1 exhibit ramping to reward activity that depends on the animals' reward expectation.

3. Inhibition of VTA dopaminergic neurons largely replicates the effects of extinguishing reward expectation, indicating that reward expectation restructures CA1 cognitive maps by modulating VTA DA inputs to dorsal CA1.

Chapter 3: Distinct sets of dopaminergic inputs in hippocampal CA1 transmit contrasting signals during behavior in a changing world

1. During exploration of familiar environments, VTA axons in dorsal CA1 exhibit ramping to reward activity while LC axon activity is correlated to the animals' velocity and increases prior to motion initiation.

2. LC axon activity sharply and persistantly increases following exposure to a novel environemnt, while VTA axon ramping to reward activity disapears. These findings demonstrate distinct activity dynamics in VTA and LC axons during spatial navigation.

4.2 Discussion and Future Directions

Dopaminergic inputs to the dorsal hippocampus in reward location encoding

Here we demonstrate strong ramping to reward activity in VTA DA inputs to the dorsal hippocampus, that depends on the animals' reward expectation. While we did not observe reward related activity in LC axons in dCA1, it has been reported that these inputs have increased activity at new reward locations (Kaufman, Geiller, and Losonczy 2020). These findings support the that LC axons play a role in the establishment of overrepresentation of reward locations (Gauthier and Tank 2018; Kaufman, Geiller, and Losonczy 2020), while VTA DA axons are involved in the maintenance of place fields in rewarded environments. Indeed, while LC inputs are not active at familiar reward location but quickly develop activity at new reward locaitons (Kaufman, Geiller, and Losonczy 2020), while VTA DA ramp to familiar rewarded locations but take time to develop ramping activity to novel reward location (Krishnan et al. 2022). Furthermore, inhibition of VTA DA neurons mimicked the effects of extinction of reward expectation on place cells but did not completely eliminate overrepresentation of reward locations, suggesting it modulates place fields throughout rewarded environments but is not solely responsible for overrepresentatio of reward locations. In contrast, inhibition of LC-CA1 axons eliminated overrepresentation of new reward locations, while excitation of this inputs can enrich place cells near familiar rewarded environments (Kaufman, Geiller, and Losonczy 2020), demonstratitng a critical role for the establishment of overrepresentation of rewarded locations. Further experiments should be conducted to establish the role of these two inputs in other goal-oriented task.

Dopaminergic inputs to the dorsal hippocampus in novelty encoding

While it had previously been shown that VTA and LC neurons increase in activity following exposure to a novel envionrment (Takeuchi et al. 2016), here we only observed novelty induced activity in LC inputs to dCA1. Combined with other studies, this demonstrates a role of LC but not VTA inputs in the encoding of novel environments in the hippocampus

(Takeuchi et al. 2016; Wagatsuma et al. 2018; Chowdhury et al. 2022). While, these experiments did not demonstrate an effect on the stability of place fields in a novel environment across days, our findings of a brief large increase in LC activity in a novel environment suggest they may play a role in the development of instant versus delayed place fields that occur in across a similar timescale (Dong, Madar, and M. E. J. Sheffield 2021). Additionally, this activity may influence the trial by trial stability of new place fields, or influence their backwards shifting over time (Dong, Madar, and M. E. J. Sheffield 2021). Further experiments should be conducted to investigate the role of this novelty induced LC input activity in hippocampal function.

It has been proposed that VTA DA inputs serve as a detector of common novelty, or novel experiences that share common aspects with past experiences. In contast, LC neurons are thought to serve as a detector of distinct novelty (Duszkiewicz et al. 2019). It is possible that our novel VR environments served as distinct novelty, activating LC but not VTA DA axons. To investigate this, experiments should be conducted introducing or removing objects and rewards and observing the activity of VTA and LC axons during these changes. It is possible VTA DA inputs or LC inputs could respond to these changes in reward and object locations and are involved in the flexible encoding of rewards and objects seen during these experiments (Gauthier and Tank 2018; Bourboulou et al. 2019).

Mechanisms of action of VTA and LC inputs to the dorsal hippocampus

One caveat of our experiments is we inhibited all VTA DA Neurons and did not directly manipulate the VTA DA projections to dCA1. Therefore, the effects of VTA DA neuron inhibition on hippocampal neuron activity cannot be attributed directly to VTA DA inputs to dCA1. VTA DA neurons project to many brain regions important for reward learning and motivation and may be impacting hippocampal function through these inputs. Therefore, further experiments should be conducted, directly manipulating VTA DA inputs to dCA1 to examine the role of this pathway in reward expectations effects on hippocampal function.

We demonstrate distinct activity dynamics in VTA DA and LC inputs to the dorsal hippocampus indicating a role for VTA DA axons in reward expectation dependent modulation of place fields and LC neurons in novelty encoding. However, we did not investigate the mechanisms through which these inputs impact hippocampal function. Investigating hippocampal pyramidal neuron dendirites during spatial navigation has revealed the subcompartment dynamics play a role in place field development (M. E. J. Sheffield and Daniel A. Dombeck 2015; Mark EJ Sheffield and Daniel A Dombeck 2019; Mark E.J. Sheffield, Adoff, and Daniel A. Dombeck 2017). Investigating how VTA and LC inputs influence these dynamics and shape place field activity may reveal important insight into the cellular mechanisms through which these inputs influence hippocampal encoding.

There is evidence that both VTA and LC inputs could act through interneurons (Adeyelu and Ogundele 2023; Kaufman, Geiller, and Losonczy 2020), while DA receptors are also expressed on pyramidal neurons (Yao, Spealman, and J. Zhang 2008; C Charuchinda et al. 1987) suggesting they may impact these neurons directly. Additionally, reward related activity has been observed in both VIP (Turi et al. 2019) and CCK interneurons and astrocytes in the hippocampus, indicating they their involvement in reward encoding in the hippocampus. Experiments investigating the effects of VTA DA and LC inputs on these neurons may provide insight into how these sparse inputs can influence entire populations of hippocampal place cells. The findings in this thesis support distinct roles of VTA DA and LC inputs to the hippocampus in learning and spatial navigation which should be tested in future experiments. Ultimately, these findings bring us closer to an understanding of how neuromodulatory inputs influence hippocampal function and episodic learning and memory.

BIBLIOGRAPHY

Foerde, Karin and Daphna Shohamy (Nov. 2011). "The role of the basal ganglia in learning and memory: Insight from Parkinson's disease". In: *Neurobiology of learning and memory* 96.4, pp. 624–636. ISSN: 1074-7427. DOI: 10.1016/j.nlm.2011.08.006. URL: https://www.ncbi.nlm.nih.gov/pmc/articles/PMC3772079/ (visited on 08/11/2023).

H, Mochizuki-Kawai (July 2008). "[Neural basis of procedural memory]". In: *Brain and nerve = Shinkei kenkyu no shinpo* 60.7. Publisher: Brain Nerve. ISSN: 1881-6096. URL: https://pubmed.ncbi.nlm.nih.gov/18646622/ (visited on 08/11/2023).

Squire, Larry R. (Nov. 1, 2004). "Memory systems of the brain: A brief history and current perspective". In: *Neurobiology of Learning and Memory*. Multiple Memory Systems 82.3, pp. 171–177. ISSN: 1074-7427. DOI: 10.1016/j.nlm.2004.06.005. URL: https://www.sciencedirect.com/science/article/pii/S1074742704000735 (visited on 08/11/2023).

Scoville, William Beecher and Brenda Milner (Feb. 1, 1957). "LOSS OF RECENT MEMORY AFTER BILATERAL HIPPOCAMPAL LESIONS". In: *Journal of Neurology, Neurosurgery & Psychiatry* 20.1, p. 11. DOI: 10.1136/jnnp.20.1.11. URL: http://jnnp.bmj.com/content/20/1/11.abstract.

Corkin, Suzanne, David G. Amaral, R. Gilberto González, Keith A. Johnson, and Bradley T. Hyman (May 15, 1997). "H. M.'s Medial Temporal Lobe Lesion: Findings from Magnetic Resonance Imaging". In: *Journal of Neuroscience* 17.10. Publisher: Society for Neuroscience Section: Articles, pp. 3964–3979. ISSN: 0270-6474, 1529-2401. DOI: 10.1523/JNEUROSCI.17-10-03964.1997. URL: https://www.jneurosci.org/content/17/10/3964 (visited on 08/11/2023).

Annese, Jacopo, Natalie M. Schenker-Ahmed, Hauke Bartsch, Paul Maechler, Colleen Sheh, Natasha Thomas, Junya Kayano, Alexander Ghatan, Noah Bresler, Matthew P. Frosch, Ruth Klaming, and Suzanne Corkin (Jan. 28, 2014). "Postmortem examination of patient H.M.'s brain based on histological sectioning and digital 3D reconstruction". In: *Nature Communications* 5, p. 3122. ISSN: 2041-1723. DOI: 10.1038/ncomms4122. URL: https://www.ncbi.nlm.nih.gov/pmc/articles/PMC3916843/ (visited on 08/11/2023).

O'Keefe, J. and J. Dostrovsky (Nov. 1971). "The hippocampus as a spatial map. Preliminary evidence from unit activity in the freely-moving rat". In: *Brain Research* 34.1, pp. 171–175. ISSN: 00068993. DOI: 10.1016/0006-8993(71)90358-1. URL: https://linkinghub.elsevier.com/retrieve/pii/0006899371903581 (visited on 08/29/2019).

O'Keefe, John and Lynn Nadel (1978). *The hippocampus as a cognitive map*. Oxford : New York: Clarendon Press ; Oxford University Press. 570 pp. ISBN: 978-0-19-857206-0.

Wilson, MA and BL McNaughton (July 29, 1994). "Reactivation of hippocampal ensemble memories during sleep". In: *Science* 265.5172, p. 676. DOI: 10.1126/science.8036517. URL: http://science.sciencemag.org/content/265/5172/676.abstract.

Krishnan, Seetha, Chad Heer, Chery Cherian, and Mark E. J. Sheffield (Nov. 4, 2022). "Reward expectation extinction restructures and degrades CA1 spatial maps through loss of a dopaminergic reward proximity signal". In: *Nature Communications* 13.1, p. 6662. ISSN: 2041-1723. DOI: 10.1038/s41467-022-34465-5. URL: https://www.nature.com/articles/s41467-022-34465-5 (visited on 06/20/2023).

Carr, Margaret F, Shantanu P Jadhav, and Loren M Frank (Feb. 2011). "Hippocampal replay in the awake state: a potential substrate for memory consolidation and retrieval". In: *Nature Neuroscience* 14.2, pp. 147–153. ISSN: 1097-6256, 1546-1726. DOI: 10.1038/nn.2732. URL: http://www.nature.com/articles/nn.2732 (visited on 07/25/2020).

Foster, David J. and Matthew A. Wilson (Mar. 2006). "Reverse replay of behavioural sequences in hippocampal place cells during the awake state". In: *Nature* 440.7084, pp. 680–683. ISSN: 0028-0836, 1476-4687. DOI: 10.1038/nature04587. URL: http://www.nature.com/articles/nature04587 (visited on 07/25/2020).

Sadowski, Josef H.L.P., Matthew W. Jones, and Jack R. Mellor (Mar. 2016). "Sharp-Wave Ripples Orchestrate the Induction of Synaptic Plasticity during Reactivation of Place Cell Firing Patterns in the Hippocampus". In: *Cell Reports* 14.8, pp. 1916–1929. ISSN: 22111247. DOI: 10.1016/j.celrep.2016.01.061. URL: https://linkinghub.elsevier.com/retrieve/pii/S2211124716300390 (visited on 07/25/2020).

Ven, Gido M. van de, Stéphanie Trouche, Colin G. McNamara, Kevin Allen, and David Dupret (Dec. 2016). "Hippocampal Offline Reactivation Consolidates Recently Formed Cell Assembly Patterns during Sharp Wave-Ripples". In: *Neuron* 92.5, pp. 968–974. ISSN: 08966273. DOI: 10.1016/j.neuron.2016.10.020. URL: https://linkinghub.elsevier.com/retrieve/pii/S0896627316307218 (visited on 07/25/2020).

Eichenbaum, Howard (Aug. 2017). "On the Integration of Space, Time, and Memory". In: *Neuron* 95.5, pp. 1007–1018. ISSN: 08966273. DOI: 10.1016/j.neuron.2017.06.036. URL: https://linkinghub.elsevier.com/retrieve/pii/S0896627317305603 (visited on 08/29/2019).

Leutgeb, S. (July 22, 2005). "Independent Codes for Spatial and Episodic Memory in Hippocampal Neuronal Ensembles". In: *Science* 309.5734, pp. 619–623. ISSN: 0036-8075, 1095-9203. DOI: 10.1126/science.1114037. URL: http://www.sciencemag.org/cgi/doi/10.1126/science.1114037 (visited on 08/29/2019).

Save, Etienne, Ludek Nerad, and Bruno Poucet (2000). "Contribution of multiple sensory information to place field stability in hippocampal place cells". In: *Hippocampus* 10.1, pp. 64–76. ISSN: 1050-9631, 1098-1063. DOI: 10.1002/(SICI)1098-1063(2000)10:1<64::AID-HIPO7>3.0.CO;2-Y. URL: http://doi.wiley.com/10.1002/%28SICI%291098-1063%282000%2910%3A1%3C64%3A%3AAID-HIPO7%3E3.0.CO%3B2-Y (visited on 08/29/2019).

Zhang, Sijie and Denise Manahan-Vaughan (Feb. 2015). "Spatial Olfactory Learning Contributes to Place Field Formation in the Hippocampus". In: *Cerebral Cortex* 25.2, pp. 423–432. ISSN: 1460-2199, 1047-3211. DOI: 10.1093/cercor/bht239. URL: https://academic.oup.com/cercor/article-lookup/doi/10.1093/cercor/bht239 (visited on 08/29/2019).

Hollup, Stig A., Sturla Molden, James G. Donnett, May-Britt Moser, and Edvard I. Moser (Mar. 1, 2001). "Accumulation of Hippocampal Place Fields at the Goal Location in an Annular Watermaze Task". In: *The Journal of Neuroscience* 21.5, pp. 1635–1644. ISSN: 0270-6474, 1529-2401. DOI: 10.1523/JNEUROSCI.21-05-01635.2001. URL: http://www.jneurosci.org/lookup/doi/10.1523/JNEUROSCI.21-05-01635.2001 (visited on 09/04/2019).

Kobayashi, T, A.H Tran, H Nishijo, T Ono, and G Matsumoto (Apr. 2003). "Contribution of hippocampal place cell activity to learning and formation of goal-directed navigation in rats". In: *Neuroscience* 117.4, pp. 1025–1035. ISSN: 03064522. DOI: 10.1016/S0306-4522(02)00700-5. URL: https://linkinghub.elsevier.com/retrieve/pii/S0306452202007005 (visited on 09/04/2019).

Dupret, David, Joseph O'Neill, Barty Pleydell-Bouverie, and Jozsef Csicsvari (Aug. 2010). "The reorganization and reactivation of hippocampal maps predict spatial memory performance". In: *Nature Neuroscience* 13.8, pp. 995–1002. ISSN: 1097-6256, 1546-1726. DOI: 10.1038/nn.2599. URL: http://www.nature.com/articles/nn.2599 (visited on 09/04/2019).

McKenzie, S., N. T. M. Robinson, L. Herrera, J. C. Churchill, and H. Eichenbaum (June 19, 2013). "Learning Causes Reorganization of Neuronal Firing Patterns to Represent Related Experiences within a Hippocampal Schema". In: *Journal of Neuroscience* 33.25, pp. 10243–10256. ISSN: 0270-6474, 1529-2401. DOI: 10.1523/JNEUROSCI.0879-13.2013. URL: http://www.jneurosci.org/cgi/doi/10.1523/JNEUROSCI.0879-13.2013 (visited on 09/04/2019).

Mizumori, Sheri J.Y. and Valerie L. Tryon (2015). "Integrative hippocampal and decision-making neurocircuitry during goal-relevant predictions and encoding". In: *Progress in Brain Research*. Vol. 219. Elsevier, pp. 217–242. ISBN: 978-0-444-63549-5. DOI: 10.1016

/bs.pbr.2015.03.010. URL: https://linkinghub.elsevier.com/retrieve/pii/S00
79612315000448 (visited on 09/04/2019).

Zaremba, Jeffrey D, Anastasia Diamantopoulou, Nathan B Danielson, Andres D Grosmark, Patrick W Kaifosh, John C Bowler, Zhenrui Liao, Fraser T Sparks, Joseph A Gogos, and Attila Losonczy (Nov. 2017). "Impaired hippocampal place cell dynamics in a mouse model of the 22q11.2 deletion". In: *Nature Neuroscience* 20.11, pp. 1612–1623. ISSN: 1097-6256, 1546-1726. DOI: 10.1038/nn.4634. URL: http://www.nature.com/articles/nn.4634 (visited on 09/04/2019).

Gauthier, Jeffrey L. and David W. Tank (July 11, 2018). "A Dedicated Population for Reward Coding in the Hippocampus". In: *Neuron* 99.1, 179–193.e7. ISSN: 0896-6273. DOI: 10.1016/j.neuron.2018.06.008. URL: https://www.sciencedirect.com/science/article/pii/S0896627318304768.

Knudsen, Eric B. and Joni D. Wallis (Sept. 2, 2021). "Hippocampal neurons construct a map of an abstract value space". In: *Cell* 184.18, 4640–4650.e10. ISSN: 0092-8674. DOI: 10.1016/j.cell.2021.07.010. URL: https://www.sciencedirect.com/science/article/pii/S0092867421008369.

Engelhardt, Eliasz (2016). "Hippocampus discovery First steps". In: *Dementia & Neuropsychologia* 10.1, pp. 58–62. ISSN: 1980-5764. DOI: 10.1590/S1980-57642016DN10100011. URL: https://www.ncbi.nlm.nih.gov/pmc/articles/PMC5674916/ (visited on 08/13/2023).

Allen, Timothy A. and Norbert J. Fortin (June 18, 2013). "The evolution of episodic memory". In: *Proceedings of the National Academy of Sciences* 110 (supplement_2). Publisher: Proceedings of the National Academy of Sciences, pp. 10379–10386. DOI: 10.1073/pnas.1301199110. URL: https://www.pnas.org/doi/10.1073/pnas.1301199110 (visited on 08/13/2023).

Teyler, T. J. and P. DiScenna (Apr. 1986). "The hippocampal memory indexing theory". In: *Behavioral Neuroscience* 100.2, pp. 147–154. ISSN: 0735-7044. DOI: 10.1037//0735-7044.100.2.147.

Martin, S. J., P. D. Grimwood, and R. G. Morris (2000). "Synaptic plasticity and memory: an evaluation of the hypothesis". In: *Annual Review of Neuroscience* 23, pp. 649–711. ISSN: 0147-006X. DOI: 10.1146/annurev.neuro.23.1.649.

Citri, Ami and Robert C. Malenka (Jan. 2008). "Synaptic plasticity: multiple forms, functions, and mechanisms". In: *Neuropsychopharmacology: Official Publication of the American College of Neuropsychopharmacology* 33.1, pp. 18–41. ISSN: 0893-133X. DOI: 10.1038/sj.npp.1301559.

Magee, Jeffrey C. and Christine Grienberger (July 8, 2020). "Synaptic Plasticity Forms and Functions". In: *Annual Review of Neuroscience* 43, pp. 95–117. ISSN: 1545-4126. DOI: 10.1146/annurev-neuro-090919-022842.

Dayan, Peter (Oct. 2012). "Twenty-Five Lessons from Computational Neuromodulation". In: *Neuron* 76.1, pp. 240–256. ISSN: 08966273. DOI: 10.1016/j.neuron.2012.09.027. URL: https://linkinghub.elsevier.com/retrieve/pii/S0896627312008628 (visited on 07/25/2019).

Palacios-Filardo, Jon and Jack R Mellor (Feb. 2019). "Neuromodulation of hippocampal long-term synaptic plasticity". In: *Current Opinion in Neurobiology* 54, pp. 37–43. ISSN: 0959-4388. DOI: 10.1016/j.conb.2018.08.009. URL: https://www.ncbi.nlm.nih.gov/pmc/articles/PMC6367596/ (visited on 08/13/2023).

Silva, Weber C.N. da, Cristiano C. Köhler, Andressa Radiske, and Martín Cammarota (Feb. 1, 2012). "D1/D5 dopamine receptors modulate spatial memory formation". In: *Neurobiology of Learning and Memory* 97.2, pp. 271–275. ISSN: 1074-7427. DOI: 10.1016/j.nlm.2012.01.005. URL: https://www.sciencedirect.com/science/article/pii/S1074742712000068.

McNamara, Colin G, Álvaro Tejero-Cantero, Stéphanie Trouche, Natalia Campo-Urriza, and David Dupret (Dec. 1, 2014). "Dopaminergic neurons promote hippocampal reactivation and spatial memory persistence". In: *Nature Neuroscience* 17.12, pp. 1658–1660. ISSN: 1546-1726. DOI: 10.1038/nn.3843. URL: https://doi.org/10.1038/nn.3843.

Lisman, John E. and Anthony A. Grace (June 2, 2005). "The Hippocampal-VTA Loop: Controlling the Entry of Information into Long-Term Memory". In: *Neuron* 46.5, pp. 703–713. ISSN: 0896-6273. DOI: 10.1016/j.neuron.2005.05.002. URL: https://www.sciencedirect.com/science/article/pii/S0896627305003971.

Edelmann, Elke and Volkmar Lessmann (Sept. 1, 2018). "Dopaminergic innervation and modulation of hippocampal networks". In: *Cell and Tissue Research* 373.3, pp. 711–727. ISSN: 1432-0878. DOI: 10.1007/s00441-018-2800-7. URL: https://doi.org/10.1007/s00441-018-2800-7.

Chowdhury, Ananya, Alessandro Luchetti, Giselle Fernandes, Daniel Almeida Filho, George Kastellakis, Alexandra Tzilivaki, Erica M. Ramirez, Mary Y. Tran, Panayiota Poirazi, and Alcino J. Silva (Aug. 2022). "A locus coeruleus-dorsal CA1 dopaminergic circuit modulates memory linking". In: *Neuron*, S0896627322007073. ISSN: 08966273. DOI: 10.1016/j.neuron.2022.08.001. URL: https://linkinghub.elsevier.com/retrieve/pii/S0896627322007073 (visited on 09/07/2022).

Wagatsuma, Akiko, Teruhiro Okuyama, Chen Sun, Lillian M. Smith, Kuniya Abe, and Susumu Tonegawa (Jan. 9, 2018). "Locus coeruleus input to hippocampal CA3 drives single-trial learning of a novel context". In: *Proceedings of the National Academy of Sciences* 115.2, E310–E316. ISSN: 0027-8424, 1091-6490. DOI: 10.1073/pnas.1714082115. URL: http://www.pnas.org/lookup/doi/10.1073/pnas.1714082115 (visited on 03/14/2019).

Kempadoo, Kimberly A., Eugene V. Mosharov, Se Joon Choi, David Sulzer, and Eric R. Kandel (Dec. 20, 2016). "Dopamine release from the locus coeruleus to the dorsal hippocampus promotes spatial learning and memory". In: *Proceedings of the National Academy of Sciences* 113.51. Publisher: Proceedings of the National Academy of Sciences, pp. 14835–14840. DOI: 10.1073/pnas.1616515114. URL: https://www.pnas.org/doi/10.1073/pnas.1616515114 (visited on 06/20/2023).

Tsetsenis, Theodoros, Julia Kathleen Badyna, Manivanan Subramaniyan, Rebecca Li, Kechun Yang, and John A. Dani (2019). "Dopamine and Norepinephrine Modulate the Formation of Aversive Memories in the Hippocampus". In: *SSRN Electronic Journal*. ISSN: 1556-5068. DOI: 10.2139/ssrn.3509875. URL: https://www.ssrn.com/abstract=3509875 (visited on 01/21/2020).

Hansen, N. and D. Manahan-Vaughan (Apr. 1, 2014). "Dopamine D1/D5 Receptors Mediate Informational Saliency that Promotes Persistent Hippocampal Long-Term Plasticity". In: *Cerebral Cortex* 24.4, pp. 845–858. ISSN: 1047-3211, 1460-2199. DOI: 10.1093/cercor/bhs362. URL: https://academic.oup.com/cercor/article-lookup/doi/10.1093/cercor/bhs362 (visited on 06/18/2019).

Assar, Nasim, Dorna Mahmoudi, Ali Farhoudian, Mohammad Hasan Farhadi, Zahra Fatahi, and Abbas Haghparast (Oct. 2016). "D1- and D2-like dopamine receptors in the CA1 region of the hippocampus are involved in the acquisition and reinstatement of morphine-induced conditioned place preference". In: *Behavioural Brain Research* 312, pp. 394–404. ISSN: 01664328. DOI: 10.1016/j.bbr.2016.06.061. URL: https://linkinghub.elsevier.com/retrieve/pii/S0166432816304259 (visited on 04/30/2020).

Azevedo, Estefania P., Lisa Pomeranz, Jia Cheng, Marc Schneeberger, Roger Vaughan, Sarah A. Stern, Bowen Tan, Katherine Doerig, Paul Greengard, and Jeffrey M. Friedman (May 2019). "A Role of Drd2 Hippocampal Neurons in Context-Dependent Food Intake". In: *Neuron* 102.4, 873–886.e5. ISSN: 08966273. DOI: 10.1016/j.neuron.2019.03.011. URL: https://linkinghub.elsevier.com/retrieve/pii/S0896627319302181 (visited on 05/23/2019).

Takeuchi, Tomonori, Adrian J. Duszkiewicz, Alex Sonneborn, Patrick A. Spooner, Miwako Yamasaki, Masahiko Watanabe, Caroline C. Smith, Guillén Fernández, Karl Deisseroth, Robert W. Greene, and Richard G. M. Morris (Sept. 2016). "Locus coeruleus and dopamin-

ergic consolidation of everyday memory". In: *Nature* 537.7620, pp. 357–362. ISSN: 0028-0836, 1476-4687. DOI: 10.1038/nature19325. URL: http://www.nature.com/articles/nature19325 (visited on 03/19/2019).

Duszkiewicz, Adrian J., Colin G. McNamara, Tomonori Takeuchi, and Lisa Genzel (Feb. 1, 2019). "Novelty and Dopaminergic Modulation of Memory Persistence: A Tale of Two Systems". In: *Trends in Neurosciences* 42.2, pp. 102–114. ISSN: 0166-2236. DOI: 10.1016/j.tins.2018.10.002. URL: https://www.sciencedirect.com/science/article/pii/S016622361830273X.

Jean-Martin Beaulieu and Raul R. Gainetdinov (Mar. 1, 2011). "The Physiology, Signaling, and Pharmacology of Dopamine Receptors". In: *Pharmacological Reviews* 63.1. Ed. by David R. Sibley, p. 182. DOI: 10.1124/pr.110.002642. URL: http://pharmrev.aspetjournals.org/content/63/1/182.abstract.

Gangarossa, Giuseppe, Sophie Longueville, Dimitri De Bundel, Julie Perroy, Denis Hervé, Jean-Antoine Girault, and Emmanuel Valjent (Dec. 1, 2012). "Characterization of dopamine D1 and D2 receptor-expressing neurons in the mouse hippocampus". In: *Hippocampus* 22.12. Publisher: John Wiley & Sons, Ltd, pp. 2199–2207. ISSN: 1050-9631. DOI: 10.1002/hipo.22044. URL: https://doi.org/10.1002/hipo.22044 (visited on 08/13/2023).

Wei, Xiaoyan, Tengfei Ma, Yifeng Cheng, Cathy C.Y. Huang, Xuehua Wang, Jiayi Lu, and Jun Wang (Mar. 1, 2018). "Dopamine D1 or D2 receptor-expressing neurons in the central nervous system". In: *Addiction Biology* 23.2. Publisher: John Wiley & Sons, Ltd, pp. 569–584. ISSN: 1355-6215. DOI: 10.1111/adb.12512. URL: https://doi.org/10.1111/adb.12512 (visited on 08/13/2023).

Yao, Wei-Dong, Roger D. Spealman, and Jingping Zhang (June 1, 2008). "Dopaminergic signaling in dendritic spines". In: *Biochemical Pharmacology* 75.11, pp. 2055–2069. ISSN: 0006-2952. DOI: 10.1016/j.bcp.2008.01.018. URL: https://www.sciencedirect.com/science/article/pii/S0006295208000956.

C Charuchinda, P Supavilai, M Karobath, and JM Palacios (May 1, 1987). "Dopamine D2 receptors in the rat brain: autoradiographic visualization using a high-affinity selective agonist ligand". In: *The Journal of Neuroscience* 7.5, p. 1352. DOI: 10.1523/JNEUROSCI.07-05-01352.1987. URL: http://www.jneurosci.org/content/7/5/1352.abstract.

Puighermanal, Emma, Laura Cutando, Jihane Boubaker-Vitre, Eve Honoré, Sophie Longueville, Denis Hervé, and Emmanuel Valjent (May 2017). "Anatomical and molecular characterization of dopamine D1 receptor-expressing neurons of the mouse CA1 dorsal hippocampus". In: *Brain Structure and Function* 222.4, pp. 1897–1911. ISSN: 1863-2653, 1863-2661. DOI: 10.1007/s00429-016-1314-x. URL: http://link.springer.com/10.1007/s00429-016-1314-x (visited on 07/15/2019).

Chen, Zhixiong, Satoshi Fujii, Ken-Ichi Ito, Hiroshi Kato, Kenya Kaneko, and Hiroyoshi Miyakawa (Mar. 31, 1995). "Activation of dopamine D1 receptors enhances long-term depression of synaptic transmission induced by low frequency stimulation in rat hippocampal CA1 neurons". In: *Neuroscience Letters* 188.3, pp. 195–198. ISSN: 0304-3940. DOI: 10.1016/0304-3940(95)11430-5. URL: https://www.sciencedirect.com/science/article/pii/0304394095114305.

Rocchetti, Jill, Elsa Isingrini, Gregory Dal Bo, Sara Sagheby, Aurore Menegaux, François Tronche, Daniel Levesque, Luc Moquin, Alain Gratton, Tak Pan Wong, Marcelo Rubinstein, and Bruno Giros (Mar. 15, 2015). "Presynaptic D2 Dopamine Receptors Control Long-Term Depression Expression and Memory Processes in the Temporal Hippocampus". In: *N-Methyl-D-Aspartate Receptor Deficits and Schizophrenia* 77.6, pp. 513–525. ISSN: 0006-3223. DOI: 10.1016/j.biopsych.2014.03.013. URL: https://www.sciencedirect.com/science/article/pii/S0006322314001668.

Huang, YAN-You and Eric R Kandel (n.d.). "D1/D5 receptor agonists induce a protein synthesis-dependent late potentiation in the CAl region of the hippocampus". In: (), p. 5.

Hagena, Hardy and Denise Manahan-Vaughan (2013). "Differentiation in the protein synthesis-dependency of persistent synaptic plasticity in mossy fiber and associational/commissural CA3 synapses in vivo". In: *Frontiers in Integrative Neuroscience* 7. ISSN: 1662-5145. DOI: 10.3389/fnint.2013.00010. URL: http://journal.frontiersin.org/article/10.3389/fnint.2013.00010/abstract (visited on 08/30/2019).

Kusuki, Tsukasa, Yoshio Imahori, Satoshi Ueda, and Kaoru Inokuchi (1997). "Dopaminergic modulation of LTP induction in the dentate gyrus of intact brain". In: *NeuroReport* 8.8. ISSN: 0959-4965. URL: https://journals.lww.com/neuroreport/Fulltext/1997/05260/Dopaminergic_modulation_of_LTP_induction_in_the.46.aspx.

Wieschollek, Valentina and Denise Manahan-Vaughan (Dec. 1, 2014). "Antagonism of D1/D5 receptors prevents long-term depression (LTD) and learning-facilitated LTD at the perforant path–dentate gyrus synapse in freely behaving rats". In: *Hippocampus* 24.12. Publisher: John Wiley & Sons, Ltd, pp. 1615–1622. ISSN: 1050-9631. DOI: 10.1002/hipo.22340. URL: https://doi.org/10.1002/hipo.22340 (visited on 08/13/2023).

Zhang, Ji-Chuan, Pak-Ming Lau, and Guo-Qiang Bi (Aug. 4, 2009). "Gain in sensitivity and loss in temporal contrast of STDP by dopaminergic modulation at hippocampal synapses". In: *Proceedings of the National Academy of Sciences* 106.31. Publisher: Proceedings of the National Academy of Sciences, pp. 13028–13033. DOI: 10.1073/pnas.0900546106. URL: https://www.pnas.org/doi/full/10.1073/pnas.0900546106 (visited on 08/13/2023).

Edelmann, Elke and Volkmar Lessmann (2011). "Dopamine Modulates Spike Timing-Dependent Plasticity and Action Potential Properties in CA1 Pyramidal Neurons of Acute Rat Hippocampal Slices". In: *Frontiers in Synaptic Neuroscience* 3. ISSN: 1663-3563. URL: https://www.frontiersin.org/articles/10.3389/fnsyn.2011.00006.

Yang, Kechun and John A. Dani (Nov. 26, 2014). "Dopamine D1 and D5 Receptors Modulate Spike Timing-Dependent Plasticity at Medial Perforant Path to Dentate Granule Cell Synapses". In: *The Journal of Neuroscience* 34.48, pp. 15888–15897. ISSN: 0270-6474. DOI: 10.1523/JNEUROSCI.2400-14.2014. URL: https://www.ncbi.nlm.nih.gov/pmc/articles/PMC4244463/ (visited on 08/13/2023).

Cumming, Paul (Sept. 2011). "Absolute abundances and affinity states of dopamine receptors in mammalian brain: A review". In: *Synapse (New York, N.Y.)* 65.9, pp. 892–909. ISSN: 1098-2396. DOI: 10.1002/syn.20916.

O'Carroll, C. M., S. J. Martin, J. Sandin, B. Frenguelli, and R. G.M. Morris (Nov. 1, 2006). "Dopaminergic modulation of the persistence of one-trial hippocampus-dependent memory". In: *Learning & Memory* 13.6, pp. 760–769. ISSN: 1072-0502. DOI: 10.1101/lm.321006. URL: http://www.learnmem.org/cgi/doi/10.1101/lm.321006 (visited on 09/04/2019).

Xing, B., H. Kong, X. Meng, S. G. Wei, M. Xu, and S. B. Li (Sept. 15, 2010). "Dopamine D1 but not D3 receptor is critical for spatial learning and related signaling in the hippocampus". In: *Neuroscience* 169.4, pp. 1511–1519. ISSN: 1873-7544. DOI: 10.1016/j.neuroscience.2010.06.034.

Granado, Noelia, Oskar Ortiz, Luz M. Suárez, Eduardo D. Martín, Valentín Ceña, José M. Solís, and Rosario Moratalla (Jan. 2008). "D1 but not D5 dopamine receptors are critical for LTP, spatial learning, and LTP-Induced arc and zif268 expression in the hippocampus". In: *Cerebral Cortex (New York, N.Y.: 1991)* 18.1, pp. 1–12. ISSN: 1460-2199. DOI: 10.1093/cercor/bhm026.

Burgdorf, Caitlin E., Kathryn C. Schierberl, Anni S. Lee, Delaney K. Fischer, Tracey A. Van Kempen, Vladimir Mudragel, Richard L. Huganir, Teresa A. Milner, Michael J. Glass, and Anjali M. Rajadhyaksha (Dec. 6, 2017). "Extinction of Contextual Cocaine Memories Requires Ca $_{v}$ 1.2 within D1R-Expressing Cells and Recruits Hippocampal Ca $_{v}$ 1.2-Dependent Signaling Mechanisms". In: *The Journal of Neuroscience* 37.49, pp. 11894–11911. ISSN: 0270-6474, 1529-2401. DOI: 10.1523/JNEUROSCI.2397-17.2017. URL: http://www.jneurosci.org/lookup/doi/10.1523/JNEUROSCI.2397-17.2017 (visited on 04/30/2020).

Tang, Jianrong and John A. Dani (Sept. 10, 2009). "Dopamine Enables In Vivo Synaptic Plasticity Associated with the Addictive Drug Nicotine". In: *Neuron* 63.5, pp. 673–682.

ISSN: 0896-6273. DOI: 10.1016/j.neuron.2009.07.025. URL: https://www.ncbi.nlm.nih.gov/pmc/articles/PMC2746116/ (visited on 08/14/2023).

Li, Shaomin, William K. Cullen, Roger Anwyl, and Michael J. Rowan (May 2003). "Dopamine-dependent facilitation of LTP induction in hippocampal CA1 by exposure to spatial novelty". In: *Nature Neuroscience* 6.5, pp. 526–531. ISSN: 1097-6256, 1546-1726. DOI: 10.1038/nn1049. URL: http://www.nature.com/articles/nn1049 (visited on 08/30/2019).

Liu, Jue, Wei Wang, Fang Wang, Fei Cai, Zhuang-Li Hu, Yuan-Jian Yang, Jin Chen, and Jian-Guo Chen (Aug. 2009). "Phosphatidylinositol-linked novel D(1) dopamine receptor facilitates long-term depression in rat hippocampal CA1 synapses". In: *Neuropharmacology* 57.2, pp. 164–171. ISSN: 1873-7064. DOI: 10.1016/j.neuropharm.2009.05.001.

Moncada, Diego and Haydée Viola (July 11, 2007). "Induction of long-term memory by exposure to novelty requires protein synthesis: evidence for a behavioral tagging". In: *The Journal of Neuroscience: The Official Journal of the Society for Neuroscience* 27.28, pp. 7476–7481. ISSN: 1529-2401. DOI: 10.1523/JNEUROSCI.1083-07.2007.

Sheffield, Mark E.J., Michael D. Adoff, and Daniel A. Dombeck (Oct. 11, 2017). "Increased Prevalence of Calcium Transients across the Dendritic Arbor during Place Field Formation". In: *Neuron* 96.2, 490–504.e5. ISSN: 0896-6273. DOI: 10.1016/j.neuron.2017.09.029. URL: https://www.sciencedirect.com/science/article/pii/S0896627317308735.

Schultz, Wolfram (July 1, 1998). "Predictive Reward Signal of Dopamine Neurons". In: *Journal of Neurophysiology* 80.1, pp. 1–27. ISSN: 0022-3077, 1522-1598. DOI: 10.1152/jn.1998.80.1.1. URL: https://www.physiology.org/doi/10.1152/jn.1998.80.1.1 (visited on 07/25/2020).

Sutton, Richard S. and Andrew G. Barto (1981). "Toward a modern theory of adaptive networks: Expectation and prediction." In: *Psychological Review* 88. Place: US Publisher: American Psychological Association, pp. 135–170. ISSN: 1939-1471 (Electronic), 0033-295X (Print). DOI: 10.1037/0033-295X.88.2.135.

Dabney, Will, Zeb Kurth-Nelson, Naoshige Uchida, Clara Kwon Starkweather, Demis Hassabis, Rémi Munos, and Matthew Botvinick (Jan. 15, 2020). "A distributional code for value in dopamine-based reinforcement learning". In: *Nature*. ISSN: 0028-0836, 1476-4687. DOI: 10.1038/s41586-019-1924-6. URL: http://www.nature.com/articles/s41586-019-1924-6 (visited on 01/16/2020).

Engelhard, Ben, Joel Finkelstein, Julia Cox, Weston Fleming, Hee Jae Jang, Sharon Ornelas, Sue Ann Koay, Stephan Y. Thiberge, Nathaniel D. Daw, David W. Tank, and Ilana B. Witten (June 1, 2019). "Specialized coding of sensory, motor and cognitive variables in

VTA dopamine neurons". In: *Nature* 570.7762, pp. 509–513. ISSN: 1476-4687. DOI: 10.1038/s41586-019-1261-9. URL: https://doi.org/10.1038/s41586-019-1261-9.

Kim, HyungGoo R., Athar N. Malik, John G. Mikhael, Pol Bech, Iku Tsutsui-Kimura, Fangmiao Sun, Yajun Zhang, Yulong Li, Mitsuko Watabe-Uchida, Samuel J. Gershman, and Naoshige Uchida (Dec. 10, 2020). "A Unified Framework for Dopamine Signals across Timescales". In: *Cell* 183.6, 1600–1616.e25. ISSN: 0092-8674. DOI: 10.1016/j.cell.2020.11.013. URL: https://www.sciencedirect.com/science/article/pii/S0092867420315300.

Mohebi, Ali, Jeffrey R. Pettibone, Arif A. Hamid, Jenny-Marie T. Wong, Leah T. Vinson, Tommaso Patriarchi, Lin Tian, Robert T. Kennedy, and Joshua D. Berke (June 1, 2019). "Dissociable dopamine dynamics for learning and motivation". In: *Nature* 570.7759, pp. 65–70. ISSN: 1476-4687. DOI: 10.1038/s41586-019-1235-y. URL: https://doi.org/10.1038/s41586-019-1235-y.

Howe, Mark W., Patrick L. Tierney, Stefan G. Sandberg, Paul E. M. Phillips, and Ann M. Graybiel (Aug. 1, 2013). "Prolonged dopamine signalling in striatum signals proximity and value of distant rewards". In: *Nature* 500.7464, pp. 575–579. ISSN: 1476-4687. DOI: 10.1038/nature12475. URL: https://doi.org/10.1038/nature12475.

Adeniyi, Philip A., Amita Shrestha, and Olalekan M. Ogundele (Oct. 15, 2020). "Distribution of VTA Glutamate and Dopamine Terminals, and their Significance in CA1 Neural Network Activity". In: *Neuroscience* 446, pp. 171–198. ISSN: 1873-7544. DOI: 10.1016/j.neuroscience.2020.06.045.

Adeyelu, Tolulope and Olalekan M. Ogundele (July 2023). "VTA multifaceted modulation of CA1 local circuits". In: *Neurobiology of Learning and Memory* 202, p. 107760. ISSN: 10747427. DOI: 10.1016/j.nlm.2023.107760. URL: https://linkinghub.elsevier.com/retrieve/pii/S1074742723000412 (visited on 06/14/2023).

Rosen, Zev B, Stephanie Cheung, and Steven A Siegelbaum (Dec. 2015). "Midbrain dopamine neurons bidirectionally regulate CA3-CA1 synaptic drive". In: *Nature Neuroscience* 18.12, pp. 1763–1771. ISSN: 1097-6256, 1546-1726. DOI: 10.1038/nn.4152. URL: http://www.nature.com/articles/nn.4152 (visited on 05/13/2019).

Rice, Margaret E. and Jyoti C. Patel (July 5, 2015). "Somatodendritic dopamine release: recent mechanistic insights". In: *Philosophical Transactions of the Royal Society of London. Series B, Biological Sciences* 370.1672, p. 20140185. ISSN: 1471-2970. DOI: 10.1098/rstb.2014.0185.

Borroto-Escuela, Dasiel O., Luigi F. Agnati, Karl Bechter, Anders Jansson, Alexander O. Tarakanov, and Kjell Fuxe (July 5, 2015). "The role of transmitter diffusion and flow

versus extracellular vesicles in volume transmission in the brain neural-glial networks". In: *Philosophical Transactions of the Royal Society of London. Series B, Biological Sciences* 370.1672, p. 20140183. ISSN: 1471-2970. DOI: 10.1098/rstb.2014.0183.

Agnati, L. F., M. Zoli, I. Strömberg, and K. Fuxe (Dec. 1995). "Intercellular communication in the brain: wiring versus volume transmission". In: *Neuroscience* 69.3, pp. 711–726. ISSN: 0306-4522. DOI: 10.1016/0306-4522(95)00308-6.

Han, Yuan, Yi Zhang, Haram Kim, Viktoriya S. Grayson, Vladimir Jovasevic, Wenjie Ren, Maria V. Centeno, Anita L. Guedea, Mariah A. A. Meyer, Yixin Wu, Philipp Gutruf, Dalton J. Surmeier, Can Gao, Marco Martina, Apkar V. Apkarian, John A. Rogers, and Jelena Radulovic (Dec. 2020). "Excitatory VTA to DH projections provide a valence signal to memory circuits". In: *Nature Communications* 11.1. ISSN: 2041-1723. DOI: 10.1038/s41467-020-15035-z. URL: http://www.nature.com/articles/s41467-020-15035-z (visited on 03/26/2020).

Morales, Marisela and Elyssa B. Margolis (Feb. 2017). "Ventral tegmental area: cellular heterogeneity, connectivity and behaviour". In: *Nature Reviews. Neuroscience* 18.2, pp. 73–85. ISSN: 1471-0048. DOI: 10.1038/nrn.2016.165.

Gasbarri, A., C. Verney, R. Innocenzi, E. Campana, and C. Pacitti (Dec. 30, 1994). "Mesolimbic dopaminergic neurons innervating the hippocampal formation in the rat: a combined retrograde tracing and immunohistochemical study". In: *Brain Research* 668.1, pp. 71–79. ISSN: 0006-8993. DOI: 10.1016/0006-8993(94)90512-6. URL: https://www.sciencedirect.com/science/article/pii/0006899394905126.

Mamad, Omar, Lars Stumpp, Harold M. McNamara, Charu Ramakrishnan, Karl Deisseroth, Richard B. Reilly, and Marian Tsanov (Sept. 12, 2017). "Place field assembly distribution encodes preferred locations". In: *PLOS Biology* 15.9. Publisher: Public Library of Science, e2002365. DOI: 10.1371/journal.pbio.2002365. URL: https://doi.org/10.1371/journal.pbio.2002365.

Booker, Sam A. and Imre Vida (Sept. 1, 2018). "Morphological diversity and connectivity of hippocampal interneurons". In: *Cell and Tissue Research* 373.3, pp. 619–641. ISSN: 1432-0878. DOI: 10.1007/s00441-018-2882-2. URL: https://doi.org/10.1007/s00441-018-2882-2 (visited on 08/11/2023).

Borgkvist, Anders, Torun Malmlöf, Kristin Feltmann, Maria Lindskog, and Björn Schilström (May 1, 2012). "Dopamine in the hippocampus is cleared by the norepinephrine transporter". In: *International Journal of Neuropsychopharmacology* 15.4, pp. 531–540. ISSN: 1461-1457. DOI: 10.1017/S1461145711000812. URL: https://doi.org/10.1017/S1461145711000812 (visited on 08/15/2023).

Aston-Jones, G. and F. E. Bloom (Aug. 1981). "Norepinephrine-containing locus coeruleus neurons in behaving rats exhibit pronounced responses to non-noxious environmental stimuli". In: *The Journal of Neuroscience: The Official Journal of the Society for Neuroscience* 1.8, pp. 887–900. ISSN: 0270-6474. DOI: 10.1523/JNEUROSCI.01-08-00887.1981.

McCarley, R. W. and J. A. Hobson (July 4, 1975). "Neuronal excitability modulation over the sleep cycle: a structural and mathematical model". In: *Science (New York, N.Y.)* 189.4196, pp. 58–60. ISSN: 0036-8075. DOI: 10.1126/science.1135627.

Isaac, Stuart O. and Craig W. Berridge (Oct. 2003). "Wake-promoting actions of dopamine D1 and D2 receptor stimulation". In: *The Journal of Pharmacology and Experimental Therapeutics* 307.1, pp. 386–394. ISSN: 0022-3565. DOI: 10.1124/jpet.103.053918.

Reimer, Jacob, Matthew J McGinley, Yang Liu, Charles Rodenkirch, Qi Wang, David A McCormick, and Andreas S Tolias (Dec. 2016). "Pupil fluctuations track rapid changes in adrenergic and cholinergic activity in cortex". In: *Nature Communications* 7.1. ISSN: 2041-1723. DOI: 10.1038/ncomms13289. URL: http://www.nature.com/articles/ncomms13289 (visited on 08/27/2019).

Shulman, G. L., R. W. Remington, and J. P. McLean (Aug. 1979). "Moving attention through visual space". In: *Journal of Experimental Psychology. Human Perception and Performance* 5.3, pp. 522–526. ISSN: 0096-1523. DOI: 10.1037//0096-1523.5.3.522.

Bouret, Sebastien and Susan J. Sara (Dec. 2002). "Locus coeruleus activation modulates firing rate and temporal organization of odour-induced single-cell responses in rat piriform cortex". In: *The European Journal of Neuroscience* 16.12, pp. 2371–2382. ISSN: 0953-816X. DOI: 10.1046/j.1460-9568.2002.02413.x.

Martins, Ana Raquel O. and Robert C. Froemke (Oct. 2015). "Coordinated forms of noradrenergic plasticity in the locus coeruleus and primary auditory cortex". In: *Nature Neuroscience* 18.10, pp. 1483–1492. ISSN: 1546-1726. DOI: 10.1038/nn.4090.

Waterhouse, Barry D. and Rachel L. Navarra (Apr. 15, 2019). "The locus coeruleus norepinephrine system and sensory signal processing: A historical review and current perspectives". In: *Behavioral Consequences of Noradrenergic Actions in Sensory Networks* 1709, pp. 1–15. ISSN: 0006-8993. DOI: 10.1016/j.brainres.2018.08.032. URL: https://www.sciencedirect.com/science/article/pii/S0006899318304542.

Eschenko, Oxana (2018). "The Role of the Locus Coeruleus in Cellular and Systems Memory Consolidation". In: *Handbook of Behavioral Neuroscience*. Vol. 28. Elsevier, pp. 327–347. ISBN: 978-0-12-812028-6. DOI: 10.1016/B978-0-12-812028-6.00018-5. URL: https://linkinghub.elsevier.com/retrieve/pii/B9780128120286000185 (visited on 04/09/2019).

Yamasaki, Miwako and Tomonori Takeuchi (2017). "Locus Coeruleus and Dopamine-Dependent Memory Consolidation". In: *Neural Plasticity* 2017, pp. 1–15. ISSN: 2090-5904, 1687-5443. DOI: 10.1155/2017/8602690. URL: https://www.hindawi.com/journals/np/2017/8602690/ (visited on 04/09/2019).

Noei, Shahryar, Ioannis S. Zouridis, Nikos K. Logothetis, Stefano Panzeri, and Nelson K. Totah (May 3, 2022). "Distinct ensembles in the noradrenergic locus coeruleus are associated with diverse cortical states". In: *Proceedings of the National Academy of Sciences* 119.18. Publisher: Proceedings of the National Academy of Sciences, e2116507119. DOI: 10.1073/pnas.2116507119. URL: https://www.pnas.org/doi/10.1073/pnas.2116507119 (visited on 08/14/2023).

Chandler, Daniel J., Wen-Jun Gao, and Barry D. Waterhouse (May 6, 2014). "Heterogeneous organization of the locus coeruleus projections to prefrontal and motor cortices". In: *Proceedings of the National Academy of Sciences of the United States of America* 111.18, pp. 6816–6821. ISSN: 1091-6490. DOI: 10.1073/pnas.1320827111.

Kebschull, Justus M., Pedro Garcia da Silva, Ashlan P. Reid, Ian D. Peikon, Dinu F. Albeanu, and Anthony M. Zador (Sept. 7, 2016). "High-Throughput Mapping of Single-Neuron Projections by Sequencing of Barcoded RNA". In: *Neuron* 91.5, pp. 975–987. ISSN: 1097-4199. DOI: 10.1016/j.neuron.2016.07.036.

Uematsu, Akira, Bao Zhen Tan, Edgar A. Ycu, Jessica Sulkes Cuevas, Jenny Koivumaa, Felix Junyent, Eric J. Kremer, Ilana B. Witten, Karl Deisseroth, and Joshua P. Johansen (Nov. 2017). "Modular organization of the brainstem noradrenaline system coordinates opposing learning states". In: *Nature Neuroscience* 20.11, pp. 1602–1611. ISSN: 1546-1726. DOI: 10.1038/nn.4642.

Loy, R., D. A. Koziell, J. D. Lindsey, and R. Y. Moore (Feb. 15, 1980). "Noradrenergic innervation of the adult rat hippocampal formation". In: *The Journal of Comparative Neurology* 189.4, pp. 699–710. ISSN: 0021-9967. DOI: 10.1002/cne.901890406.

Segal, M., H. Markram, and G. Richter-Levin (1991). "Actions of norepinephrine in the rat hippocampus". In: *Progress in Brain Research* 88, pp. 323–330. ISSN: 0079-6123. DOI: 10.1016/s0079-6123(08)63819-4.

Edison, Hilary T. and Carolyn W. Harley (Mar. 2012). "Medial and lateral perforant path evoked potentials are selectively modulated by pairing with glutamatergic activation of locus coeruleus in the dentate gyrus of the anesthetized rat". In: *Hippocampus* 22.3, pp. 501–509. ISSN: 1098-1063. DOI: 10.1002/hipo.20916.

Hagena, Hardy and Denise Manahan-Vaughan (2012). "Learning-facilitated long-term depression and long-term potentiation at mossy fiber-CA3 synapses requires activation of

-adrenergic receptors". In: *Frontiers in Integrative Neuroscience* 6, p. 23. ISSN: 1662-5145. DOI: 10.3389/fnint.2012.00023.

Goh, Jinzhong Jeremy and Denise Manahan-Vaughan (Dec. 2013). "Hippocampal long-term depression in freely behaving mice requires the activation of beta-adrenergic receptors". In: *Hippocampus* 23.12, pp. 1299–1308. ISSN: 1098-1063. DOI: 10.1002/hipo.22168.

Ji, Jinzhao, Xuehan Zhang, and Baoming Li (Dec. 2003). "beta-adrenergic modulation of in vivo long-term potentiation in area CA1 and its role in spatial learning in rats". In: *Science in China. Series C, Life Sciences* 46.6, pp. 605–614. ISSN: 1006-9305. DOI: 10.1360/02yc0243.

Ji, J.-Z., X.-H. Zhang, and B.-M. Li (Dec. 2003). "Deficient spatial memory induced by blockade of beta-adrenoceptors in the hippocampal CA1 region". In: *Behavioral Neuroscience* 117.6, pp. 1378–1384. ISSN: 0735-7044. DOI: 10.1037/0735-7044.117.6.1378.

Gibbs, Marie E. and Roger J. Summers (Aug. 2002). "Role of adrenoceptor subtypes in memory consolidation". In: *Progress in Neurobiology* 67.5, pp. 345–391. ISSN: 0301-0082. DOI: 10.1016/s0301-0082(02)00023-0.

Thomas, Steven A. (Apr. 2015). "Neuromodulatory Signaling in Hippocampus-Dependent Memory Retrieval". In: *Hippocampus* 25.4, pp. 415–431. ISSN: 1050-9631. DOI: 10.1002/hipo.22394. URL: https://www.ncbi.nlm.nih.gov/pmc/articles/PMC9484472/ (visited on 08/14/2023).

André, Marion Agnès Emma, Oliver T. Wolf, and Denise Manahan-Vaughan (2015). "Beta-adrenergic receptors support attention to extinction learning that occurs in the absence, but not the presence, of a context change". In: *Frontiers in Behavioral Neuroscience* 9, p. 125. ISSN: 1662-5153. DOI: 10.3389/fnbeh.2015.00125.

Hagena, Hardy, Niels Hansen, and Denise Manahan-Vaughan (Apr. 1, 2016). "-Adrenergic Control of Hippocampal Function: Subserving the Choreography of Synaptic Information Storage and Memory". In: *Cerebral Cortex* 26.4, pp. 1349–1364. ISSN: 1047-3211. DOI: 10.1093/cercor/bhv330. URL: https://doi.org/10.1093/cercor/bhv330 (visited on 07/31/2023).

Kaufman, Alexandra Mansell, Tristan Geiller, and Attila Losonczy (Mar. 18, 2020). "A Role for the Locus Coeruleus in Hippocampal CA1 Place Cell Reorganization during Spatial Reward Learning". In: *Neuron* 105.6, 1018–1026.e4. ISSN: 0896-6273. DOI: 10.1016/j.neuron.2019.12.029. URL: https://www.sciencedirect.com/science/article/pii/S0896627319310955.

Colgin, Laura Lee, Edvard I. Moser, and May-Britt Moser (Sept. 1, 2008). "Understanding memory through hippocampal remapping". In: *Trends in Neurosciences* 31.9, pp. 469–477. ISSN: 0166-2236. DOI: 10.1016/j.tins.2008.06.008. URL: https://www.sciencedirect.com/science/article/pii/S0166223608001677.

Bostock, Elizabeth, Robert U. Muller, and John L. Kubie (Apr. 2, 1991). "Experience-dependent modifications of hippocampal place cell firing". In: *Hippocampus* 1.2. Publisher: John Wiley & Sons, Ltd, pp. 193–205. ISSN: 1050-9631. DOI: 10.1002/hipo.450010207. URL: https://doi.org/10.1002/hipo.450010207 (visited on 06/20/2023).

Ziv, Yaniv, Laurie D Burns, Eric D Cocker, Elizabeth O Hamel, Kunal K Ghosh, Lacey J Kitch, Abbas El Gamal, and Mark J Schnitzer (Mar. 1, 2013). "Long-term dynamics of CA1 hippocampal place codes". In: *Nature Neuroscience* 16.3, pp. 264–266. ISSN: 1546-1726. DOI: 10.1038/nn.3329. URL: https://doi.org/10.1038/nn.3329.

Dong, Can, Antoine D. Madar, and Mark E. J. Sheffield (May 20, 2021). "Distinct place cell dynamics in CA1 and CA3 encode experience in new environments". In: *Nature Communications* 12.1, p. 2977. ISSN: 2041-1723. DOI: 10.1038/s41467-021-23260-3. URL: https://doi.org/10.1038/s41467-021-23260-3.

Hainmueller, Thomas and Marlene Bartos (June 1, 2018). "Parallel emergence of stable and dynamic memory engrams in the hippocampus". In: *Nature* 558.7709, pp. 292–296. ISSN: 1476-4687. DOI: 10.1038/s41586-018-0191-2. URL: https://doi.org/10.1038/s41586-018-0191-2.

RU Muller and JL Kubie (July 1, 1987). "The effects of changes in the environment on the spatial firing of hippocampal complex-spike cells". In: *The Journal of Neuroscience* 7.7, p. 1951. DOI: 10.1523/JNEUROSCI.07-07-01951.1987. URL: http://www.jneurosci.org/content/7/7/1951.abstract.

Goode, Travis D., Kazumasa Z. Tanaka, Amar Sahay, and Thomas J. McHugh (Sept. 9, 2020). "An Integrated Index: Engrams, Place Cells, and Hippocampal Memory". In: *Neuron* 107.5, pp. 805–820. ISSN: 0896-6273. DOI: 10.1016/j.neuron.2020.07.011. URL: https://www.sciencedirect.com/science/article/pii/S0896627320305286.

Robinson, Nick T.M., Lucie A.L. Descamps, Lloyd E. Russell, Moritz O. Buchholz, Brendan A. Bicknell, Georgy K. Antonov, Joanna Y.N. Lau, Rebecca Nutbrown, Christoph Schmidt-Hieber, and Michael Häusser (Dec. 10, 2020). "Targeted Activation of Hippocampal Place Cells Drives Memory-Guided Spatial Behavior". In: *Cell* 183.6, 1586–1599.e10. ISSN: 0092-8674. DOI: 10.1016/j.cell.2020.09.061. URL: https://www.sciencedirect.com/science/article/pii/S0092867420313027.

Michael I. Anderson and Kathryn J. Jeffery (Oct. 1, 2003). "Heterogeneous Modulation of Place Cell Firing by Changes in Context". In: *The Journal of Neuroscience* 23.26, p. 8827. DOI: 10.1523/JNEUROSCI.23-26-08827.2003. URL: http://www.jneurosci.org/content/23/26/8827.abstract.

Kentros, Clifford G, Naveen T Agnihotri, Samantha Streater, Robert D Hawkins, and Eric R Kandel (Apr. 22, 2004). "Increased Attention to Spatial Context Increases Both Place Field Stability and Spatial Memory". In: *Neuron* 42.2. Publisher: Elsevier, pp. 283–295. ISSN: 0896-6273. DOI: 10.1016/S0896-6273(04)00192-8. URL: https://doi.org/10.1016/S0896-6273(04)00192-8 (visited on 06/20/2023).

André A. Fenton, William W. Lytton, Jeremy M. Barry, Pierre-Pascal Lenck-Santini, Larissa E. Zinyuk, Štepan Kubík, Jan Bureš, Bruno Poucet, Robert U. Muller, and Andrey V. Olypher (Mar. 31, 2010). "Attention-Like Modulation of Hippocampus Place Cell Discharge". In: *The Journal of Neuroscience* 30.13, p. 4613. DOI: 10.1523/JNEUROSCI.5576-09.2010. URL: http://www.jneurosci.org/content/30/13/4613.abstract.

Wood, Emma R., Paul A. Dudchenko, R.Jonathan Robitsek, and Howard Eichenbaum (Sept. 1, 2000). "Hippocampal Neurons Encode Information about Different Types of Memory Episodes Occurring in the Same Location". In: *Neuron* 27.3, pp. 623–633. ISSN: 0896-6273. DOI: 10.1016/S0896-6273(00)00071-4. URL: https://www.sciencedirect.com/science/article/pii/S0896627300000714.

Zhao, Xinyu, Ching-Lung Hsu, and Nelson Spruston (Jan. 5, 2022). "Rapid synaptic plasticity contributes to a learned conjunctive code of position and choice-related information in the hippocampus". In: *Neuron* 110.1, 96–108.e4. ISSN: 0896-6273. DOI: 10.1016/j.neuron.2021.10.003. URL: https://www.sciencedirect.com/science/article/pii/S0896627321007716.

Kinsky, Nathaniel R., William Mau, David W. Sullivan, Samuel J. Levy, Evan A. Ruesch, and Michael E. Hasselmo (May 15, 2020). "Trajectory-modulated hippocampal neurons persist throughout memory-guided navigation". In: *Nature Communications* 11.1, p. 2443. ISSN: 2041-1723. DOI: 10.1038/s41467-020-16226-4. URL: https://doi.org/10.1038/s41467-020-16226-4.

Marta A. P. Moita, Svetlana Rosis, Yu Zhou, Joseph E. LeDoux, and Hugh T. Blair (Aug. 4, 2004). "Putting Fear in Its Place: Remapping of Hippocampal Place Cells during Fear Conditioning". In: *The Journal of Neuroscience* 24.31, p. 7015. DOI: 10.1523/JNEUROSCI.5492-03.2004. URL: http://www.jneurosci.org/content/24/31/7015.abstract.

Peter J. Schuette, Fernando M. C. V. Reis, Sandra Maesta-Pereira, Meghmik Chakerian, Anita Torossian, Garrett J. Blair, Weisheng Wang, Hugh T. Blair, Michael S. Fanselow, Jonathan C. Kao, and Avishek Adhikari (Oct. 21, 2020). "Long-Term Characterization of

Hippocampal Remapping during Contextual Fear Acquisition and Extinction". In: *The Journal of Neuroscience* 40.43, p. 8329. DOI: 10.1523/JNEUROSCI.1022-20.2020. URL: http://www.jneurosci.org/content/40/43/8329.abstract.

Rouhani, Nina and Yael Niv (Mar. 4, 2021). "Signed and unsigned reward prediction errors dynamically enhance learning and memory". In: *eLife* 10. Ed. by Thorsten Kahnt and Christian Büchel. Publisher: eLife Sciences Publications, Ltd, e61077. ISSN: 2050-084X. DOI: 10.7554/eLife.61077. URL: https://doi.org/10.7554/eLife.61077.

Jang, Anthony I., Matthew R. Nassar, Daniel G. Dillon, and Michael J. Frank (July 1, 2019). "Positive reward prediction errors during decision-making strengthen memory encoding". In: *Nature Human Behaviour* 3.7, pp. 719–732. ISSN: 2397-3374. DOI: 10.1038/s41562-019-0597-3. URL: https://doi.org/10.1038/s41562-019-0597-3.

Stanek, Jessica K., Kathryn C. Dickerson, Kimberly S. Chiew, Nathaniel J. Clement, and R. Alison Adcock (Oct. 1, 2019). "Expected Reward Value and Reward Uncertainty Have Temporally Dissociable Effects on Memory Formation". In: *Journal of Cognitive Neuroscience* 31.10, pp. 1443–1454. ISSN: 0898-929X. DOI: 10.1162/jocn_a_01411. URL: https://doi.org/10.1162/jocn_a_01411 (visited on 06/20/2023).

Éléonore Duvelle, Roddy M. Grieves, Vincent Hok, Bruno Poucet, Angelo Arleo, Kate J. Jeffery, and Etienne Save (Mar. 27, 2019). "Insensitivity of Place Cells to the Value of Spatial Goals in a Two-Choice Flexible Navigation Task". In: *The Journal of Neuroscience* 39.13, p. 2522. DOI: 10.1523/JNEUROSCI.1578-18.2018. URL: http://www.jneurosci.org/content/39/13/2522.abstract.

Tabuchi, E., A.B. Mulder, and S.I. Wiener (Jan. 1, 2003). "Reward value invariant place responses and reward site associated activity in hippocampal neurons of behaving rats". In: *Hippocampus* 13.1. Publisher: John Wiley & Sons, Ltd, pp. 117–132. ISSN: 1050-9631. DOI: 10.1002/hipo.10056. URL: https://doi.org/10.1002/hipo.10056 (visited on 06/20/2023).

Wikenheiser, Andrew M. and A. David Redish (Aug. 1, 2011). "Changes in reward contingency modulate the trial-to-trial variability of hippocampal place cells". In: *Journal of Neurophysiology* 106.2. Publisher: American Physiological Society, pp. 589–598. ISSN: 0022-3077. DOI: 10.1152/jn.00091.2011. URL: https://doi.org/10.1152/jn.00091.2011 (visited on 06/20/2023).

Lee, Inah, Amy L. Griffin, Eric A. Zilli, Howard Eichenbaum, and Michael E. Hasselmo (Sept. 7, 2006). "Gradual Translocation of Spatial Correlates of Neuronal Firing in the Hippocampus toward Prospective Reward Locations". In: *Neuron* 51.5, pp. 639–650. ISSN: 0896-6273. DOI: 10.1016/j.neuron.2006.06.033. URL: https://www.sciencedirect.com/science/article/pii/S0896627306005836.

Poucet, B. and V. Hok (2017). "Remembering goal locations." In: *Current Opinion in Behavioral Sciences* 17. Place: Netherlands Publisher: Elsevier Science, pp. 51–56. ISSN: 2352-1554(Electronic),2352-1546(Print). DOI: 10.1016/j.cobeha.2017.06.003.

Martig, Adria K. and Sheri J.Y. Mizumori (Feb. 1, 2011). "Ventral tegmental area disruption selectively affects CA1/CA2 but not CA3 place fields during a differential reward working memory task". In: *Hippocampus* 21.2. Publisher: John Wiley & Sons, Ltd, pp. 172–184. ISSN: 1050-9631. DOI: 10.1002/hipo.20734. URL: https://doi.org/10.1002/hipo.20734 (visited on 06/20/2023).

Sosa, Marielena and Lisa M. Giocomo (Aug. 1, 2021). "Navigating for reward". In: *Nature Reviews Neuroscience* 22.8, pp. 472–487. ISSN: 1471-0048. DOI: 10.1038/s41583-021-00479-z. URL: https://doi.org/10.1038/s41583-021-00479-z.

Guru, Akash, Changwoo Seo, Ryan J. Post, Durga S. Kullakanda, Julia A. Schaffer, and Melissa R. Warden (May 22, 2020). *Ramping activity in midbrain dopamine neurons signifies the use of a cognitive map*. preprint. Neuroscience. DOI: 10.1101/2020.05.21.108886. URL: http://biorxiv.org/lookup/doi/10.1101/2020.05.21.108886 (visited on 05/28/2020).

McNaughton, B. L., C. A. Barnes, and J. O'Keefe (Sept. 1, 1983). "The contributions of position, direction, and velocity to single unit activity in the hippocampus of freely-moving rats". In: *Experimental Brain Research* 52.1, pp. 41–49. ISSN: 1432-1106. DOI: 10.1007/BF00237147. URL: https://doi.org/10.1007/BF00237147.

Chen, Tsai-Wen, Trevor J. Wardill, Yi Sun, Stefan R. Pulver, Sabine L. Renninger, Amy Baohan, Eric R. Schreiter, Rex A. Kerr, Michael B. Orger, Vivek Jayaraman, Loren L. Looger, Karel Svoboda, and Douglas S. Kim (July 1, 2013). "Ultrasensitive fluorescent proteins for imaging neuronal activity". In: *Nature* 499.7458, pp. 295–300. ISSN: 1476-4687. DOI: 10.1038/nature12354. URL: https://doi.org/10.1038/nature12354.

Pettit, Noah L., Xintong C. Yuan, and Christopher D. Harvey (May 1, 2022). "Hippocampal place codes are gated by behavioral engagement". In: *Nature Neuroscience* 25.5, pp. 561–566. ISSN: 1546-1726. DOI: 10.1038/s41593-022-01050-4. URL: https://doi.org/10.1038/s41593-022-01050-4.

Beatty, Jackson (1982). "Task-evoked pupillary responses, processing load, and the structure of processing resources." In: *Psychological Bulletin* 91. Place: US Publisher: American Psychological Association, pp. 276–292. ISSN: 1939-1455(Electronic),0033-2909(Print). DOI: 10.1037/0033-2909.91.2.276.

Bradley, Margaret M., Laura Miccoli, Miguel A. Escrig, and Peter J. Lang (July 1, 2008). "The pupil as a measure of emotional arousal and autonomic activation". In: *Psychophys-*

iology 45.4. Publisher: John Wiley & Sons, Ltd, pp. 602–607. ISSN: 0048-5772. DOI: 10.1111/j.1469-8986.2008.00654.x. URL: https://doi.org/10.1111/j.1469-8986.2008.00654.x (visited on 06/20/2023).

Rotenberg, Alexander, Mark Mayford, Robert D Hawkins, Eric R Kandel, and Robert U Muller (Dec. 27, 1996). "Mice Expressing Activated CaMKII Lack Low Frequency LTP and Do Not Form Stable Place Cells in the CA1 Region of the Hippocampus". In: *Cell* 87.7. Publisher: Elsevier, pp. 1351–1361. ISSN: 0092-8674. DOI: 10.1016/S0092-8674(00)81829-2. URL: https://doi.org/10.1016/S0092-8674(00)81829-2 (visited on 06/20/2023).

Schultz, Wolfram, Peter Dayan, and P. Read Montague (Mar. 14, 1997). "A Neural Substrate of Prediction and Reward". In: *Science* 275.5306. Publisher: American Association for the Advancement of Science, pp. 1593–1599. DOI: 10.1126/science.275.5306.1593. URL: https://doi.org/10.1126/science.275.5306.1593 (visited on 06/20/2023).

Armbruster, Blaine N., Xiang Li, Mark H. Pausch, Stefan Herlitze, and Bryan L. Roth (Mar. 20, 2007). "Evolving the lock to fit the key to create a family of G protein-coupled receptors potently activated by an inert ligand". In: *Proceedings of the National Academy of Sciences* 104.12. Publisher: Proceedings of the National Academy of Sciences, pp. 5163–5168. DOI: 10.1073/pnas.0700293104. URL: https://doi.org/10.1073/pnas.0700293104 (visited on 06/20/2023).

Nagai, Yuji, Naohisa Miyakawa, Hiroyuki Takuwa, Yukiko Hori, Kei Oyama, Bin Ji, Manami Takahashi, Xi-Ping Huang, Samuel T. Slocum, Jeffrey F. DiBerto, Yan Xiong, Takuya Urushihata, Toshiyuki Hirabayashi, Atsushi Fujimoto, Koki Mimura, Justin G. English, Jing Liu, Ken-ichi Inoue, Katsushi Kumata, Chie Seki, Maiko Ono, Masafumi Shimojo, Ming-Rong Zhang, Yutaka Tomita, Jin Nakahara, Tetsuya Suhara, Masahiko Takada, Makoto Higuchi, Jian Jin, Bryan L. Roth, and Takafumi Minamimoto (Sept. 1, 2020). "Deschloroclozapine, a potent and selective chemogenetic actuator enables rapid neuronal and behavioral modulations in mice and monkeys". In: *Nature Neuroscience* 23.9, pp. 1157–1167. ISSN: 1546-1726. DOI: 10.1038/s41593-020-0661-3. URL: https://doi.org/10.1038/s41593-020-0661-3.

Tarder-Stoll, Hannah, Manasi Jayakumar, Halle R. Dimsdale-Zucker, Eren Günseli, and Mariam Aly (Feb. 17, 2020). "Dynamic internal states shape memory retrieval". In: *Neuropsychologia* 138, p. 107328. ISSN: 0028-3932. DOI: 10.1016/j.neuropsychologia.2019.107328. URL: https://www.sciencedirect.com/science/article/pii/S0028393219303719.

Tryon, Valerie L., Marsha R. Penner, Shawn W. Heide, Hunter O. King, Joshua Larkin, and Sheri J. Y. Mizumori (July 1, 2017). "Hippocampal neural activity reflects the economy of choices during goal-directed navigation". In: *Hippocampus* 27.7. Publisher: John Wiley

& Sons, Ltd, pp. 743–758. ISSN: 1050-9631. DOI: 10.1002/hipo.22720. URL: https://doi.org/10.1002/hipo.22720 (visited on 06/20/2023).

Singer, Annabelle C. and Loren M. Frank (Dec. 24, 2009). "Rewarded Outcomes Enhance Reactivation of Experience in the Hippocampus". In: *Neuron* 64.6, pp. 910–921. ISSN: 0896-6273. DOI: 10.1016/j.neuron.2009.11.016. URL: https://www.sciencedirect.com/science/article/pii/S089662730900899X.

Durstewitz, Daniel, Nicole M. Vittoz, Stan B. Floresco, and Jeremy K. Seamans (May 13, 2010). "Abrupt Transitions between Prefrontal Neural Ensemble States Accompany Behavioral Transitions during Rule Learning". In: *Neuron* 66.3, pp. 438–448. ISSN: 0896-6273. DOI: 10.1016/j.neuron.2010.03.029. URL: https://www.sciencedirect.com/science/article/pii/S0896627310002321.

Karlsson, Mattias P., Dougal G. R. Tervo, and Alla Y. Karpova (Oct. 5, 2012). "Network Resets in Medial Prefrontal Cortex Mark the Onset of Behavioral Uncertainty". In: *Science* 338.6103. Publisher: American Association for the Advancement of Science, pp. 135–139. DOI: 10.1126/science.1226518. URL: https://doi.org/10.1126/science.1226518 (visited on 06/20/2023).

Smith, David M. and Sheri J.Y. Mizumori (Sept. 1, 2006). "Hippocampal place cells, context, and episodic memory". In: *Hippocampus* 16.9. Publisher: John Wiley & Sons, Ltd, pp. 716–729. ISSN: 1050-9631. DOI: 10.1002/hipo.20208. URL: https://doi.org/10.1002/hipo.20208 (visited on 06/20/2023).

Barter, Joseph W., Suellen Li, Dongye Lu, Ryan A. Bartholomew, Mark A. Rossi, Charles T. Shoemaker, Daniel Salas-Meza, Erin Gaidis, and Henry H. Yin (2015). "Beyond reward prediction errors: the role of dopamine in movement kinematics". In: *Frontiers in Integrative Neuroscience* 9. ISSN: 1662-5145. URL: https://www.frontiersin.org/articles/10.3389/fnint.2015.00039.

Watanabe, Masataka (Aug. 1, 1996). "Reward expectancy in primate prefrental neurons". In: *Nature* 382.6592, pp. 629–632. ISSN: 1476-4687. DOI: 10.1038/382629a0. URL: https://doi.org/10.1038/382629a0.

Gomperts, Stephen N, Fabian Kloosterman, and Matthew A Wilson (Oct. 14, 2015). "VTA neurons coordinate with the hippocampal reactivation of spatial experience". In: *eLife* 4. Ed. by Howard Eichenbaum. Publisher: eLife Sciences Publications, Ltd, e05360. ISSN: 2050-084X. DOI: 10.7554/eLife.05360. URL: https://doi.org/10.7554/eLife.05360.

Jennings, Alistair, Olga Tyurikova, Lucie Bard, Kaiyu Zheng, Alexey Semyanov, Christian Henneberger, and Dmitri A. Rusakov (Mar. 2017). "Dopamine elevates and lowers as-

troglial Ca2+ through distinct pathways depending on local synaptic circuitry". In: *Glia* 65.3, pp. 447–459. ISSN: 0894-1491. DOI: 10.1002/glia.23103. URL: https://www.ncbi.nlm.nih.gov/pmc/articles/PMC5299530/ (visited on 06/20/2023).

Wildenberg, Gregg, Anastasia Sorokina, Jessica Koranda, Alexis Monical, Chad Heer, Mark Sheffield, Xiaoxi Zhuang, Daniel McGehee, and Bobby Kasthuri (Dec. 29, 2021). "Partial connectomes of labeled dopaminergic circuits reveal non-synaptic communication and axonal remodeling after exposure to cocaine". In: *eLife* 10. Ed. by Yukiko Goda, Michael A Taffe, and Yukiko Goda. Publisher: eLife Sciences Publications, Ltd, e71981. ISSN: 2050-084X. DOI: 10.7554/eLife.71981. URL: https://doi.org/10.7554/eLife.71981.

Tritsch, Nicolas X. and Bernardo L. Sabatini (Oct. 4, 2012). "Dopaminergic modulation of synaptic transmission in cortex and striatum". In: *Neuron* 76.1, pp. 33–50. ISSN: 0896-6273. DOI: 10.1016/j.neuron.2012.09.023. URL: https://www.ncbi.nlm.nih.gov/pmc/articles/PMC4386589/ (visited on 06/20/2023).

Sheffield, Mark E. J. and Daniel A. Dombeck (Jan. 2015). "Calcium transient prevalence across the dendritic arbour predicts place field properties". In: *Nature* 517.7533. Number: 7533 Publisher: Nature Publishing Group, pp. 200–204. ISSN: 1476-4687. DOI: 10.1038/nature13871. URL: https://www.nature.com/articles/nature13871 (visited on 06/20/2023).

Rolls, Edmund T. (Nov. 2007). "An attractor network in the hippocampus: theory and neurophysiology". In: *Learning & Memory (Cold Spring Harbor, N.Y.)* 14.11, pp. 714–731. ISSN: 1549-5485. DOI: 10.1101/lm.631207.

Ambrose, R. Ellen, Brad E. Pfeiffer, and David J. Foster (Sept. 7, 2016). "Reverse Replay of Hippocampal Place Cells Is Uniquely Modulated by Changing Reward". In: *Neuron* 91.5, pp. 1124–1136. ISSN: 0896-6273. DOI: 10.1016/j.neuron.2016.07.047. URL: https://www.sciencedirect.com/science/article/pii/S0896627316304639.

Bhattarai, Baburam, Jong Won Lee, and Min Whan Jung (Jan. 7, 2020). "Distinct effects of reward and navigation history on hippocampal forward and reverse replays". In: *Proceedings of the National Academy of Sciences* 117.1. Publisher: Proceedings of the National Academy of Sciences, pp. 689–697. DOI: 10.1073/pnas.1912533117. URL: https://www.pnas.org/doi/10.1073/pnas.1912533117 (visited on 06/20/2023).

Gillespie, Anna K., Daniela A. Astudillo Maya, Eric L. Denovellis, Daniel F. Liu, David B. Kastner, Michael E. Coulter, Demetris K. Roumis, Uri T. Eden, and Loren M. Frank (Oct. 6, 2021). "Hippocampal replay reflects specific past experiences rather than a plan for subsequent choice". In: *Neuron* 109.19, 3149–3163.e6. ISSN: 1097-4199. DOI: 10.1016/j.neuron.2021.07.029.

Bouret, Sebastien and Susan J. Sara (Aug. 2004). "Reward expectation, orientation of attention and locus coeruleus-medial frontal cortex interplay during learning". In: *The European Journal of Neuroscience* 20.3, pp. 791–802. ISSN: 0953-816X. DOI: 10.1111/j.1460-9568.2004.03526.x.

Dombeck, Daniel A., Christopher D. Harvey, Lin Tian, Loren L. Looger, and David W. Tank (Nov. 2010). "Functional imaging of hippocampal place cells at cellular resolution during virtual navigation". In: *Nature Neuroscience* 13.11. Number: 11 Publisher: Nature Publishing Group, pp. 1433–1440. ISSN: 1546-1726. DOI: 10.1038/nn.2648. URL: https://www.nature.com/articles/nn.2648 (visited on 06/20/2023).

Heys, James G., Krsna V. Rangarajan, and Daniel A. Dombeck (Dec. 3, 2014). "The functional micro-organization of grid cells revealed by cellular-resolution imaging". In: *Neuron* 84.5, pp. 1079–1090. ISSN: 1097-4199. DOI: 10.1016/j.neuron.2014.10.048.

Aronov, Dmitriy and David W. Tank (Oct. 22, 2014). "Engagement of neural circuits underlying 2D spatial navigation in a rodent virtual reality system". In: *Neuron* 84.2, pp. 442–456. ISSN: 1097-4199. DOI: 10.1016/j.neuron.2014.08.042.

Bourboulou, Romain, Geoffrey Marti, François-Xavier Michon, Elissa El Feghaly, Morgane Nouguier, David Robbe, Julie Koenig, and Jerome Epsztein (Mar. 1, 2019). "Dynamic control of hippocampal spatial coding resolution by local visual cues". In: *eLife* 8. Ed. by Neil Burgess, Timothy E Behrens, and Sara N Burke. Publisher: eLife Sciences Publications, Ltd, e44487. ISSN: 2050-084X. DOI: 10.7554/eLife.44487. URL: https://doi.org/10.7554/eLife.44487 (visited on 06/20/2023).

Pachitariu, Marius, Carsen Stringer, Mario Dipoppa, Sylvia Schröder, L. Federico Rossi, Henry Dalgleish, Matteo Carandini, and Kenneth D. Harris (July 20, 2017). *Suite2p: beyond 10,000 neurons with standard two-photon microscopy*. Pages: 061507 Section: New Results. DOI: 10.1101/061507. URL: https://www.biorxiv.org/content/10.1101/061507v2 (visited on 06/20/2023).

Stringer, Carsen and Marius Pachitariu (Apr. 1, 2019). "Computational processing of neural recordings from calcium imaging data". In: *Current Opinion in Neurobiology*. Machine Learning, Big Data, and Neuroscience 55, pp. 22–31. ISSN: 0959-4388. DOI: 10.1016/j.conb.2018.11.005. URL: https://www.sciencedirect.com/science/article/pii/S0959438818300977 (visited on 06/20/2023).

Larkin, Margaret Carr, Christine Lykken, Lynne D. Tye, Jeanette Graham Wickelgren, and Loren M. Frank (July 2014). "Hippocampal output area CA1 broadcasts a generalized novelty signal during an object-place recognition task: Generalized Novelty Signals in The Hippocampus". In: *Hippocampus* 24.7, pp. 773–783. ISSN: 10509631. DOI: 10.1002/hipo.22268. URL: http://doi.wiley.com/10.1002/hipo.22268 (visited on 08/29/2019).

Retailleau, Aude and Genela Morris (Mar. 2018). "Spatial Rule Learning and Corresponding CA1 Place Cell Reorientation Depend on Local Dopamine Release". In: *Current Biology* 28.6, 836–846.e4. ISSN: 09609822. DOI: 10.1016/j.cub.2018.01.081. URL: https://linkinghub.elsevier.com/retrieve/pii/S0960982218301477 (visited on 02/15/2019).

Lemon, N. and D. Manahan-Vaughan (Sept. 1, 2012). "Dopamine D1/D5 Receptors Contribute to De Novo Hippocampal LTD Mediated by Novel Spatial Exploration or Locus Coeruleus Activity". In: *Cerebral Cortex* 22.9, pp. 2131–2138. ISSN: 1047-3211, 1460-2199. DOI: 10.1093/cercor/bhr297. URL: https://academic.oup.com/cercor/article-lookup/doi/10.1093/cercor/bhr297 (visited on 04/09/2019).

Chu, Hong-Yuan, Qianqian Wu, Shanglin Zhou, Xiaohua Cao, Ao Zhang, Guo-Zhang Jin, Guo-Yuan Hu, and Xuechu Zhen (Aug. 2011). "SKF83959 suppresses excitatory synaptic transmission in rat hippocampus via a dopamine receptor-independent mechanism". In: *Journal of Neuroscience Research* 89.8, pp. 1259–1266. ISSN: 03604012. DOI: 10.1002/jnr.22653. URL: http://doi.wiley.com/10.1002/jnr.22653 (visited on 08/30/2019).

Zhuang, Xiaoxi, Justine Masson, Jay A. Gingrich, Stephen Rayport, and René Hen (Apr. 2005). "Targeted gene expression in dopamine and serotonin neurons of the mouse brain". In: *Journal of Neuroscience Methods* 143.1, pp. 27–32. ISSN: 01650270. DOI: 10.1016/j.jneumeth.2004.09.020. URL: https://linkinghub.elsevier.com/retrieve/pii/S0165027004003504 (visited on 08/30/2019).

Redondo, Roger L. and Richard G. M. Morris (Jan. 2011). "Making memories last: the synaptic tagging and capture hypothesis". In: *Nature Reviews. Neuroscience* 12.1, pp. 17–30. ISSN: 1471-0048. DOI: 10.1038/nrn2963.

Ihalainen, J.A, P Riekkinen Jr, and M.G.P Feenstra (Dec. 24, 1999). "Comparison of dopamine and noradrenaline release in mouse prefrontal cortex, striatum and hippocampus using microdialysis". In: *Neuroscience Letters* 277.2, pp. 71–74. ISSN: 0304-3940. DOI: 10.1016/S0304-3940(99)00840-X. URL: https://www.sciencedirect.com/science/article/pii/S030439409900840X.

Cohen, Jeremy D, Mark Bolstad, and Albert K Lee (July 25, 2017). "Experience-dependent shaping of hippocampal CA1 intracellular activity in novel and familiar environments". In: *eLife* 6. ISSN: 2050-084X. DOI: 10.7554/eLife.23040. URL: https://elifesciences.org/articles/23040 (visited on 03/28/2019).

Lima, Karine Ramires, Liane da Silva de Vargas, Bruna Ramborger, Rafael Roehrs, Dieuwke Sevenster, Iván Izquierdo, Rudi D'Hooge, and Pâmela B Mello-Carpes (Oct. 3, 2019). "Noradrenergic and dopaminergic involvement in novelty modulation of aversive memory generalization of adult rats". In: *Behavioural Brain Research* 371, p. 111991. ISSN: 0166-

4328. DOI: 10.1016/j.bbr.2019.111991. URL: https://www.sciencedirect.com/science/article/pii/S0166432819303201.

Moreno-Castilla, Perla, Rodrigo Pérez-Ortega, Valeria Violante-Soria, Israela Balderas, and Federico Bermúdez-Rattoni (May 1, 2017). "Hippocampal release of dopamine and norepinephrine encodes novel contextual information". In: *Hippocampus* 27.5. Publisher: John Wiley & Sons, Ltd, pp. 547–557. ISSN: 1050-9631. DOI: 10.1002/hipo.22711. URL: https://doi.org/10.1002/hipo.22711 (visited on 09/08/2023).

London, Tanisha D., Julia A. Licholai, Ilona Szczot, Mohamed A. Ali, Kimberly H. LeBlanc, Wambura C. Fobbs, and Alexxai V. Kravitz (Apr. 4, 2018). "Coordinated Ramping of Dorsal Striatal Pathways preceding Food Approach and Consumption". In: *The Journal of Neuroscience* 38.14, pp. 3547–3558. ISSN: 0270-6474, 1529-2401. DOI: 10.1523/JNEUROSCI.2693-17.2018. URL: http://www.jneurosci.org/lookup/doi/10.1523/JNEUROSCI.2693-17.2018 (visited on 04/25/2019).

Jeong, Huijeong, Annie Taylor, Joseph R Floeder, Martin Lohmann, Stefan Mihalas, Brenda Wu, Mingkang Zhou, Dennis A Burke, and Vijay Mohan K Namboodiri (Dec. 23, 2022). "Mesolimbic dopamine release conveys causal associations". In: *Science* 378.6626, eabq6740. ISSN: 0036-8075, 1095-9203. DOI: 10.1126/science.abq6740. URL: https://www.science.org/doi/10.1126/science.abq6740 (visited on 03/22/2023).

Sheffield, Mark EJ and Daniel A Dombeck (Feb. 2019). "Dendritic mechanisms of hippocampal place field formation". In: *Current Opinion in Neurobiology* 54, pp. 1–11. ISSN: 09594388. DOI: 10.1016/j.conb.2018.07.004. URL: https://linkinghub.elsevier.com/retrieve/pii/S0959438818300734 (visited on 09/04/2019).

Turi, Gergely Farkas, Wen-Ke Li, Spyridon Chavlis, Ioanna Pandi, Justin O'Hare, James Benjamin Priestley, Andres Daniel Grosmark, Zhenrui Liao, Max Ladow, Jeff Fang Zhang, Boris Valery Zemelman, Panayiota Poirazi, and Attila Losonczy (Mar. 2019). "Vasoactive Intestinal Polypeptide-Expressing Interneurons in the Hippocampus Support Goal-Oriented Spatial Learning". In: *Neuron* 101.6, 1150–1165.e8. ISSN: 08966273. DOI: 10.1016/j.neuron.2019.01.009. URL: https://linkinghub.elsevier.com/retrieve/pii/S0896627319300108 (visited on 02/12/2020).